Functional Multi-Omics Investigation of Macrophage Immune Regulation

Doctoral thesis at the Medical University of Vienna
for obtaining the academic degree

Doctor of Philosophy

Submitted by

Peter Traxler, BSc. MSc.

Supervisor:
Univ.-Prof. Dr. Christoph Bock
CeMM Research Center for Molecular Medicine
of the Austrian Academy of Sciences
Lazarettgasse 14, AKH BT 25.3
1090 Vienna, Austria

Vienna, 10/2025

Declaration

I, Peter Traxler, hereby declare that this thesis, titled “Functional Multi-Omics Investigation of Macrophage Immune Regulation”, represents my original work and has not been submitted, either in part or in full, for any other academic degree or qualification. The work presented in this thesis was carried out under the supervision of Univ.-Prof. Dr. Christoph Bock at the CeMM Research Center for Molecular Medicine of the Austrian Academy of Sciences, Vienna, Austria, and in the laboratory of my mentor Matthias Farlik at the Department of Dermatology, University of Vienna, Vienna, Austria, in accordance with the study program UN094 of the Medical University of Vienna, Austria. This thesis was conducted according to the guidelines for “Good Scientific Practice”[1] of the Medical University of Vienna.

Results of this thesis have been published, and articles are referenced (see *Publications arising from the thesis project*) or included in the Results section according to the thesis outline[2] of the Medical University of Vienna. The included publication “Integrated time-series analysis and high-content CRISPR screening delineate the dynamics of macrophage immune regulation” is distributed under the Creative Commons CC-BY license[3] which permits reuse of the article[4]. Authorship and funding contributions pertaining to the findings of this thesis are listed in the included publication (see Results section).

Christoph Bock and Matthias Farlik provided valuable feedback on an earlier draft of the thesis manuscript.

Declaration of AI-assisted technologies and writing tools:

When writing this document, the author made use of ChatGPT (Version 3.5, OpenAI, https://chatgpt.com/), Le Chat (Mistral AI, https://chat.mistral.ai/chat) and Microsoft Word (Version 16.95.1, Microsoft) in order to improve grammar, vocabulary, spelling and phrasing. The use of the large language model/AI tools (ChatGPT and Le Chat) falls under the “AI assisted

[1] Good Scientific Practice, Medical University of Vienna, 3. Auflage. Wien, 2021, ISBN 978-3-902610-47-8 https://www.meduniwien.ac.at/web/en/rechtliches/good-scientific-practice/

[2] Recommended Thesis Outline, Medical University of Vienna, Wien, 10.12.2024, https://www.meduniwien.ac.at/web/fileadmin/content/serviceeinrichtungen/studienabteilung/studium/PhD/PDF_2024/Thesis_Outline_10.12.2024b.pdf

[3] Creative Commons Attribution 4.0 International, https://creativecommons.org/licenses/by/4.0/ (accessed 09.09.2025)

[4] CCC RightsLink, https://s100.copyright.com/AppDispatchServlet?publisherName=ELS&contentID=S2405471225001796&orderBeanReset=true&orderSource=Phoenix (accessed 09.09.2025)

copy editing" purpose/definition[5] used and accepted by Nature journals without need of declaration for scientific publishing.

Zotero (7.0.11, https://www.zotero.org/) was used as reference manager to organize the manually selected bibliography.

The author assumes full responsibility for the content.

[5] "The use of an LLM (or other AI-tool) for "AI assisted copy editing" purposes does not need to be declared. In this context, we define the term "AI assisted copy editing" as AI-assisted improvements to human-generated texts for readability and style, and to ensure that the texts are free of errors in grammar, spelling, punctuation and tone. These AI-assisted improvements may include wording and formatting changes to the texts, but do not include generative editorial work and autonomous content creation. In all cases, there must be human accountability for the final version of the text and agreement from the authors that the edits reflect their original work."

Springer Nature, Editorial Policies, Artificial Intelligence (AI), Nature, https://www.nature.com/nature/editorial-policies/ai (accessed 2025.04.01)

Table of Contents

Abstract

Technological advancements drive scientific progress. They enable novel perspectives and foster experimentation at unprecedented scale. The recent discovery and adaptation of the CRISPR-Cas systems for mammalian genome editing coupled with robust single cell sequencing workflows emerge as a promising approach to address myriad questions of fundamental cellular biology. Pairing single cell transcriptome readout to individual genetic perturbations enables a comprehensive understanding of the functional impact of the respective genetic loci. Early efforts demonstrated the feasibility and insightful data richness in immune cells such as T and dendritic cells. Building on these approaches we set out to address macrophage immune regulation, specifically focusing on the role of transcription factors and epigenetic regulators. Macrophages perform a variety of tasks, depending on their environmental context and previous encounters, and as such are very plastic. Yet this great potential can be misapplied or even corrupted in certain disease states. Therefore, a better understanding of the involved regulators in cellular homeostasis and immune response will conceivably open up novel therapeutic angles to regulate a host of chronic or acute immune states.

In the course of this thesis, we adapted and optimized high content CRISPR perturbation screening to macrophages. Specifically, we collected a dense time-series of gene expression and chromatin accessibility changes following a variety of immune stimuli and then functionally assessed the role of 135 potential regulators in macrophage homeostasis and exposure to the intracellular pathogen *Listeria monocytogenes*. With this approach we were able to cluster genes based on their dynamic relationship between chromatin openness and gene expression and link transcriptional regulators back to them. Furthermore, we described novel roles for genes such as the lineage determining transcription factor *Spi1*/PU.1, JAK-STAT pathway members, and several genes encoding epigenetic factors such as *Ep300* (histone acetyltransferase), and *Sfpq*, (splicing factor). Importantly, we charted functional relationships between the regulators, independent of mechanistic constraints, purely based on their perturbation outcome on the transcriptome. This offers an additional perspective towards a systems-level understanding. Overall, we developed robust workflows enabling the generation of high-quality data sets and demonstrated their biological utility in uncovering macrophage immune regulation.

Zusammenfassung

Technologische Weiterentwicklungen treiben wissenschaftlichen Fortschritt an. Sie ermöglichen neue Perspektiven und fördern noch nicht da gewesene Skalierung experimenteller Versuche. Die kürzliche Entdeckung und Adaptierung des CRISPR-Cas Systems für Genom-Editierung in Säugetieren gekoppelt mit robusten Einzelzell-Sequenzierungs-Arbeitsabläufen zeichnen sich als vielversprechende Ansätze ab um zahlreiche Fragen der fundamentalen Zellbiologie zu adressieren. Die Verbindung von Einzelzell-Transkriptom-Auslesung und individuellen genetischen Perturbationen ermöglicht ein umfassendes Verständnis von den funktionalen Auswirkungen der respektiven genetischen Loci. Anfängliche Bestrebungen demonstrierten die Durchführbarkeit und aufschlussreiche Datenfülle in Immunzellen wie etwa T und Dendritischen Zellen. Aufbauend auf diesen Methoden begannen wir Fragen der Makrophagen Immunregulation zu adressieren, mit speziellem Fokus auf die Rolle von Transkriptionsfaktoren und Epigenetischen Regulatoren. Makrophagen führen eine Vielzahl an Aufgaben durch, abhängig von ihrem Umgebungskontext und früheren Begegnungen und sind somit sehr plastisch. Jedoch kann dieses große Potential in gewissen Krankheitszuständen falsch angewendet oder sogar korrumpiert werden. Ein besseres Verständnis der involvierten Regulatoren in zellulärer Homöostase und während einer Immunantwort wird daher denkbarerweise neue therapeutische Blickwinkel eröffnen, um eine Vielzahl von chronischen und akuten Immunzuständen zu regulieren.

Im Zuge dieser These, haben wir High-Content CRISPR Perturbations-Screenings auf Makrophagen angepasst und optimiert. Wir haben eine dichte Zeitreihe von Genexpressions- und Chromatin Zugänglichkeits-Änderungen nach einer Vielfalt von Immunstimuli erfasst und danach funktionell die Rolle von 135 potenziellen Regulatoren in der Makrophagen Homöostase und nach Exposition mit dem intrazellulären Pathogen *Listeria monocytogenes* ausgewertet. Mittels dieser Herangehensweise war es uns möglich, Gene auf Grund ihrer dynamischen Beziehung zwischen Chromatin Zugänglichkeit und Genexpression zu clustern und die transkriptionellen Regulatoren mit diesen rückwirkend zu verbinden. Des Weiteren haben wir neue Rollen für Gene wie den Lineage-bestimmenden Transkriptionsfaktor *Spi1*/PU.1, Mitglieder des JAK-STAT Signalweges, und einige epigenetischen Faktoren wie etwa *Ep300* (Histon Acetyltransferase) und *Sfpq* (Splicing Faktor) beschrieben. Hervorzuheben ist, dass wir die funktionellen Beziehungen zwischen Regulatoren kartiert haben, unabhängig von mechanistischen Beschränkungen und allein basierend auf Grund von den Perturbationsauswirkungen auf das Transkriptom. Dies ermöglicht eine weitere Perspektive zu einem System-Verständnisses. Zusammengefasst haben wir eine robuste Herangehensweise für die Generierung von

hoch-qualitativen Datensätzen entwickelt und deren biologische Nützlichkeit in der Aufdeckung der Makrophagen Immunantwort demonstriert.

Publications arising from the thesis project

Publication included in this thesis

Traxler, P.*, Reichl, S.*, Folkman, L., Shaw, L., Fife, V., Nemc, A., Pasajlic, D., Kusienicka, A., Barreca, D., Fortelny, N., Rendeiro, A.F., Halbritter, F., Weninger, W., Decker, T., Farlik, M.#, Bock, C.#, 2025. Integrated time-series analysis and high-content CRISPR screening delineate the dynamics of macrophage immune regulation. Cell Systems 16, 101346. https://doi.org/10.1016/j.cels.2025.101346

* shared first authors

shared senior authors

Related publications not included in this thesis

Boccuni, L., Podgorschek, E., Schmiedeberg, M., Platanitis, E., Traxler, P., Fischer, P., Schirripa, A., Novoszel, P., Nebreda, A.R., Arthur, J.S.C., Fortelny, N., Farlik, M., Sexl, V., Bock, C., Sibilia, M., Kovarik, P., Müller, M., Decker, T., 2022. Stress signaling boosts interferon-induced gene transcription in macrophages. Sci. Signal. 15, eabq5389. https://doi.org/10.1126/scisignal.abq5389

Datlinger, P., Rendeiro, A.F., Schmidl, C., Krausgruber, T., Traxler, P., Klughammer, J., Schuster, L.C., Kuchler, A., Alpar, D., Bock, C., 2017. Pooled CRISPR screening with single-cell transcriptome readout. Nat Methods 14, 297–301. https://doi.org/10.1038/nmeth.4177

Abbreviations

Abbreviation	Definition
5mC	5-methylcytosine
APC	Antigen presenting cell
BCR	B cell receptor
BMDM	Bone marrow derived macrophage
CAR	Chimeric antigen receptor
CAR-M	Chimeric antigen receptor macrophages
CAR-T	Chimeric antigen receptor T cell
CRISPR	Clustered regularly interspaced short palindromic repeats
CRISPRa	CRISPR activation
CRISPRi	CRISPR interference
DAMP	Danger-associated molecular patterns
DC	Dendritic cell
DNA	Deoxyribonucleic acid
dsDNA	Double stranded DNA
FACS	Fluorescence-activated cell sorting
FISH	Fluorescence in situ hybridization
GFP	Green fluorescent protein
gRNA	Guide RNA
HAT	Histone acetyl transferase
HDAC	Histone deacetyl transferase
HMT	Histone methyl transferase
HSC	hematopoietic stem cell
INDEL	Insertion-deletion
IRF	Interferon regulatory factor
ISG	Interferon stimulated gene
ISGF3	Interferon stimulated gene factor 3
lncRNA	Long non-coding RNA
LPS	Lipopolysaccharide
LTR	Long terminal repeat
miRNA	MicroRNA
MOI	Multiplicity of infection
mRNA	Messenger RNA
NHEJ	Non-homologous end joining

NK	Natural killer
NLR	Nod-like receptor
PAM	protospacer-adjacent motif
PAMP	Pathogen-associated molecular patterns
PRG	Primary response genes
PRR	Pattern recognition receptor
RISC	RNA-induced silencing complex
RLR	RIG-I-like RNA sensor
RNA	Ribonucleic acid
RNAi	RNA interference
scRNA-seq	Single cell RNA-seq
shRNA	Small hairpin RNA
siRNA	Small interfering RNA
SLC	Solute carriers
SRG	Secondary response genes
TAD	Topologically associated domains
TALE	Transcription activator-like effector
TALEN	Transcription activator-like effector nuclease
TAM	Tumor associated macrophage
TCR	T cell receptor
TF	Transcription factor
TLR	Toll-like receptor
UMI	Unique molecular identifier

Acknowledgments

I would like to express my deepest gratitude to my advisor, Christoph Bock, who allowed me to explore fascinating project directions and supported me when it was time to focus and persevere. I have learned an immense amount about science, professionalism and myself and I am forever grateful for the nurturing environment, constructive criticism, and novel perspectives vital for my scientific development.

I also extend my thanks to my mentor, Matthias Farlik, for introducing me to the fascinating world of macrophages and guiding this project towards fruition. I deeply appreciate the in-depth explorations, timely reassurances and growth opportunities that emerged throughout this project.

Next up: Mum, Dad and Flo! My basin of stability, for which I hope my “thank you”s echo long after my voice falters.

Thanks, and hugs to friends that kicked my butt, that built me up and that let me be; and a dinosaur I was fortunate to learn more closely from.

My scientific colleagues of past, present (and future!) I am beyond lucky as you all are unfortunately too numerous to mention by name. I cherish every word of advice, every “hmm?” that made me (re)think in more depth and every smile that calmed and motivated!

Paul, thanks for teaching me on so many aspects of science and lab guitars!

Fangwen, thanks for the companionship and both literal and metaphorical pineapples!

Namesake, thanks for the stimulating discussions and nourishing s(up)port!

Stephan, thanks for the healthy mix of goal-oriented pragmatism and boundless optimism!

Lastly, I would like to thank the many science communicators, ambassadors, infrastructure creators and donors who foster scientific thinking, exchange and access to literature and materials. Carefully curated databanks, qualitative plasmid distribution systems, freely shared code scripts and accessible scientific publications all contribute immensely to the day-to-day scientific work and thus human progress!

CHAPTER ONE: Introduction

1.1 Immune system

1.1.1 Parts protecting the greater whole:

Multicellular organisms face continuous challenges to their integrity at several scales, from genetic information to cellular metabolism and general organ function (Paludan *et al*, 2021). These challenges or stressors come from an immensely broad range of environmental origins including physical wounding, foreign objects (splinters, asbestos), toxic substances (venom/poison), mutagens (chemical/radiation) and other causes leading to sterile inflammation (Chen & Nuñez, 2010); biological infections by pathogenic bacteria, viruses, fungi and prions (Casadevall & Pirofski, 2002; Caughey & Baron, 2006); and parasitic agents such as multicellular and protozoan parasites (Zaccone *et al*, 2008) and transmissible cancer (Ashall, 1986; Burioli *et al*, 2021; Callaway, 2015). As such, various lifeforms have developed ways to fend off both external threats and internally corrupted processes as well as to remove or restore affected parts. The biological mechanisms and actors at play to keep an organism "healthy" from infections and safeguard against abnormal cellular behavior are generally grouped under the term immune system.

A widely used subcategorization within these mechanisms is drawn between innate abilities (i.e. determined by evolutionary processes and "bestowed" to the organism) and adaptive abilities (i.e. a framework requiring some form of training via exposure to subsequently mount a rather specific defense). This differentiation is often employed when talking about subgroups of hematopoietic cells of complex multicellular organisms, such as humans, which specialize on dealing with immune challenges. Amongst the innate immune cells are myeloid-derived ones such as macrophages, dendritic cells, granulocytes and mast cells as well as innate lymphoid cells like natural killer (NK) cells. On the other hand, lymphoid-lineage T and B cells capable of recombining their DNA at V(D)J loci to create antigen-specific binding receptors (Roth, 2014), TCR and BCR respectively, are part of the adaptive immune response. While this latter adaptation to previously encountered antigens was for a long time seen as a pinnacle of complex life major discoveries surrounding the CRISPR system in procaryotes both widened the definition of adaptive response (Van Der Oost *et al*, 2009) and provided revolutionary cell engineering tools discussed and utilized in this work below. Similarly, while innate immune cells possess intrinsic pathogen-responses the strength and character of response can be influenced based on previous exposures, blurring the line between innate and adaptive abilities as previously understood. In the course of this work, we focused on primary responses

in macrophages, yet the time-series data sets created during this work contain insights towards macrophages readiness for future challenges.

1.2 Macrophage Biology

1.2.1 Mac' of all trades:

Macrophages, as part of the innate immune arm are often regarded as sentinels and among the first to recognize and respond to infectious challenges though their contributions extend far beyond immediate pathogenic threats (Park *et al*, 2022). They occur throughout all human organs, from (opportunistic) pathogen-exposed mucosal membranes, such as the lung (Kulle *et al*, 2022) and intestine (Mowat & Bain, 2011), to the circulatory and lymphatic systems (Gray & Cyster, 2012) and the toxin-removing liver (Kulle *et al*, 2022), and even in immune-privileged organs like the testis (Rival *et al*, 2008), eye (Chinnery *et al*, 2017), and central nervous system (Carson *et al*, 2006; Smyth & Kipnis, 2025). Macrophages can be derived either from early developmental progenitors in the yolk sac and subsequently the fetal liver or be supplied throughout life from hematopoietic stem cells residing in the bone-marrow. Tissue resident macrophages can persist and self-maintain in adult tissue though major replenishing later in life is performed by bone marrow derived monocytes. Hence, in a relatively disease-free adult the majority of microglia are of yolk sac origin; tissue-resident macrophages in epidermis, lung and liver are derived largely from fetal liver; while most macrophages in the heart and gut tissue are replaced by bone marrow derived macrophages (Ginhoux & Guilliams, 2016; Wu & Hirschi, 2021). Tissue-resident macrophages from distinct developmental phases can co-exist within the same tissue and largely exhibit the same functionality. This ties in with the great plasticity exhibited by macrophages. When analyzing the transcriptome of various tissue-resident macrophages, Gautier *et al.* and the Immunological Genome Consortium identified only 39 genes that were shared by four macrophage populations (splenic red pulp, lung, peritoneum, and microglia) and expressed at a higher level than in closely related dendritic cells (Immunological Genome Consortium *et al*, 2012). While the above study revealed the strong tissue-specificity of macrophage gene expression profiles, Lavin *et al.* proved functionally that macrophages largely adapt to their environment instead of persisting with a previously developed phenotype. They expanded the transcriptome findings by including Kupffer cells of the liver, ileal- and colonic macrophages of the gastrointestinal tract, and bone-marrow derived monocytes. Furthermore, they transferred peritoneal macrophages into lung tissue and observed large transcriptomic changes towards lung expression profiles within the original peritoneal macrophages (Lavin *et al*, 2014).

A further indicator for the plasticity of macrophages can be found in tumor microenvironments where, similar to cancer-associated fibroblasts, macrophages are often corrupted by the signaling milieu to support various pro-tumorigenic features. Understanding the driving factors of these tumor-associated macrophages offers novel routes to support tumor immunotherapy (Khan *et al*, 2023).

Taken together, macrophages and specifically their expression profile can vary a lot depending on the environment they are in and understanding the contributing factors at play may allow favorable reprogramming toward patient-beneficial macrophage behavior.

1.2.2 Master of some:

Macrophages are aptly named for their size and one of their key strengths: to surround and break down extracellular objects, a process termed phagocytosis. Additionally, they perform a plethora of functions to keep bodily homeostasis, respond to threats and ultimately in reestablishing normal tissue function. Some recent review works have tried to define hallmarks of healthy macrophages such as (Wynn *et al*, 2013) and (Sheu & Hoffmann, 2022). In broad strokes, major shared functional hallmarks of macrophages are phagocytosis, sensing danger to tissue and host, release of antimicrobial substances, programmed cell death, cytokine and chemokine release, antigen presentation, tissue remodeling, and motility.

Phagocytosis:

The aforementioned capability to surround large objects, such as extracellular microorganisms, marks them as a vital player in infectious disease response as they can engulf and break down pathogens (Uribe-Querol & Rosales, 2020). Once an extracellular object is surrounded in a phagosome the vesicle fuses with the lysosome creating a phagolysosome, a highly acidic environment in which specialized enzymes degrade the contents, allowing reuse of components, expulsion or antigen presentation. Phagocytosis both helps to eliminate an active threat as well as clean up after the immediate danger is contained.

Macrophages are also professional efferocytes (Boada-Romero *et al*, 2020), that is, they can eat and reabsorb dead, dying or otherwise unwanted cells. This function is utilized from early on in development with a notable example being applied to apoptotic cells resulting from limb formation and the clearance necessary for individual digit formation (Hernández-García *et al*, 2024). Similarly, clearing of partial cell or extracellular material is crucial in respective tissue (re)modeling: microglia aid neuronal health as they prune synapses in the central nervous system; macrophages reabsorb extruded nuclei from erythrocytes in hematopoietic niches;

and specialized macrophages called osteoclasts reabsorb bone tissue and shape bone-marrow cavities (Wynn *et al*, 2013). Importantly, macrophages can suppress unwanted inflammation when clearing apoptotic cells and debris and ward off autoimmunity towards self-antigens.

Sensing danger to tissue and host

To enable the various outcomes of phagocytosis, macrophages need to sense and differentiate a broad range of stimuli (Uribe-Querol & Rosales, 2020). In general, efferocytosis of live cells is inhibited by the expression of CD47 on human cells, often called the “don’t eat me” signal, which binds SIRPα and other inhibitory receptors on macrophages preventing phagocytosis (Boada-Romero *et al*, 2020).

On the other hand, specific signals exposed during apoptotic processes, such as phosphatidylserine or calreticulin on the outer plasma membrane, initiate phagocytic processes of host cells. Receptors that induce phagocytosis are grouped into opsonic and non-opsonic receptors (Uribe-Querol & Rosales, 2020). The latter group contains scavenger-, dectin-, mannose receptors, and CD14 that either directly recognize the aforementioned apoptotic signals or components of bacterial or fungal cell walls. Opsonic receptors encompass receptors recognizing the conserved domains of antibodies (Fc-Receptors such as FCGR1/CD64) and complement receptors. As such they provide macrophages with the capability to efficiently clear recognized immunological threats.

Both phagocytic receptor groups work in coordination with pattern recognition receptors (PRRs), which recognize a broad range of conserved structural classes. Among the PRRs that sense damage- or pathogen-associated molecular patterns (DAMPs and PAMPs respectively) are Toll-like Receptors (TLR) mainly expressed on the cell surface and endosomes, NOD-like receptors (NLR) in the cytosol, RIG-I-like RNA sensors (RLR) and cGAS which recognizes DNA (Dvorkin *et al*, 2024). These are the result of evolutionary adaptation to common threats and represent the prime recognition system of innate immunity. Many of these receptors bind to a multitude of ligands and therefore enable a constant survey of a broad DAMP and PAMP landscape. These PRRs act in coordination with phagocytic receptors to increase efficiency and decide whether or not the phagocytosed particle warrants a pro- or anti-inflammatory response. Notably, some receptors are both PRRs and phagocytic, such as Dectins, while the common TLRs are considered non-phagocytic (Uribe-Querol & Rosales, 2020).

Furthermore, macrophages express a variety of cytokine and chemokine receptors to coordinate their behavior with other immune cells and the wider host body at large.

Cytokine and chemokine release

In addition to their effector functions in eliminating pathogens macrophages are also regarded as a major immune sentinel. They are capable of producing and releasing a broad range of cytokines and chemokines to attract other immune cells and influence their behavior in response to danger (Arango Duque & Descoteaux, 2014). Alongside their paracrine effects they can also act autocrine, i.e. on the secreting macrophage itself, to reinforce signaling cascades. One classic example is the type I interferon IFN-β which macrophages produce in response to interferon regulatory factor (IRF) activation following TLR receptor engagement. In turn, IFN-β activates JAK-STAT signaling culminating in the formation of the interferon-stimulated gene factor 3 (ISGF3) complex (comprising STAT1, STAT2, and IRF9) as well as alternative complexes (Platanitis *et al*, 2019).

This complex kickstarts an interferon response program in neighboring cells irrespective of their exposure to DAMPs and PAMPs and thus prepares them for infectious encounters. Other well studied examples of pro-inflammatory cytokines released by macrophages are TNF, IL-6, and IL-1β, all endogenous pyrogens (substances that are fever inducing) with multiple roles in immune activation. Though similar to their role in kickstarting an immune response, macrophages can also maintain or revert to homeostasis by releasing a host of anti-inflammatory cytokines. One prominent example is IL-10, which inhibits macrophage function and especially antigen presentation via MHC-II molecules. Another is TGF-β, which next to a plethora of other functions is important for Treg development. Furthermore, macrophages express various checkpoint inhibitors like PD-L1 and PD-L2 that suppress the adaptive immune response.

Next to regulating the immune status of cells macrophages release a number of specialized cytokines, called chemokines, to influence migration of other immune cells. Receiving cells follow the direction of increasing chemokine concentration and thus arrive at the source, the site of pathogen encounter or the tumor microenvironment. Among the main chemokines produced by macrophages are CXCLs such as CXCL1/2 and 8 which recruit neutrophils, and interferon inducible CXCL9 and 11 which mainly recruit T cells, as well as CXCL10 (IP-10) and CCL5 (RANTES) which attract T cells, NK and dendritic cells. Furthermore, they can recruit other monocytes and macrophages via secretion of CCL2 (MCP1) (Arango Duque & Descoteaux, 2014).

Release of antimicrobial and cytotoxic substances

Next to the phagocytosis of invading pathogens macrophages produce antimicrobial peptides and proteins (e.g. defensins, cathelicidins, lysozyme) that lead to lysis of bacterial cell membranes or inhibit their growth as well as regulate other aspects of the immune response (Lai & Gallo, 2009). Furthermore, macrophages produce nitric oxides and reactive oxygen species

to help with clearance of pathogens by creating a hostile environment. However, these effects can lead to widespread tissue damage, as they react unspecific and induce damage on cells of the host organism. Thus, these mechanisms need to be limited to acute stresses and not prolonged beyond the clearance of the immediate threat.

Programmed cell death

Being on the front line of infections comes with danger to be parasitized by the very threat a macrophage is supposed to deal with. This most strikingly happens in certain viral infections (such as HIV-1) or intracellular bacteria (such as *Legionella, Listeria, Mycobacteria*) that specialize to invade cells including macrophages and exploit their metabolism and motility to proliferate and spread throughout the multicellular organism (Price & Vance, 2014; Reece *et al*, 2021). Next to classic cell apoptosis, a non-inflammatory cell death, a macrophage can initiate various pro-inflammatory cell death fates. Makuch et al. summarize three distinct programs: pyroptosis, necroptosis and ferroptosis.

In case of pyroptosis the inflammasome, a PRR complex, capable of triggering the caspase cascade, is activated and subsequently leads to gasdermin D pore formation on the plasma membrane resulting in the release of cellular contents increasing an overall inflammatory response. While this results in cell death, the process remains reversible even after cell swelling and leakage through gasdermin D pores has started. Necroptosis can be triggered by FAS, TNF or TRAIL signaling via RIPK proteins in the absence of caspase 8 leading to MLKL pore formation and is different from necrotic cell death due to cell injury. Similar to pyroptosis, the formation of MLKL pores is to a certain extend a reversible process. The third process, ferroptosis, is a recently discovered pathway dependent on iron levels and leads to increased lipid peroxidation in the membrane compared to other cell death pathways (Makuch *et al*, 2024).

Antigen presentation

In addition to recruiting the adaptive arm of the immune system macrophages, alongside dendritic cells and certain B cells, are professional antigen presenting cells (APCs) (Roche & Furuta, 2015). While every cell type presents intracellular self-antigens via MHC class I molecules APCs express an array of MHC class II molecules which focus on presenting peptides taken up from the environment and then processed in the endosomes and lysosomes. Antigens presented on MHC class II molecules are recognized by CD4+ T helper cells with a matching TCR. These activated CD4+ T helper cells, in turn, orchestrate the adaptive immune response.

Additionally, APCs can cross-present foreign antigens on their MHC class I molecules which stimulates cytotoxic CD8+ T cells (Muntjewerff & Meesters, 2020). The activation of naïve CD8+ T cells is best studied in DCs and relies on co-expression of costimulatory receptors

such as CD80 and CD86 and cytokine IL-12. In a recent study, monocytes were observed to acquire preformed antigen peptide-MHC class I complexes from neighboring cells and present them instead, a process called cross-dressing (Elewaut *et al*, 2025). Besides the activation of naïve CD8+ cells macrophages are equipped for local re-activation of cytotoxic T cells or vice-versa their suppression via anti-inflammatory signaling.

Tissue remodeling

Next to their ability to phagocytose extracellular material macrophages are actively involved in tissue remodeling both during homeostasis as well as after tissue damage occurred. They release proteases like matrix metalloproteases that cleave the extracellular matrix or remodelers like lysyl hydroxylases, which drive collagen cross links. Furthermore, they release a number of growth factors to influence fibrotic processes (TGF-β), proliferation of various structural (PDGF, IGF-1) and stem cell populations (WNT3A), and angiogenesis (VEGF) (Wynn & Vannella, 2016). Better understanding of the complicated interplay of macrophages in wound repair and tissue remodeling has further garnered attention when it became clear that these processes are often exploited within tumors to strengthen or enable several pro-tumorigenic properties. This includes aberrant growth signaling, mediating cell migration, driving permissive blood vasculature and intravasation of cancer cells into the blood stream increasing metastatic spread.

Motility

Macrophages are able to break down the extracellular matrix and release chemokines that direct motility in other cells and themselves. Bone-marrow derived monocytes and macrophages travel via the circulatory system throughout the whole body to sites of inflammation, even into immune-privileged areas such as the brain (Carson *et al*, 2006). In local tissues macrophages migrate both amoeboid as well as mesenchymal depending on the extracellular environment (Van Goethem *et al*, 2010). Their ability to invade tissues and patrol aids them in constantly surveying the host for damage and pathogens.

1.2.3 Signaling in macrophages

As described above, macrophages sense and survey their environment constantly with their specialized PRRs, IFNARs, TNFRs, mechanoreceptors, and others. Once a suitable ligand binds with sufficient strength a handful of intracellular mediators are activated. Sheu and Hoffmann list the key players MYD88, TRIF, TRAF, MAVS, STING and ASC. TLR and IL-1 receptors signal via MYD88, with the exception of TLR3, a double stranded RNA binding receptor not present on the cell surface but in endosomes. TLR3 and TLR4 from within the endosome can activate TRIF (Sheu & Hoffmann, 2022). Thus, even in a supposedly simple sensing of

lipopolysaccharide (LPS), a cell membrane component of gram-negative bacteria, via TLR4 two different signaling pathways are engaged depending on the localization of the TLR4 receptor complex and receptor internalization and endosome maturation. Once activated, MYD88 leads to an early NFκB peak irrespective of the actual amount of LPS, whereas TRIF induced signaling is prolonged and much more responsive to ligand concentration (Cheng *et al*, 2015; Sheu & Hoffmann, 2022). TNFR signaling via TRAFs leads to activation of NFκB, stress signaling, or cell death. Intracellular NLRs sense peptidoglycans the main component of gram-positive bacterial cell walls and other components like flagellins, and in turn activate caspase-1 and ASC (PYCARD) leading to inflammasome formation and pyroptosis (Franchi *et al*, 2009). Nucleic acid sensors measure RNA (by RIG-1 like receptors) or DNA (by cGAS) in the cytosol. The former activates MAVS leading to TBK1/IKKε induction. Activation of cGAS on the other hand by long double-stranded DNA (dsDNA) in the cytosol leads to the production of cGAMP (2'3' cyclic GMP-AMP). This messenger molecule activates the endoplasmic reticulum membrane protein STING and initiates its transfer to the Golgi where it activates TBK1.

These signaling pathways mostly converge on a handful of kinase transcription factors. TRIFs, MAVS and STING lead to strong activation of IRF3; MYD88 heavily induces p38 MAPKs; and NFκB and JNK/ERK are universally activated by the signaling pathways outlined above (Sheu & Hoffmann, 2022).

At first glance it seems that while PRR recognize and differentiate a broad range of PAMPs and DAMPs via their binding affinities and localization, the downstream signaling is mainly performed by the same transcription factors and hence should display a largely shared signaling response. However, recent studies have indicated that depending on the stimulus and concentration triggering the signal also transcriptional regulation displays a heterogeneous behaviour in their response. An important study described six different response patterns of NFκB that vary from static to oscillatory with varying activation speed, peak amplitude, duration and overall activity (Adelaja *et al*, 2021). Furthermore, the transcriptional response may depend on previously established chromatin accessibility enabling a permissive landscape without transcription, in other words those loci display epigenetic potential (Krausgruber *et al*, 2020). With many immune genes, termed primary response genes (PRG), able to be activated with minimal delay by available but inactive transcription factors (Pope & Medzhitov, 2018) and some genes (PRG-I) already exhibiting transcription associated epigenetic marks at promoter histones and pre-assembled RNA polymerase II (Hargreaves *et al*, 2009). The latter being constrained at the level of transcriptional elongation and mRNA processing to avoid aberrant signaling. Indeed, an investigation of PRG-Is compared to housekeeping genes, that is, genes generally active in cells to fulfill maintenance tasks, found that albeit both are marked by Pol II occupancy, PRG-Is are also bound by corepressors such as histone deacetylase

(HDAC) complexes. Their activation therefore relies on a “de-repression” (Hargreaves *et al*, 2009) or in other words, certain immune genes are in a constant state of dual-regulation with their figurative gas and brake pedal constantly engaged.

In contrast, PRG-IIs were found to be GC poor without constant Pol II occupancy. Nevertheless, they display activation associated H3 acetylation and H3K4me^3 and are speculated to denote more cell-type specific genes (Hargreaves *et al*, 2009) and/or are associated with specialized roles such as IFN-β induced genes (Ramirez-Carrozzi *et al*, 2009). Genes whose signal-induced transcription requires protein translation (e.g. of an activating transcription factor) and chromatin remodeling are termed secondary response genes (SRG). Overall, macrophages and the innate immune response have served as a great model to study stimulus-response triggered gene expression processes (Sheu & Hoffmann, 2022).

1.3 Transcriptional and epigenetic regulation

1.3.1 Elements of mRNA transcription

Gene transcription is a multi-faceted process with several key players and a plethora of contributing and fine-tuning mechanisms in place to ensure the appropriate level of mRNA production at any point in time. Cramer summarized the general process of gene transcription in a comprehensive review in 2019 (Cramer, 2019). Every protein-coding gene has (at least) one promoter where the RNA polymerase II pre-initiation complex can form, separate the DNA strands and start transcription of the gene.

Promoters for housekeeping genes, which are constitutively expressed in a variety of cell types, generally contain CpG islands. These islands obstruct formation of dense nucleosome packaging of the DNA and hence keep the promoter open and accessible, unless the DNA itself gets methylated. On the other hand, many cell-type or context specific genes rely more on specialized elements, like the TATA box and specific transcription factor binding sites whose combination and localization coordinates transcription. In macrophages, response genes induced by NFκB and the MAP kinase pathway, which are activated by a wide array of stimuli, contain CpGs and are rather devoid of nucleosomes even in a basal state. On the other hand, the IFN-β response relies less on CpG islands and rather depends on nucleosome rearrangement to free the promoter region for transcriptional activity (Ramirez-Carrozzi *et al*, 2009).

The majority of the roughly 1600 known transcription factors bind nucleosome-free DNA acting on open chromatin regions. Pioneering factors on the other hand are capable of binding nucleosome-bound DNA. They open up previously closed promoters and thus enable the differentiation into a specific cell type. Pioneering factors likely act in concert with chromatin remodeling complexes that can evict nucleosomes, replace histones, or shift around their location. Furthermore, recruitment of histone acetyltransferases (HAT) aid in establishing these now permissive promoters. HATs introduce acetyl groups onto positively charged lysines on the histones. This weakens the interaction with the negatively charged backbone of DNA, leading to a looser, i.e. more open promoter region.

In principle, human mRNA transcription of a gene thus requires both the gene body and a promoter sequence amenable to assembly of the polymerase initiation complex. This is often exploited in cell engineering where an exogenous DNA containing a protein-coding gene after a common mammalian promoter (e.g. CMV, EF1α) is sufficient to direct expression of the gene of interest. An example is the plasmid CROPseq-Guide-Puro, Addgene #86708 from our study where an EF1α promoter drives expression of a puromycin resistance gene (Datlinger *et al*, 2017).

Transcription in endogenous loci is also influenced by enhancer regions. These are genomic regions in *cis* or *trans* where additional transcription factors can bind, get into close proximity and interact with proteins and complexes from the promoter region. Macrophages rely heavily on enhancer regulated transcription to define tissue resident functions (Lavin *et al*, 2014). The pioneering factor PU.1 opens many macrophage specific enhancer sequences during differentiation and prepares them for subsequent stimulus specific activation (Kaikkonen *et al*, 2013; Ostuni *et al*, 2013).

Promoters can be influenced by various enhancer sequences, with the expression level correlating with the amount of enhancers (Denisenko *et al*, 2017). Enhancers are often specific for a cell type and stimulus and aid in recruitment of other co-activators such as the mediator complex. This complex has recently been described to aid cell type specific transcriptional expression patterns (Jaeger *et al*, 2020).

Polymerase initiation, elongation and pausing are regulated as well as several mRNA processing steps that happen simultaneously with elongation such as splicing. Transcription factors, due to their specific binding to promoter and enhancer DNA sequences and subsequent recruitment functions, are considered key regulators of transcription pattern control. Therefore, deciphering the transcription factor code promises to reveal the transcription programs governing cell behavior (Pope & Medzhitov, 2018). A proposed hierarchical model suggests that pioneering/lineage determining factors open up genomic loci during differentiation. Then a

second layer made up of primer factors may keep the loci in an inactive but ready form, enabling rapid upregulation by exchange with/being bound by stimulus induced transcription factors, preferentially from the same protein family (Garber *et al*, 2012). Interestingly, while transcription factors can co-occupy the same promoter, they may not necessarily act directly cooperative, but rather in sequential steps to control the immune response (Cheng *et al*, 2017). Deciphering the transcription factor code may not be easy and in and of itself sufficient to understand gene expression. An in-depth study of NFκB and IRF3 co-occupancy revealed their target genes to be regulated in unique and individual ways (Tong *et al*, 2016).

Next to transcription factors acting in concert, additional layers such as epigenetic regulation allow a cell a more plastic adaption to environmental signals than relying on DNA encoded sequences and their respective transcription factor proteins alone.

1.3.2 Chromatin and nucleosomes

DNA is seldom free and unbound within a cell but rather packed in various densities. The typical double-stranded DNA molecule wraps almost twice around histone octamers with about 147 bp of DNA per protein core (Chen *et al*, 2020). Each octamer contains two copies of histone H2A, H2B, H3 and H4 and once DNA-bound these units are termed nucleosomes. A linker histone H1 exists which does not sit within the octamer bead but between them and helps with the compaction of chromatin fibers. The full-length DNA-protein complex is called chromatin and, in this configuration, referred to as resembling “beads on a string” based on their appearance in electron microscopy image. The first study describing this analogy used the word “particles” instead of the hitherto common “beads” (Olins & Olins, 1974). This structure called “euchromatin” is relatively open for interaction with other proteins for transcriptional control, though can condense by packing the nucleosomes into approximately 30 nm fibers referred to as heterochromatin. This densely packed form is generally considered transcriptionally inactive. Heterochromatin can in turn coil up further ultimately resulting in tightly packed chromosomes.

1.3.3 DNA methylation

Various covalent changes can be performed on chromatin in turn influencing the various accessibility states. The DNA itself can be methylated, which in eukaryotes generally refers to the addition of a methyl group to a cytosine (5-methylcytosine, 5mC) (Moore *et al*, 2013). Especially at CpG island promoters, DNA methylation is associated with inactivation and denser nucleosome packaging. 5mC methyl groups can be established de novo by DNMT3A and DNMT3B or on the newly synthesized strand during DNA replication by DNMT1 based on

the previous methylation status (CpG is palindromic, i.e. it is matched on the complementary strand by a CpG sequence).

Removal of 5mC can occur in different ways, such as by deamination by AID/APOBEC into thymine, yet the predominant removal in human and mouse cells is performed by TET proteins which oxidize 5mC into various intermediates (Prasad *et al*, 2021). The resulting G/T mismatch from the conversion to thymine or the various intermediate products from TET oxidation can be repaired using the base excision repair mechanism. This dependence leads to a higher mutation rate at CpG sites. While methylated DNA may directly decrease the affinity of certain transcription factors specific methyl-CpG-binding domain (MBD) proteins bind to methylated DNA and in turn prohibit gene expression (Kaluscha *et al*, 2022; Valinluck, 2004). Given both the ability to change DNA methylation status based on a cell's experience as well as the ability to persist and even bequeath CpG methylations to daughter cells positions this mechanism as a promising malleable layer for therapeutic intervention.

1.3.4 Histone codes

A further epigenetic layer involves nucleosomes, specifically the histones. As mentioned above, DNA void of nucleosomes is more accessible. Specialized ATP-dependent chromatin remodeler complexes slide nucleosomes, evict or reinstall nucleosomes. Four families of chromatin remodelers have been described so far: SWI/SNF, ISWI, CHD and INO80 which are heavily associated with cell differentiation, gene expression and DNA repair (Tyagi *et al*, 2016).

The IFN-β response depends on SWI/SNF induced chromatin rearrangement for expression, which may not only increase specificity but also reduce unwanted basal or tonic response (Ramirez-Carrozzi *et al*, 2009). This dependence may be an important evolutionary safeguard as excessive type I signaling is involved in many autoimmune and autoinflammatory diseases, so called interferonopathies (Crow & Casanova, 2024).

Besides their ability to reposition nucleosomes, chromatin remodelers can affect histone subcomponents of a nucleosome and exchange them with a different variant. Indeed, several specialized histone variants have been identified and correlated with specific processes (Quénet, 2018). A majority of variants are expressed in the S phase and cell-cycle associated or expressed in specific tissues and cell types. Among the more specialized yet universally expressed histone varieties, H3.3 is associated with general transcription, H2A.X with DNA damage repair, H2A.Zs with both, and macroH2A with heterochromatin repression as well as specialized transcriptional activation (Chen *et al*, 2014; Recoules *et al*, 2022).

In addition to repositioning and exchange of histone variants many different forms of post-translational modifications have been discovered. While DNA tightly wraps around the histone octamer the N-terminal ends of histones extend beyond nucleosomes and are accessible to specialized epigenetic factors that actively read, write and erase these histone modifications (Chen *et al*, 2020). These modifications can take many forms such as methylation, acetylation, ubiquitination and sumoyulation all occurring predominantly at lysines, as well as phosphorylation of serines and threonines, citrullination, ADP-ribosylation, and proline isomerization (Niu *et al*, 2022). These modifications can be found in concert affecting amino acids at different positions but also mutually exclusive on key amino acids. The well-studied lysine group at position 27 of histone H3 can be found either methylated (H3K27me) or acetylated (H3K27ac). The methylation mark, introduced by histone methyl transferases (HMT), can be either mono-, di- or trimethylated (H3K27me3) and is associated with inhibition of transcription. Reports in macrophages indicate that JMJD3 a demethylase is upregulated after macrophage stimulation by either LPS (Chen *et al*, 2012; De Santa *et al*, 2009) or IL4 (Ishii *et al*, 2009) and demethylates H3K27me3 at a large proportion of response genes. In turn, H3K27ac, introduced by the histone acetyltransferase p300 (*EP300*) is associated with active promoter and enhancer regions (Ghisletti *et al*, 2010; Kano *et al*, 2024; Schmidt *et al*, 2016). While histone acetylation is generally considered a transcription activation mark, methylation is not necessarily an inhibitory mark. Indeed triple methylation of H3K4me3 at promoter sites correlates with transcriptional activity, while H3K4me1 is a feature of active or poised enhancers (Barski *et al*, 2007). Thus, deciphering the histone code involves knowledge of the modifications at precise amino acid positions, the specific histone variant used and where the nucleosome is positioned along the DNA.

1.3.5 Chromatin in 3D

A higher order layer of epigenetic regulation is the localization of chromatin in 3D. As mentioned, chromatin can coil into more denser areas but likewise it can bring distal sites such as *cis*- and even *trans*-enhancers into proximity of the respective gene body. The cohesin complex, a ring-like structure, together with CTCF forms large scale loops with increased proximity of the associated chromatin. These so called topologically associated domains (TAD) have been implicated in cell type differences. In line, a study by Stik *et al.* found that disruption of these TADs via induced CTCF degradation diminished LPS response in macrophages (Stik *et al*, 2020).

Furthermore, genetic loci can localize to various nuclear bodies such as the nucleolus, associated with ribosomal RNA transcription, or paraspeckles involved in gene splicing. Association with polycomb bodies or the nuclear lamina is often linked to transcriptional repression

(Mao *et al*, 2011; Van Steensel & Belmont, 2017). These membrane-less substructures involve an assortment of specialized proteins and RNAs enabling or increasing the efficiency of transcriptional regulation.

1.3.6 Non-coding RNA

Apart from the assembly of the aforementioned nuclear bodies, another layer of epigenetic regulation is mediated by non-coding RNAs such as microRNAs (miRNA) and long non-coding RNAs (lncRNA). For miRNAs longer precursor molecules are processed by specialized machinery to produce short RNA snippets of around 22 bp capable of binding a complementary mRNA sequence (Shang *et al*, 2023). The miRNAs interact with Argonaute proteins to bind to mRNA, which stops translation or even induce the degradation of the mRNA. Therefore, the miRNA system is considered a repressive mechanism. Indeed, macrophages reacting to LPS stimulation phosphorylate AGO2 to disrupt miRNA/AGO complexes, which in turn derepresses proinflammatory response genes (Mazumder *et al*, 2013).

On the other hand, long non-coding RNAs (lengths over 200 bps) contain various binding sites and motif structures to coordinate the interactions with regulatory proteins, RNA, or DNA sequences. Long non-coding RNAs are a diverse class with estimates ranging from 10-100 thousand lncRNAs existing in the human genome (Statello *et al*, 2021). Insights into their exact gene regulatory roles will likely reveal further fine-tuning mechanisms. One example of a lncRNA active in macrophages is transcribed from an intergenic region in the Cox2 gene, lincRNA-Cox2, which itself is upregulated in response to LPS and other bacterial stimuli. Based on perturbation experiments, lincRNA-Cox2 seems to repress certain ISGs in homeostatic conditions while expression of specific inflammatory genes, such as IL6 may be positively influenced by lincRNA-Cox2 (Carpenter *et al*, 2013).

1.4 Trained immunity/stimulus memory

While macrophages are innately equipped with pattern recognition receptors, they are not only responding to the current environment based on evolutionary hardcoded rules, but also adapt their signaling responses based on prior exposures. Evidence for innate immune memory accumulated around a century ago with multicellular organisms exhibiting a diminished response to repeated pathogen or LPS exposure (Van Epps, 2006). Macrophages were soon identified as a major contributor that showed a weakened transcriptional response to LPS after an initial exposure to high-concentrated dose (100 ng/ml) of LPS *in vitro* (Foster *et al*, 2007; Mages *et al*, 2008). This phenomenon is termed immune tolerance and can help the host organism to avoid detrimental immune over-reactions inducing too much collateral damage, for example, in an attempt to clear a persistent infection.

Similarly, the opposite side of the coin can be observed in a process called immune priming where an initial stimulus of IFN-γ leads to an increased subsequent immune response to LPS (Gifford & Lohmann-Matthes, 1987). Hereby the induction of a low-level interferon stimulus primes macrophages in the vicinity to enable a quick ramp up of immune response genes once the actual threat is encountered. Interestingly, a low-dose pretreatment with LPS can prime macrophages as well, meaning that the induced memory is reliant not only on the stimulant itself but also the encountered concentration (Deng *et al*, 2013) leading to drastically different outcomes (tolerance or priming). Furthermore, memory can result in repeated simulation with the same factor (LPS followed by LPS), or by differing signals (IFN-γ followed by LPS). However, priming is now understood to mean a stronger secondary response, without an intermediary drop of response gene expression to homeostatic levels. This latter case, a first stimulus followed by a period of basal level expression, but a stronger secondary response to either the same treatment or even a different class of stimulants was later termed trained immunity in the immunological field (Netea *et al*, 2011).

Investigations of molecular mechanisms generating stimulus memory indicate epigenetic and metabolic changes as likely causative processes. A study of *ex vivo* monocyte to macrophage differentiation with either β-glucan induced immune training or LPS induced tolerance found widespread changes in distal regulatory elements. An initial stimulus lead to chromatin opening associated with increased H3K27ac and H3K4me1 marks with the methylation mark persisting after the initial response (Saeed *et al*, 2014). Subsequent work described involvement of certain long non-coding RNAs in the regulation of groups of immune response genes, such as chemokines elicited after β-glucan. The upregulation of a specific human lncRNA UMLILO after the first stimulus helped recruit H3K4me3 writers to certain CXCL promoters, even in murine cells which lack this specific lncRNA (Fanucchi *et al*, 2019).

Crucially, macrophage states remain plastic. A previously established tolerant state with LPS can be reverted to a trained state by β-glucan treatment (Novakovic *et al*, 2016) indicating that in a complex situation innate immune cells likely adapt dynamically to their environment. This finding highlights the complexity involved in immune memory both advocating careful experimental designs to derive meaningful conclusions while simultaneously emphasizing the potential of this semi-stable, malleable layer for therapeutic interventions.

It is important to note that similar to “epigenetic memory/inheritance”, the scale of memory in immunity is not universally defined. As such, stimulus memory could apply to 1) a single cell exposed twice without intermediate cell division, 2) the same cell type with cell divisions where daughter cells retain parental memory 3) a memory kept during cell differentiation from a progenitor cell or 4) a memory inherited from a parental individual to its (sexually reproduced) offspring (transgenerational effects have been described in cohorts impacted by famines

(González-Rodríguez *et al*, 2023), though this process presumably does not apply to macrophages). For immune memory the separation between “central trained immunity” and “peripheral trained immunity” has been proposed, with the former including training events in bone-marrow residing progenitor cells passed to circulating immune cells and the latter describing similar stimulation but observing trained effects in cells not in circulation, i.e. in the periphery (Vuscan *et al*, 2024).

Overall, this property of responding to prior exposure and subsequent memory based on changes to the intrinsic epi-genome resembles characteristics of the adaptive immune response. Therefore, trained immunity may be seen as a bridging phenomenon between those two categorical definitions (Netea *et al*, 2019). Apart from updating our definitions and categorial views two take aways for human medicine could be stated as:
i) Macrophages are reprogrammable by influencing their epigenome. In general, epigenetic factors are considered druggable (Ganesan *et al*, 2019) compared to transcription factors that often do not provide binding sites for traditional small-molecule inhibitors. ii) Furthermore, keeping exceptions in mind, once they are trained the memory persists and can be propagated to daughter cells. A feature that may be exploitable for ex-vivo cell engineering with subsequent re-introduction of fine-tuned macrophages into tumor sites or chronic autoimmune contexts to alleviate aberrant immune milieus. Cell engineering of macrophages to, at first, better understand the function of each component and later create an optimized macrophage for the respective immune challenges has garnered increasing attention (Sloas *et al*, 2021).

1.5 Genetic engineering of cells

1.5.1 Double-strand breaks and targeted genome editing

Modifying the genetic information of cells or whole organisms promises incredible therapeutic opportunities to treat or even revert many diseases and serve as invaluable resource for experimental manipulation.

Early efforts of genetic manipulation of target cells focused on homologous recombination (Fernández *et al*, 2017; Smithies *et al*, 1985). This natural process contributes to genetic diversity during meiosis, provides an opportunity to repair damaged DNA and enables lateral/horizontal gene transfer. In general, homologous recombination comes into play once a DNA double-strand break is recognized within a cell. As the name suggests, it works to repair the break via a homologous copy of the genetic information. In short, this copy serves as a template for DNA polymerases to synthesize new DNA to make up for previously lost or mutated genetic information. While sufficiently strong homology is needed to anneal adjacent

regions during the repair process, novel genetic information can be provided within the homologous DNA strand to be incorporated during template-directed DNA synthesis.

Pioneering work in mammalian cells focused on genetic engineering of knockout mice by targeted introduction of exogenous homologous templates into mouse embryonic stem cells for which Oliver Smithies, Mario Capecchi and Martin Evans received the 2007 Nobel Prize in Physiology and Medicine (Mak, 2007). Early efforts reported a rather low efficiency of around one in thousand cells with a successful integration event (Smithies *et al*, 1985). It was soon recognized that artificial induction of double strand breaks around the target site improved the number of successful gene editing events via homologous recombination. This led to a search for ever better methods to introduce DNA damage at the intended target site. A first milestone was the application of I-*Sce*I, a yeast meganuclease which homes in on a specific 18 base pair long target site (One DNA strand of the target site in 5'-3' orientation, arrows indicate the cut sites "TAGGG↑ATAA↓CAGGGTAAT"[6]). The nuclease creates a doubled-strand break with 3' overhangs, a feature beneficial for homologous recombination. Application of I-*Sce*I-induced double-strand breaks improved efficiencies by two orders of magnitude (Cohen-Tannoudji *et al*, 1998).

The next breakthrough was the combination of the two important functions within one engineered protein: a DNA-endonuclease domain, initially from a bacterial restriction enzyme *Fok*I, and a targeting domain for specific DNA sequences, a zinc finger motif. The latter was first described in the frog *Xenopus laevis* and the matching of zinc finger motifs to three nucleobases paired with the ability to combine multiple fingers to create a custom-made sequence-specific target domain promised precise cutting in total control of the experimenter (Pavletich & Pabo, 1991). Yet design and production of new zinc finger motifs was not routinely performed by individual molecular biology groups (Fernández *et al*, 2017).

An alternative tool soon arose based on DNA-binding motifs derived from a bacteria *Xanthomonas spp.* which injects transcription activator-like effector (TALE) proteins into plant host cells. Many naturally occurring TALE binding motifs have been discovered and, similar to zinc fingers, they can be combined to bind ever longer specific DNA sequences. Coupling them with the same nuclease domain *Fok*I created programmable nucleases termed TALE nucleases (TALENs). Various TALE sequences became readily available and could be arranged in sequence using standard cloning techniques such as restriction-ligation based protocols like the common Golden Gate cloning workflow (Bird *et al*, 2022). The availability of components

[6] Sequence taken from https://enzymefinder.neb.com/#!/isoschizomerByName/I-SceI#nebheader (accessed 07.10.2025)

and accessible workflows enabled many molecular biology labs to assemble expression plasmids locally resulting in fast and widespread adoption of TALENs to genetically modify cells (Fernández *et al*, 2017; Joung & Sander, 2013).

Easier to destroy than to repair correctly

Targeted gene replacement or insertion provided a strong incentive to invest in these technologies for the creation of novel therapeutic approaches in medicine or genetically modified organisms in agriculture. Simultaneously, introducing a targeted DNA mutation offered tremendous opportunity for basic research purposes to explore DNA sequence functions in a cellular context. For this purpose, often no templated repair via homologous recombination is needed, and rather alternative ways of DNA repair can be beneficial. One of these, termed non-homologous end joining (NHEJ) in juxtaposition to the aforementioned mechanism, is an error-prone repair of double-strand breaks that does not require a template (Chang *et al*, 2017). As such, NHEJ is generally available throughout the cell cycle whereas the homologous recombination repair machinery is restricted to the S and G2 phases of mitosis. Repair of double-strand breaks, especially when sticky ends (DNA single strand protrusions) are present, often leads to nucleotide insertions or deletions (INDELs). Based on the three-nucleotide (codon) based amino acid code any alteration of nucleotides not-divisible by three leads to a frameshift away from the original coding. Thus, the introduction of INDELs has 2 out of 3 chances not only to mutate a coding gene sequence, but outright eliminate it from being translated into the correct gene's protein. Therefore, the targeted induction of double-strand breaks is often used with the intentional goal of creating an effective knockout of a gene. While these perturbations have to be carefully validated and interpretations have to take alternative explanations into account (e.g. the creation of a truncated protein or an alternatively spliced version, instead of a knockout) the general concept of introducing double strand breaks to eliminate a specific gene's function and study the cellular effects soon became a common approach.

1.5.2 No need for translation, target identification using RNAs:

Yet apart from gene editing techniques another method provided the ability to prevent a specific gene's function which neither modified the DNA information nor required exogenous proteins to be introduced in the target cell. Like the aforementioned approaches, the technique is based on a mechanism existing in nature, specifically on the post-transcriptional inhibition machinery existing in eukaryotic cells relying on complementary single-stranded RNAs. Small-interfering RNAs (siRNAs) or miRNAs target complementary messenger RNA (mRNA) that otherwise would get translated into proteins. This process, termed RNA interference (RNAi), leads to hybridized double stranded RNA which is recognized by the RNA-induced silencing

complex (RISC). This results in translational repression or degradation of the RNA by Argonaute proteins and thus downregulation of the respective protein. Target lengths typically range between 19-27 bp with shorter sequences providing better results on average (Taxman *et al*, 2010) and the interfering RNA can either be introduced as double-stranded RNA via transfection into cells or as short hairpin RNAs (shRNA) on a vector to be transcribed within the cell. The latter is processed by the endogenous protein Dicer to produce a siRNA duplex for RNAi.

One of the benefits of RNAi is that it can efficiently target non-coding RNAs such as long-non-coding RNAs (lncRNAs), however, the suppression works primarily in the cytoplasm which may not affect non-coding RNAs remaining in the nucleus (Lucere *et al*, 2020). Another issue to be considered are off-target effects either based on the sheer number of cytoplasmic siRNAs after transfection or due to the relatively high sequence similarity, which can cause the unintended downregulation of multiple other transcripts (Taxman *et al*, 2010; Lucere *et al*, 2020). Like other knockdown methods certain functions may be hard to assess, compared to constitutive knockouts, as even trace amounts of proteins such as transcription factors (TF) or solute carriers (SLC) can be enough to maintain a wild-type phenotype.

Another benefit of RNAi is the usage of a widespread endogenous system, which means that it works readily in a wide variety of animal and cellular models once the interfering RNA component can be introduced into the respective cell. Relying only on siRNAs or shRNAs has advantages, even over more recent approaches such as CRISPR, as the shRNA cassette is a very small locus fitting into almost any vector and does not require expression of exogenous proteins (note that early CRISPR-Cas9 systems were also packaged onto a single lentiviral vector, however, the large size of ~10 kb meant straining the packaging capacity of the viral system and was often associated with low transduction rates) (Asmamaw Mengstie, 2022). Due to the small size and varieties of transfection or transduction possibilities RNAi remains a viable choice for tricky primary tissues and *in vivo* applications.

A third benefit of RNAi-based systems was the easiness to create individual knockdown constructs. Compared to zinc finger nucleases and TALENs no protein design is necessary as only a mere ~20 bp nucleotide sequence adapted to the specific target is needed. In combination with the advances in synthetic biology genome-wide targeting RNAi libraries could be synthesized and cloned in high throughput. This enabled large scale arrayed or pooled screens ushering in a new era of functional genomics based on perturbation screens focusing on the genome or transcriptome (Mohr *et al*, 2014).

1.5.3 A tool to rule, the CRISPR-Cas9 revolution:

The CRISPR (Clustered Regularly Interspaced Short Palindromic Repeats) Cas9 (CRISPR associated protein 9) system has revolutionized genetic research by making gene editing easily accessible and versatile. This mechanism naturally occurs in bacteria where it was discovered to provide an adaptive immune response to genetic threats such as bacteriophages. Both the mechanisms as well as the implications were groundbreaking and have changed the way prokaryotic defense mechanisms are viewed.

Like RNAi this approach relies on an interplay of a guiding RNA sequence and the function of proteins. The Cas9 protein can unwind and cut double-stranded DNA and is guided by two short RNAs, the first being the CRISPR RNA (crRNA) which contains a complementary sequence of about 20 base pairs to the genetic target and a hybridization domain. The latter allows it to pair with a trans-activating RNA (tracrRNA) which facilities binding with the Cas9 protein. Bacteria introduce viral DNA sequences from previous infections into their own genome in a regulated fashion (leading to the CRISPR acronym). These viral derived sequences, termed spacers, then get transcribed and serve as crRNA. This creates a simple yet versatile system where only the spacer part of the crRNA needs to be specific to the target, while the rest of the machinery can be used for multiple targets depending on which crRNA it pairs with at a time. One minor restriction of the targeting is the need of a protospacer-adjacent motif (PAM) next to the spacer-targeted site. The exact sequence varies for different Cas-proteins and for Cas9 the PAM is a three bases long sequence “NGG” directly downstream of the target site.

Jennifer Doudna and Emmanuel Charpentier were vital in the discovery of these mechanisms and their adaption to use it for genome engineering and were awarded the 2020 Nobel Prize in Chemistry. They and others, such as Georg Church and Feng Zhang, paved the way to utilize and adapt CRISPR to be used in eukaryotic cells (Cohen, 2021).

For genetic engineering purposes the crRNA and tracrRNA are often combined in a single guide RNA (gRNA) construct with the ability to self-hybridize and bind the Cas9 protein. This reduces cell engineering efforts to only two components, the gRNA and the Cas9 protein, both of which must be introduced into a eukaryotic cell. There are multiple ways in which those components can be inserted which boil down to the three main cellular information states: DNA, RNA and Protein.

A common approach is to encode gRNA and Cas9 on a vector plasmid after eukaryotic minimal promoters. After introduction of the DNA information into a cell the endogenous transcription and translation machinery will produce the necessary components which can self-assemble and in turn manipulate the host cell. Vectors can be transiently transfected into cells via

various means such as calcium phosphate, electroporation, cationic lipids or polymers. Alternatively the content can be added to the host cell's DNA via transduction by lentiviruses or retroviruses. Integration into the host's DNA offers constitutive active systems that are preserved over many cell divisions and thus offer genetic lineage tracing methods (Kebschull & Zador, 2018). Though the undirected nature of the DNA integration poses the risk of unintended disruption of the respective endogenous locus.

1.5.4 One system, many functions:

As mentioned above, the Cas9 protein essentially combines two functions, a helicase-like ability to unwind DNA at the target site and an endonuclease domain for DNA cutting. Mutation of the Cas9 protein led to a deactivated, endonuclease-dead version (dCas9) which remains capable of binding DNA based on the gRNA target though without inducing double-strand breaks. Targeting dCas9 towards a gene's promoter sequence can lead to diminished transcription due to Cas9 sterically occupying the spot other endogenous proteins need to bind to (Sapozhnikov & Szyf, 2021). Thus, this simple change led to a variation that instead of creating knockouts could be used to create knockdowns. Improvements were made to this approach termed CRISPR interference (CRISPRi) by fusing other proteins involved in transcriptional inhibition such as a KRAB domain to Cas9 (Gilbert *et al*, 2013). Of course, what can be tuned down, can also be cranked up. Fusing transcription activator domains like VP64 or VPR to Cas9 created a targeted transcriptional activator system termed CRISPR activation (CRISPRa) (Gilbert *et al*, 2013).

As such, CRISPR technology allows a tight control over a gene's mutations or it's respective transcriptional abundance. The latter wasn't restricted to tight promoter control of genes, but also allowed targeting of enhancer regions, opening up large parts of the genome to be interrogated for their contribution to a cell's properties (Chen *et al*, 2019; Hilton *et al*, 2015; Korkmaz *et al*, 2016). While artificial up or downregulation helps in understanding the potential of certain genes or genomic loci, coupling the system with epigenetic writers such as p300 (Hilton *et al*, 2015), DNMT (Vojta *et al*, 2016), and TET (Xu et al., 2016) promises ever more finetuned experimental setups to interrogate the causal contributions of epigenetic marks towards transcriptional control (Policarpi *et al*, 2024). Furthermore, CRISPR is used to change the location of chromatin within the nucleus by connecting a targeted locus to the nuclear lamina and recruiting other nuclear compartments (Wang *et al*, 2018), creating artificial chromatin loops (Hao *et al*, 2017) or establishing heterochromatin via targeted HP1α localization (Gao *et al*, 2021). Thus, this technology can be used to mechanistically address a variety of epigenetic layers implicated with transcriptional control.

Another line of CRISPR gene editing is the coupling of base-editors with dCas9 or Cas9 nickases. In the latter only one endonuclease motif is inactivated hence only one DNA strand gets cut while the other stays intact. In contrast to double-strand DNA cutting and relying on a cell's own DNA repair apparatus the goal is to introduce well defined and reliable point mutations. This got achieved by homing either cytidine (Komor *et al*, 2016) or adenine (Gaudelli *et al*, 2017) base-editors with the CRISPR system. A relatively recent addition is prime editing (Anzalone *et al*, 2019). In this method the DNA is nicked to create a single-strand break and a repair template is provided as part of the gRNA. A reverse transcriptase fused to Cas9 reads the RNA template and synthesizes a corrected DNA strand onto the originally nicked strand. Then a second cut on the opposing DNA strand favors the DNA repair incorporating the newly synthesized DNA piece in favor of the original sequence. Thus, very precise gene editing and DNA knock-ins are enabled with CRISPR editing technology.

1.5.5 Investigating specific loci

Coupling Cas9 with fluorescent proteins such as green fluorescent protein (GFP) allowed imaging analysis of genomic loci and their temporal dynamics such as telomeres in living cells (Chen *et al*, 2013). In order to amplify imaging signals many different strategies have been employed, whether by providing a protein chain able to recruit fluorescent proteins (Tanenbaum *et al*, 2014) or modification of the gRNA itself to be bound by RNA-binding proteins such as in the CRISPRainbow approach (Ma *et al*, 2016) or the modular Casilio imaging toolkit (Clow *et al*, 2022). Technological improvements allow even single gRNAs to create a reliably strong fluorescent signal for spatiotemporal imaging studies of genomic elements such as enhancers or promoters and allow the discrimination of different alleles (Maass *et al*, 2018). Taken together, the CRISPR technology enables the visualization of genomic loci and their dynamic patterns in living cells.

Another direction was the analysis of adjacent proteins and thus the uncovering of protein neighborhoods. These studies often incorporated the use of the biotin ligase BirA, a protein capable of adding biotin tags to proteins in the immediate vicinity which in turn allows the purification of biotin-labeled proteins via streptavidin pull-down. Analysis via mass-spectrometry readouts then identify the local protein neighborhoods targeted by the CRISPR system. This was applied in proof-of-concept studies on genomic loci such as telomeres by biotin labeling of Cas9 (Liu *et al*, 2017), or with coupling of Cas9 with BirA (Schmidtmann *et al*, 2016) and similar biotin-tagging proteins such as Apex2 (Gao *et al*, 2018) to investigate telomeres and centromeres. Thus, CRISPR technology can additionally be used to define and interrogate local proteome neighborhoods.

1.5.6 Large, pooled screen

Besides the incredible breath of precise perturbations that can be introduced into cells due to CRISPR based systems another important feature is scale. Irrespective of the intended manipulation the targeting mechanism of Cas9 to specific genetic loci is determined by a short span of around 20 nucleotides which sit in a separate small RNA. This feature allows the application of all the tools established to clone shRNAs and introduce them into cells to the CRISPR system. As such, large pools of oligos, targeting every human gene multiple times, can be readily synthesized and cloned into gRNA plasmid backbones. From there, the library pool can be amplified in bacterial colonies and subsequently transfected into viral packaging cells. The so produced viral library contains viral particles, each carrying only one gRNA vector. This viral library can then be used to transfect target cells. By adjusting the right ratio of viral particles to target cells the latter will mainly be transduced with one viral particle per cell, which in effect introduces one genetic perturbation per cell in an uncomplicated way. In this context the terminology of microbiology is used where the ratio of viral particles to cells is termed the multiplicity of infection (MOI). Assuming that both viral particles and target cells are homogeneous populations, where each agent or target has an equal probability of successful transduction, the necessary concentration of each can be easily derived to allow a majority of cells transduced with only one gRNA. The probability that a cell will be transduced with none, one or multiple gRNAs follows a Poisson's distribution and can be calculated as follows:

$$P(n) = \frac{m^n * e^{-m}}{n!}$$

Equation 1

Where P is the probability that a cell will get n amounts of viral vectors/gRNAs given the MOI m.

For amplification-based screens a general recommendation is to use an MOI around 0.3 to gain single transduced cells (Bock *et al*, 2022; Joung *et al*, 2017). In situations where cell numbers are limited or transduction rate is difficult to control for such as in *in vivo* screens multiple transduction events can be tolerated and complications mitigated by introducing unique molecular identifiers (UMIs) such as the iBAR gRNA design (Zhu *et al*, 2019). In cases where the general assumption is that most gRNAs will not introduce phenotypical perturbations (i.e. perturbations that become apparent at the time of the readout) improved analytical strategies can increase the power to detect meaningful effects (Gasperini *et al*, 2019). Furthermore, combinatorial effects of gRNAs could be studied by introducing multiple different perturbations into a single cell. While this can be controlled by raising the MOI multiple other

strategies, such as simultaneous introduction of two vectors (Mali *et al*, 2013) or special constructs transducing two (Replogle *et al*, 2020; Tang *et al*, 2022) or more gRNAs via the same vector (Xie *et al*, 2015; Zhou *et al*, 2021), promise a better experimental control. This ease of manipulating the entire genome in a pooled fashion enables high-throughput identification of genes of interests for particular biological questions.

1.5.7 Selection of adequate readout

Pooled CRISPR amplicon readout-based screens are either performed as positive selection screens, in which the phenotype of interest is actively enriched and selected for, or a negative selection screen (dropout), where the interesting hits are depleted from the overall pool. In the former a selective pressure, for example a drug leading to a stop in cell proliferation, would allow only successfully perturbed cells of certain genes to continue proliferating. For these types of screens a lower coverage per target is needed, given the expectation that only a minority of cells will persist in meaningful numbers at the termination of the experiment. In contrast, a dropout screen assumes that unperturbed cells survive, and only specifically perturbed cells cannot cope with the adverse selective pressure. Hence, a larger coverage of each target is needed to ascertain which hits reliably dropped out, i.e. do not persist at the termination of the screen.

Another common selective pressure is fluorescence-activated cell sorting (FACS) based on a specific marker expression. However, given the throughput of genome-wide screens these methods can get time intensive. An interesting example of an alternative readout applied to macrophage phagocytosis relied on magnetic separation of cells based on their capability to engulf magnetic particles (Haney *et al*, 2018). Careful planning is required to find a readout suitable to the research question at hand, especially, when the readout is limited to a single property such as proliferation or marker gene expression. The advent of high-throughput single cell technologies with a simultaneous readout of multiple markers up to encompassing "-ome" wide technologies such as single cell transcriptome sequencing promise a more unbiased readout capable of assessing a diverse range of phenotypes within a single experiment.

1.6 Single cell technology

1.6.1 How it works

Single cell readouts promise to assess each cell individually on a multitude of features. Traditional high-throughput screening approaches often relied on cell morphology or antibody staining followed by Fluorescent Activated Cell Sorting (FACS), which allows the separation of cells

based on one or a few parameters into separate wells. In a study of innate immune cell activation by LPS the perturbed cells were sorted for low and high TNF expression, thus separating two different classes of TNF regulators depending on their knockout effect (Parnas *et al*, 2015). While relatively easy to implement, the number of parameters to be analyzed does not scale as well as other methods (though combination with more sophisticated downstream methods is possible). The number of parameters is depended on the labelling mechanism. Besides fluorescence labelling and separation can rely on different properties such as magnetic separation that may offer a higher degree of parameters to be differentiated (Reisbeck *et al*, 2016).

Alternatively, imaging-based approaches offer data-rich readouts. Yet in the context of perturbation screens, it is technically more challenging to assess which genetic perturbation resulted in the observed phenotype. While gRNAs can be cloned separately and the screen can be conducted in an arrayed format, this shifts the logistic investment without reaping the benefits from pooled screening approaches. In the latter case, staining gRNAs with fluorescence in situ hybridization (FISH) is a common option (Emanuel *et al*, 2017; Lawson *et al*, 2017). Successful methods of image based screens include an arrayed, image-based screen of nearly 1500 genes investigating their impact on the nuclear pore complex formation and localization (De Groot *et al*, 2018); a pooled, genome-wide screen combining image based identification of phenotypes of interest with subsequent sorting and sequencing of the genetic perturbations (Kanfer *et al*, 2021); and similarly, such a strategy can exploit different photoactivation times and photoactivatable fluorescent proteins to differentiate multiple phenotypes of interest (Yan *et al*, 2021). Taken together, high-throughput, image-based screens offer readouts of various properties including the spatial location of the cell, its neighbors, and the subcellular localizations of various organelles or molecular components.

Sequences suffice

Recent advantages in single cell sequencing such as single cell RNA-sequencing (scRNA-seq) enable the readout of the expression level of thousands of genes per cell. Widely used (commercial) solutions allow the analysis of thousands of cells per reaction in a relatively simple and straightforward way (Mereu *et al*, 2020).

In early droplet-based sequencing methods like Drop-seq (Macosko *et al*, 2015) and inDrop (Klein *et al*, 2015) a single cell was encapsulated together with a bead containing adapters/primers within a liquid droplet in an oil emulsion. Within this liquid compartment (each droplet can be considered a single reaction well) cell lysis occurs and mRNA is captured by oligo-dT adaptors on the bead. The captured mRNA can then be reverse transcribed where additionally a unique molecular identifier (UMI) and cell barcode sequence is included. This way each

mRNA molecule receives both an individual barcode to reduce technical noise and an identifier to assign it to one individual cell. The capture with oligo-dT adaptors allows easy hybridization of the mRNA content of a cell and avoids undesired amplification of other abundant cellular RNAs such as ribosomal RNAs (highest abundance in human transcriptome) or tRNAs (highest molar level in human transcriptome) (Palazzo & Lee, 2015).

While an mRNA-based readout provides an unprecedented, multi-faceted snapshot of a cell's behavior it would present an excessive analytical challenge to use scRNA-seq for pooled perturbation screens without a way to assert what gene got compromised in each respective cell. There are multiple ways to gather this piece of information. For genetic knockout screens it would be conceivable to read out enough of the transcriptome via long-read sequencing to assess the actual genetic deficit each cell received. This approach promises accurateness in excluding cells that have not undergone the expected gene cutting or repaired it in a way that may result in a silent mutation or minor impact on the respective gene function. Furthermore, the data depth could allow to draw conclusions about the specific types of genetic perturbation that the repair machinery resulted in. It is conceivable that certain outcomes of a single gRNA targeting a gene could have different functional impacts. A mutation could lead to the complete loss of the protein due to nonsense-mediated mRNA decay, destroy a catalytic site, or block a protein-protein binding site. The latter two options may disable different sub-functions of a gene's impact on the cellular behavior. However, while these insights might be informative, they either require large numbers of cells to gain confidence in the data or careful follow up experiments for interesting cases.

In most common approaches of scRNA-seq readouts for perturbation screens a cells knockout is inferred by knowing which gRNA is present in the cell. However, neither artificial gRNAs nor the individual components of the bacterial system (tracrRNA and crRNA) contain poly-A tails and thus were not captured by early droplet-based sequencing technologies. To enable the assignment the first CRISPR coupled single-cell screens read out a barcode introduced together with the gRNA (Adamson *et al*, 2016; Dixit *et al*, 2016; Jaitin *et al*, 2016; Xie *et al*, 2017). However, this method is both technically cumbersome and introduces a potential source of error due to recombination events mixing up barcodes and gRNAs in pooled cloning approaches (Hill *et al*, 2018).

At the start of this thesis project, we explored a different approach. By changing the location of the gRNA expression locus into the 3' long terminal repeat (LTR) region of a lentiviral vector the same region would be transcribed in two different ways. One, started by human U6, a Type III RNA-polymerase promoter which results in the typical gRNA directing the Cas9 protein to the target site. Further upstream, a second promoter, EF-1a, recruits a type II polymer-

ase and enables the expression of proteins such as an antibiotic resistance gene. Interestingly, the resulting mRNA extends into the 3' LTR. Thereby, the whole gRNA locus is transcribed as well into a polyadenylated mRNA and this transcript could be captured by classic poly-T adaptors. This method, which we published as CROP-seq (Datlinger *et al*, 2017), allows straightforward cloning of the gRNA pool and avoids the risk of recombination events leading to incorrect gRNA assignments.

Further improvements

Since then, the field of single cell sequencing has made, and continues to make, great technological leaps. Commercialization of droplet-based approaches improved the numbers of cells that could be analyzed and drastically increased robustness of the workflow (e.g. 10x Genomics) (Zheng *et al*, 2017).

Besides overall improvements, new modalities can be sequenced often in conjunction with the matching transcriptome of the same single cell. These include for example protein information via staining of cell-surface receptors (Peterson *et al*, 2017; Stoeckius *et al*, 2017), internal proteins (Gerlach *et al*, 2019; Reimegård *et al*, 2021; Rivello *et al*, 2021), TCR or BCR variable regions (Azizi *et al*, 2018; Neal *et al*, 2018), or epigenetic information (Angermueller *et al*, 2016; Hou *et al*, 2016; Hu *et al*, 2016).

The concept to read out gRNA transcripts directly was taken further and methods established to directly capture the actual polymerase type III transcribed gRNA via the introduction of a specific capture sequence for 3' based sequencing methods (Replogle *et al*, 2020) and via gRNA backbone specific reverse transcription primers in combination with 5' sequencing (Mimitou *et al*, 2019; Replogle *et al*, 2020). In our experience, the switch from 3' capture to 5' capture improved the UMI count of gRNAs 10-100-fold, allowing better discrimination of true signal to noise.

Quality in, quality out

With the improvement of single cell sequencing readouts enabling more complex setups another consideration concerns the transduction and editing efficiency affecting the quality of each cell and overall "usability" for the planned analysis. Cells that do not contain gRNAs can reliably be excluded either via antibiotic treatment (in case the gRNA containing vector includes resistance to the antibiotic) or via exclusion FACS sorting (for a co-transduced fluorescent marker gene). A trickier aspect, however, are cells that contain multiple gRNAs. Apart from specialized research questions, combinations of knockouts are often avoided. Combined effects of multiple knockouts can lead to a number explosion of cells needed to be analyzed to gain statistical significance and thus trust in the conclusions, whereas to identify singular knockout effects it is prudent to minimize the number of double strand breaks per cell. For the

transduction of amplicon screens an MOI around 0.3 (Bock *et al*, 2022; Joung *et al*, 2017) is recommended, whereas for single cell screens an MOI of 0.1 is often used to further reduce the chance of cells transduced with more than 1 gRNA. At this MOI the theoretical probability that a cell is infected with 1 gRNA is ~9%, and the probability that a cell is infected with 2 or more gRNAs is ~0.5% (see Equation 1). Thus, by first selecting for cells that contain gRNAs and only using those as input to a single cell screen, we can expect that ~5% of the resulting cells will be infected by multiple gRNAs.

1.6.2 Assumptions and considerations

While these numbers are easy to calculate and can be reasonably well dialed in, they work with the underlying assumption that all cells in culture have the same transduction rate. The more heterogeneous the cell population at the time of transduction is, the more care needs to be taken that this assumption is reasonably satisfied. Dilution curves with subsequent FACS or qPCR/droplet PCR-based quantification of overall transduction efficiency can serve as a valuable preliminary experiment. Otherwise, once the technical aspect of gRNA assignment is optimized, a small-scale single cell screening experiment can empirically reveal how the distribution of gRNAs in the respective cell line looks at a certain point of the experiment.

However, having a gRNA within a cell does not guarantee a perturbation of the cell. gRNA mediated knockouts generally work via the induction of double strand breaks. These get repaired by the cell's repair machinery and often lead to frameshifts, generally eliminating the function of the protein (see section *Double-strand breaks and targeted genome editing*). Nevertheless, the chance is given that either no frameshift occurs or if the gRNA is placed on the beginning or end of a gene that a truncated version is created which may continue most of the original protein's function. These issues are considered with better prediction algorithms creating gRNA sequences, such as the VBCscore (Michlits *et al*, 2020) which preferentially aims to cut hydrophobic sequences. This ensures, that in absence of a frameshift event, the codon for a hydrophobic amino acid is mutated to a different sequence. This often results in hydrophilic amino acids which in turn decrease protein stability and have a higher chance to disrupt protein structure and hence function all together.

The alternative to avoid dependency on DNA-damage repair are CRISPRi screens which can lead to very low levels of expression comparable to knockout screens (Sanson *et al*, 2018) in a more uniform way amongst target cells. Generally though, the best target site to downregulate a gene's expression is harder to predict, which either requires more cells to be screened with various gRNAs, or multiple gRNAs targeting the same promoter of a gene need to be introduced via more complex gRNA vectors within the same cell (hit the same gene locus at multiple sites simultaneously). Furthermore, a knockdown of certain proteins might not be

enough to ascertain the function, such as can often be seen with transcription factors or solute carrier proteins where even a relatively small number of correct proteins per cell can maintain basic functions or where redundancy in function exists between proteins (Hoja *et al*, 2016; Trescher & Leser, 2019).

Apart from methods addressing the experimental side, there are analytical strategies to mitigate the effect of unperturbed cells creating noise. One such strategy is Mixscape (Papalexi *et al*, 2021) which determines for each gRNA assigned cell how different it is to the neighboring cells containing non-targeting control gRNAs. In this way it calculates a perturbation score for each cell allowing the binary discrimination into perturbed and non-perturbed cells. Thereafter, downstream analysis can be done only on classified perturbed cells and thus result in cleaner signals. However, this is a method of post-hoc removal of cells that have already been paid for, meaning money was spent that could have otherwise contributed to greater insights by prior experimental reduction of "unperturbed cells". Furthermore, as we show in our paper ((Traxler *et al*, 2025), see results section) for *Csf1r* and *Fcgr1* a genetic perturbation can still lead to the respective protein knockout (CD115 and CD64 respectively) yet without any functional consequence for the cell in the particular context. A more in depth look at "un-/perturbed" is taken in the discussion. While financial constrains must be kept in mind, the first genome-wide screens have been performed by homing in on expressed genes within the respective cell line (Replogle *et al*, 2022). Furthermore, the field rapidly evolves, and technological improvements promise the analysis of millions of cells per sample with relative ease (Brown *et al*, 2024; Clark *et al*, 2023; Datlinger *et al*, 2021).

1.6.3 General considerations for setting up a screen:

Setting up a screen can be broken down into the following components:

a) Cell handling: how well can a near homogeneous population of cells be kept (i.e. maintain equal chance for each cell).
b) Gene editing: how to achieve a high perturbation rate while avoiding doublets (i.e. one cell contains only one perturbation).
c) Selection: how to select for high quality, single cells (i.e. be as cost/resource efficient as possible)
d) Controls: careful thought about the amount and types of positive and negative controls
e) Screen depth vs width: how many gRNAs/cells per perturbation target gene/locus
f) Sequencing depth: how much information to recover per cell

g) Type of readout: which workflows are robustly established and add valuable data, which are experimental and provide novel perspectives: e.g. transcriptome, cell-surface proteome, chromatin accessibility, DNA sequence.

The considerations for a-c) can and are often experimentally optimized beforehand and remain useful for validation experiments after a successful screen. Note should be taken to choose a timepoint early on when transcriptomic changes for the studied effect/function are starting or are fully activated. Consequently, effects like cell death or other strong stresses have not been initiated and thus high-quality transcriptomes can be expected for each perturbed cell (compared to classic amplicon screens often requiring changes in cell number induced by the “selective pressure” aimed for in the setup).

Regarding point d) about controls, a classic negative control often used are non-targeting gRNAs. These are of the same length as their homing equivalent but with a sequence not found in the genome of the cell of interest. As concerns arose, around the lack of perturbation stress (e.g. double-strand breaks and subsequent DNA repair mechanisms) some opt to target safe-harbor loci, regions of the genome expected to lead to no biological effects in the experimental model. Examples are Y-chromosomal genes and olfactory receptors (Gilbert *et al*, 2014) or regions without annotated functions (Morgens *et al*, 2017). Either way it is important to remain vigilant regarding the type of assumptions underlying each choice.

Positive controls are more elusive in single-cell screening contexts. Essential gene perturbations, as have often been used in amplicon-based screens (Wang *et al*, 2015), are mostly unsuitable as they either will not present in sufficient depth in the readout or otherwise, may be considered as a failed control. However, in most cases certain genes are already known in the field to lead to specific transcriptomic changes without drastically affecting the number of cells in the given time frame (e.g. JAK-STAT members in immune response experiments). When combining transcriptome with cell-surface protein readout we found it useful to perturb some of the proteins included in the antibody panel to look for the respective change in the target’s cell-surface availability, irrespective of more widespread cellular changes.

Question e) about how many cells are needed per target is the most challenging to answer as it depends on the efficiency of many different steps. Furthermore, any effects not observed may be due to insufficient sensitivity. Thus, conclusions about observed perturbation effects are more robust than extrapolations based on a lack of observed effects of a given target. To establish a screen in a new cellular model without any reasonable (screening) single cell data a useful recommendation is to perform a small preliminary screen with the most valuable controls and many different conditions. To keep costs low, cell hashing can help to test multiple

workflows in a single sequencing “sample” (e.g. a single 10x reaction containing multiple cell-samples labeled with a different oligo nucleotide specific to that cell sample).

Point f) is the sequencing depth and related to e), often a shallow depth can be used to identify the strongest hits for future follow up. However, deeper sequencing of each cell may make the dataset more interesting as subtle changes in transcriptome may be revealed in far more perturbations. Thus, both increasing cells-per-target and depth-per-cell can aid in characterizing target effects. A rule-of-thumb recommendation we utilized for the results discussed below and similar studies was to aim for 100 cells post quality control per target gene (e.g. 4x gRNAs for every 25 cells hitting the same gene). These numbers provide a momentary recommendation and are expected to change favorably in the near future with improvements in all areas contributing towards performance.

Lastly, point g) addresses the types of information gathered to ascertain gene perturbation effects. Transcriptome sequencing became more and more robust and commercial protocols exist to combine it with cell-surface protein analysis and VDJ recombination status. Similarly, modalities such as intracellular protein (Gerlach *et al*, 2019; Mimitou *et al*, 2021; Reimegård *et al*, 2021) or chromatin accessibility (De Rop *et al*, 2024) have been demonstrated to work as well. At the time of writing, they may require more experimental expertise to set up, yet are expected to benefit similarly from optimization efforts.

1.7 Aims of this thesis:

The focus of this thesis project was on optimizing, applying, and evaluating state of the art technologies in CRISPR perturbation and single cell sequencing methods.

1.7.1 Aim I: Optimization and application of pooled CRISPR perturbation screens with combined single-cell transcriptome and CITE-seq read out in a macrophage model

From the onset of this thesis the ability to perform functional CRISPR perturbation screens was a major technical goal to first achieve (soon realized with the author's contribution to (Datlinger *et al*, 2017)) and further optimize and upgrade with the ever-growing technological advancements of the field. A stated milestone of this thesis was to achieve a robust workflow applying CROP-seq with combined single cell transcriptome and CITE-seq readout to a biological question of macrophage biology.

1.7.2 Aim II: Analysis of dynamic epigenetic potential and relative transcriptional abundance in macrophage activation elicited by diverse immunological stimuli

Macrophages and the innate immune response have served as a valuable model of stimulus-driven transcriptional response with remarkable insights to the interplay of various epigenetic mechanisms such as CpG island methylation and dynamic histone marks (Ramirez-Carrozzi *et al*, 2009). Aim II of our study was to add to the growing list of generated systems data by establishing a high-quality dataset of transcriptome and chromatin accessibility from a single experiment of *in vitro* differentiated macrophages in response to a broad range of immunological stimuli and provide an integrated analysis of both data modalities.

1.7.3 Aim III: Characterization of key transcriptional regulators of macrophage homeostasis and immune response by combining descriptive and functional approaches

Transcriptional regulators and especially epigenetic modifiers provide a promising leverage point in various disease settings. Hence, Aim III of this study was to characterize a broad range of transcriptional regulators by combining multimodal descriptive and functional methods to investigate their contribution to homeostasis and selected time points of macrophage response to a complex immune stimulus.

CHAPTER TWO: Results

2.1 Prologue

In order to accomplish the outlined aims of this thesis project we adapted the CROP-seq method (Datlinger *et al*, 2017), in essence a pooled CRISPR knockout screen combined with single cell RNA-seq readout. It relies on a lentiviral delivery vector for gRNAs expressing a continuous mRNA transcript which encodes the gRNA sequence itself into the polyadenylated RNA making a direct readout with common 3'-based single-cell readouts possible.

After this first version, various optimizations were tried to increase the perturbation properties and efficiencies of the CRISPR-Cas9 system and the single cell read out performance, in particular, the ability to assign single guide RNAs per each cell robustly. Incorporating major advancements in the field (specifically highlighted here are three works: Direct-seq (Replogle *et al*, 2020), CITE-seq (Stoeckius *et al*, 2017) and Mixscape (Papalexi *et al*, 2021)) enabled us to reach the milestone stated in **Aim I**, a robust workflow with combined transcriptome and cell surface protein read out.

Combining this method with our expertise in executing complex *in vitro* assays with next generation sequencing workflows we chose to apply and combine multimodal readouts to assess epigenetic potential (Krausgruber *et al*, 2020) in a dynamic setting and perform integrated analysis to better understand the interplay and fulfill **Aim II**. We chose the relatively established innate immune response in macrophages due to the ability to apply methods both in cell lines, *ex vivo* differentiating and differentiated cells, and enable future work in already established constitutively Cas9-expressing mouse models (Chu *et al*, 2016; Platt *et al*, 2014). Working with macrophages allowed us to compare and benchmark our results on a technical level with excellent works in dendritic cells such as (Dixit *et al*, 2016; Jaitin *et al*, 2016), while providing novel biological insights with potentially broad therapeutic implications.

Specifically, in line with **Aim III,** we chose transcriptional regulators with a heavy focus on epigenetic modifiers for the screen, as these were implicated to be involved in a majority of transcriptional regulatory processes. Furthermore, compared to transcription factors, they are generally seen as "druggable" (Ganesan *et al*, 2019), that is, amenable to therapeutic intervention with small molecule drugs. As such, this study was conducted to provide a robust single-cell perturbation screen protocol, high-quality multimodal data, an integrated analysis workflow and novel biological insights.

These three aims culminated in the publication ((Traxler *et al*, 2025), included below), where we generated a dense time series of macrophage response to 6 selected immune stimulants

with bulk RNA-seq and ATAC-seq readout within the same experiment. The resulting data was ideally suited for integrated analysis of both modalities, revealing dynamic response regulons. We followed up the most complex of our immune stimulants , treatment with live *Listeria monocytogenes*, and applied genetic perturbation screening to investigate the contribution to transcriptional regulation of over a hundred target genes. Ultimately, we described novel transcriptional regulators and mapped their function back to the newly identified response regulons.

2.1.1 PDF of the paper: Integrated time-series analysis and high-content CRISPR screening delineate the dynamics of macrophage immune regulation

The PDF version of this article is reprinted from the journal Cell Systems where it is published under the Creative Commons CC-BY license[7] which permits reuse of the article[8]. Supplementary information is available on https://www.cell.com/cell-systems/fulltext/S2405-4712(25)00179-6#supplementary-material.

[7] Creative Commons Attribution 4.0 International, https://creativecommons.org/licenses/by/4.0/ (accessed 09.09.2025)

[8] CCC RightsLink, https://s100.copyright.com/AppDispatchServlet?publisherName=ELS&contentID=S2405471225001796&orderBeanReset=true&orderSource=Phoenix (accessed 09.09.2025)

Cell Systems

Integrated time-series analysis and high-content CRISPR screening delineate the dynamics of macrophage immune regulation

Graphical abstract

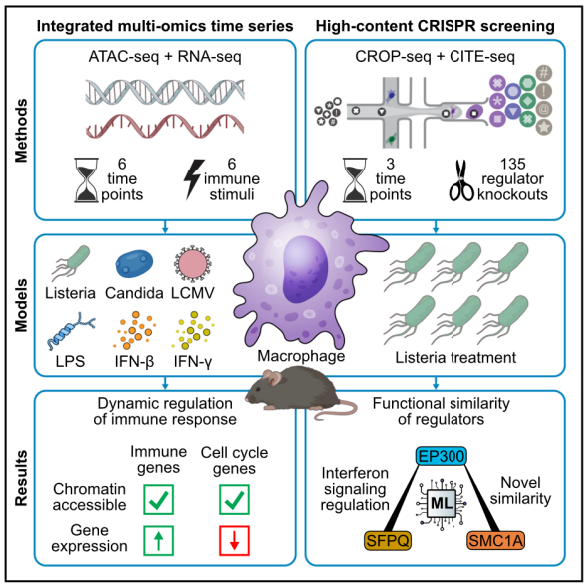

Authors

Peter Traxler, Stephan Reichl, Lukas Folkman, ..., Thomas Decker, Matthias Farlik, Christoph Bock

Correspondence

cbock@cemm.oeaw.ac.at

In brief

Traxler, Reichl, et al. combine multi-omics time series with high-content CRISPR screens to identify regulators of macrophage immune responses and map their functional similarities. This study reveals how innate immune cells adapt their regulatory states upon acute challenges, and it provides a blueprint for delineating regulatory dynamics in other contexts.

Highlights

- Transcriptome and chromatin dynamics in macrophages responding to six immune stimuli
- Epigenetic potential and transcriptional abundance foster rapid regulatory responses
- High-content CRISPR screens identify regulatory roles of SPI1, EP300, and JAK-STAT
- Machine learning establishes functional similarity graphs of regulators via regulons

Traxler et al., 2025, Cell Systems *16*, 101346
August 20, 2025
https://doi.org/10.1016/j.cels.2025.101346

CellPress

Cell Systems

CellPress
OPEN ACCESS

Methods

Integrated time-series analysis and high-content CRISPR screening delineate the dynamics of macrophage immune regulation

Peter Traxler,[1,2,10] Stephan Reichl,[1,3,10] Lukas Folkman,[1,3,4,5] Lisa Shaw,[2] Victoria Fife,[1] Amelie Nemc,[1] Djurdja Pasajlic,[2] Anna Kusienicka,[2] Daniele Barreca,[1] Nikolaus Fortelny,[1,7] André F. Rendeiro,[1] Florian Halbritter,[1,6] Wolfgang Weninger,[2] Thomas Decker,[8,9] Matthias Farlik,[1,2,11] and Christoph Bock[1,3,11,12,*]

[1]CeMM Research Center for Molecular Medicine of the Austrian Academy of Sciences, Vienna, Austria
[2]Medical University of Vienna, Department of Dermatology, Vienna, Austria
[3]Medical University of Vienna, Institute of Artificial Intelligence, Center for Medical Data Science, Vienna, Austria
[4]Southern Cross University, Faculty of Science and Engineering, Gold Coast, Australia
[5]Griffith University, Coastal and Marine Research Centre, Gold Coast, Australia
[6]St. Anna Children's Cancer Research Institute (CCRI), Vienna, Austria
[7]Center for Tumor Biology and Immunology, Department of Biosciences and Medical Biology, University of Salzburg, Salzburg, Austria
[8]Max Perutz Labs, Vienna Biocenter Campus, Vienna, Austria
[9]University of Vienna, Center for Molecular Biology, Department of Microbiology, Immunobiology and Genetics, Vienna, Austria
[10]These authors contributed equally
[11]Senior author
[12]Lead contact
*Correspondence: cbock@cemm.oeaw.ac.at
https://doi.org/10.1016/j.cels.2025.101346

SUMMARY

Macrophages are innate immune cells involved in host defense. Dissecting the regulatory landscape that enables their swift and specific response to pathogens, we performed time-series analysis of gene expression and chromatin accessibility in murine macrophages exposed to various immune stimuli, and we functionally evaluated gene knockouts at scale using a combined CROP-seq and CITE-seq assay. We identified new roles of transcription regulators such as *Spi1*/PU.1 and JAK-STAT pathway members in immune cell homeostasis and response to pathogens. Macrophage activity was modulated by splicing proteins SFPQ and SF3B1, histone acetyltransferase EP300, cohesin subunit SMC1A, and mediator complex proteins MED8 and MED14. We further observed crosstalk among immune signaling pathways and identified molecular drivers of pathogen-induced dynamics. In summary, this study establishes a time-resolved regulatory map of pathogen response in macrophages, and it describes a broadly applicable method for dissecting immune-regulatory programs through integrative time-series analysis and high-content CRISPR screening. A record of this paper's transparent peer review process is included in the supplemental information.

INTRODUCTION

Innate immunity is critical for protecting the body against pathogens. Macrophages are among the first immune cells to respond to invading pathogens, which they sense via pattern recognition receptors.[1] Detection of pathogen-associated molecular patterns (PAMPs) activates signaling cascades and transcriptional regulators such as NF-κB, IRF, and AP-1. These regulatory proteins orchestrate expression of their target genes over the course of the pathogen response and during the subsequent return to homeostasis. Co-expressed target genes are often referred to as "regulons" and constitute key components of the pathogen response in macrophages and other immune cells.

Type I interferons (IFN-I), especially IFN-β, are mediators of the early innate immune response that is triggered by pattern recognition receptors. These interferons are produced by macrophages in response to pathogen encounter, and the secreted interferons are sensed by interferon alpha receptors (IFNARs) in an autocrine and paracrine manner, resulting in activation of the JAK-STAT pathway. STAT transcription factors then induce rapid upregulation of the well-known group of interferon-stimulated genes (ISGs), which have many biological roles, including host defense and pathogen clearance.[2] In parallel, secreted IFN-I establishes an antiviral state in surrounding cells and promotes inflammation together with additional secreted cytokines, which further contributes to effective pathogen control.[3,4]

This innate immune response is widely studied as a model for signal-induced and context-dependent gene regulation, which includes dynamic and combinatorial effects of transcription

factors,[5–8] histone modifications and chromatin accessibility,[5,9–12] Pol II pausing and elongation,[10,13] higher-order chromatin confirmation changes,[14] and mRNA splicing and degradation.[6,15] The transcriptional dynamics in immune-challenged macrophages include activation of primary response genes, which are predisposed for activation and are rapidly upregulated upon stimulation, and of secondary response genes, which require preceding protein synthesis in order to be transcribed at high levels.[5,13,16]

Utilizing genetically encoded pathogen recognition and signaling, innate immune cells can induce pathogen-specific transcriptional responses.[1] Several studies investigated timelines of the transcriptional response to infection signals such as PAMPs and cytokines, both in macrophages and in dendritic cells,[6,9,17–19] and they mapped the associated changes in the chromatin and the epigenome.[5,7,10,20] To further dissect the regulatory landscape of the macrophage pathogen response, here we combined dense time-series analyses of transcription and chromatin accessibility with systematic genetic perturbation of putative immune regulators through high-content CRISPR screens.[21]

Specifically, we analyzed multi-omics time series of murine macrophages that we exposed to pathogens and infection-linked stimuli, and we evaluated perturbations of key regulators using the CROP-seq method for high-content CRISPR screening[22] (Figure 1A). Macrophages were treated with infectious bacteria (*Listeria monocytogenes*, *Listeria*), viruses (lymphocytic choriomeningitis virus, LCMV), UV-irradiated fungi (*Candida albicans*, *Candida*), bacteria-associated PAMPs (lipopolysaccharide, LPS), and interferons (IFN-β and IFN-γ), and we profiled gene expression by RNA sequencing (RNA-seq) and chromatin accessibility by ATAC-seq for six time points per stimulus over the first 24 h following stimulation. We performed integrative analysis of all data and identified both pathogen-specific and shared regulons involved in the response to the six stimuli. Finally, we functionally characterized the identified regulons in the response to *Listeria* treatment using CRISPR perturbation screens with single-cell RNA-seq readout.

In summary, we devised a high-throughput approach for dissecting immune regulation and applied it to macrophages that we exposed to pathogens and infection-linked stimuli. We observed important roles of transcription regulators such as *Ep300*, *Sfpq*, *Sf3b1*, *Smc1a*, and members of the mediator complex, and we established a time-resolved and perturbation-validated map of the regulatory programs that underlie the macrophage response to *Listeria*.

RESULTS

Time-series profiling uncovers dynamic transcriptome and chromatin landscapes in response to six stimuli

To chart the immune-regulatory landscape of macrophages, we exposed primary bone-marrow-derived macrophages (BMDMs) to six immune stimuli, including infectious pathogens, pathogen-derived stimuli, and pro-inflammatory cytokines. We established dense time series of gene expression (by RNA-seq[23]) and chromatin accessibility (by ATAC-seq[24,25]) with time points at 0, 2, 4, 6, 8, and 24 h to resolve the gene-regulatory dynamics of both the primary and secondary responses triggered by each stimulus (Figure 1A).

The signaling properties of these six immune stimuli are well established and reflect a broad spectrum of the regulatory processes involved in the macrophage response to pathogens. *Listeria* is sensed by toll-like receptor 2 (TLR2) and intracellularly by cytosolic Nod-like receptors and the DNA sensor cGas, which signals via STING.[26] LCMV induces intracellular signaling by the RNA sensors RIG-I and MDA5.[27] *Candida* is sensed mainly by Dectin-2[28] and by certain toll-like receptors (TLRs). LPS, a key component in the bacterial membrane of gram-negative bacteria, is detected by TLR4, and the signal transduction is mediated by the MyD88 and TRIF pathways.[29] Interferons are sensed by specific interferon receptors and signal via STAT1-STAT2-IRF9 complexes (which are dominant for IFN-I, including IFN-β) and via STAT1-STAT1 homodimers (which are dominant for the type II interferon IFN-γ).[30]

We generated RNA-seq and ATAC-seq profiles for 31 conditions (5 post-treatment time points for each of the 6 stimuli, plus untreated cells as a shared control), with two biological replicates for each condition. The data quality was high across all samples (Tables S1 and S2). Genes and genomic regions known to be activated by the immune stimuli showed the expected responses. For example, the *Cd69* locus displayed increased chromatin accessibility and gene expression in response to *Listeria*, LPS, and interferons (Figure 1B), while *Candida* caused increased chromatin accessibility and gene expression for *Prdm1* (at 2 h) but not for *CD69* (Figure S1). Genome browser tracks for all genes are provided on the supplementary website (http://macrophage-regulation.bocklab.org).

To assess the time-series dynamics of macrophages responding to each of the six stimuli, we performed unsupervised dimensionality reduction separately for the RNA-seq and ATAC-seq profiles (Figures 1C and S2A). Two main trajectories emerged, which were consistent across the two modalities. Starting from untreated macrophages, the first trajectory was characterized by a pronounced interferon response, while the second trajectory was linked to pathogens. IFN-β and IFN-γ treatment resulted in transcriptional changes that were similar at the 2-h time point (Figure 1C) but later diverged (in particular in the ATAC-seq data), indicating partially distinct regulatory programs. The pathogen trajectory showed a more gradual pattern with the most pronounced effects after 4 to 6 h of stimulation by *Listeria* or LPS. For LCMV, we observed a clear response only at the 24-h time point, which followed the pathogen trajectory with a delay compared with *Listeria* and LPS. Finally, treatment with UV-irradiated *Candida* resulted in initial changes along the pathogen trajectory followed by a return to homeostasis (Figure 1C).

To investigate the regulons (identified by co-expressed gene sets) that control the macrophage response to pathogens, we determined the differentially expressed genes and differentially accessible regions for each stimulus and time point relative to untreated macrophages (Tables S1 and S2). We then clustered all genes and genomic regions with statistically significant differences in at least one condition and visualized their time-series dynamics as heatmaps (Figure 1D). The results supported our observations from the unsupervised analysis (Figure 1C): (1) interferon and pathogen responses were characterized by divergent trends for both gene expression and chromatin accessibility, (2) the IFN-β and IFN-γ responses were highly similar after

Cell Systems
Methods

CellPress
OPEN ACCESS

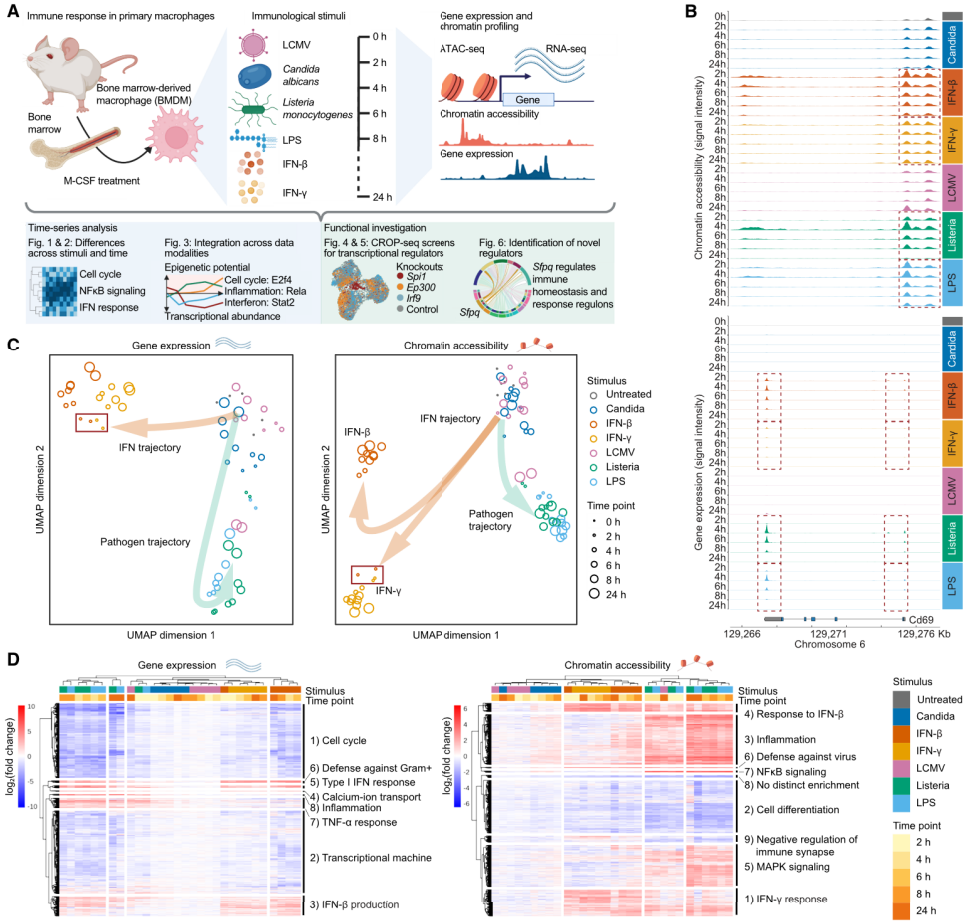

Figure 1. Time-series profiling uncovers dynamic transcriptome and chromatin landscapes in macrophages responding to six stimuli

(A) Schematic outline of the experimental and analytical approach. Macrophages were differentiated by M-CSF addition from murine bone marrow and treated with immune stimuli in two biological replicates. RNA-seq and ATAC-seq profiling were performed at six time points, and high-content CRISPR screening was performed using a combined CROP-seq and CITE-seq assay.

(B) Genome browser tracks depicting chromatin accessibility (top) and gene expression (bottom) at the *CD69* locus (the promoter is on the right and the direction of transcription is from right to left) over time across stimuli (colored) and in untreated controls (gray). Noteworthy changes are highlighted by boxes.

(C) Unsupervised uniform manifold approximation and projection (UMAP) representation of all gene expression (left, RNA-seq; GEO: GSE263759; 64 samples) and chromatin accessibility profiles (right, ATAC-seq; GEO: GSE263758; 78 samples). Stmuli are color-coded, time points are denoted by circle size, and arrows indicate shared trends. Boxes highlight the similarity of the IFN-β and IFN-γ responses at the 2-h time point.

(D) Differential gene expression (left) and chromatin accessibility (right) comparing each stimulus and time point (columns) to the untreated controls, visualized as hierarchically clustered heatmaps of effect sizes for statistically significant genes and genomic regions (rows), annotated with summarized results of gene set enrichment analyses.

2 h but subsequently diverged, and (3) LCMV treatment induced a late response that followed the early transcriptional response observed for *Listeria* and LPS.

For each of the six stimuli, more genes were downregulated than upregulated (Figures 1D and S2B). Stimulation-upregulated genes were enriched for immunological processes such as

response to interferon and TNF-α, bacterial defense, and the signaling cascade driving IFN-β production (this included *Sting1*, *Ddx58*, and *Irf7*). By contrast, downregulated genes were enriched for general metabolic processes and regulation of the cell cycle, indicative of cell-intrinsic reorganization and downregulation of energy-consuming maintenance processes in favor of pathogen defense.[31] Other enrichments were specific to certain stimuli (Figure 1D). For example, genes with higher expression upon IFN-β than IFN-γ treatment were enriched for IFN-I signaling, and genes activated more strongly by stimulation with *Listeria* than with LPS were enriched for gene functions such as negative regulation of viral genome replication and apoptotic processes and cellular response to Gram-positive bacteria (Table S1).

By contrast, chromatin accessibility was preferentially increased upon stimulation (Figures 1D and S2B). This was in part because many downregulated genes maintained high levels of chromatin accessibility, suggesting that the downregulation was temporary. For the upregulated immune genes, increased levels of gene expression often coincided with enhanced chromatin accessibility (Table S2), likely fostered by active chromatin remodeling. Consistently, genomic regions with increased chromatin accessibility upon stimulation were linked to genes with known roles in the response to pathogens, in inflammation, IFN response, mitogen-activated protein kinase (MAPK) signaling, and NF-κB signaling.

In summary, our comparative analysis of the macrophage response to pathogens and infection-linked stimuli revealed stimulus-specific changes as well as shared regulatory processes. Gene expression and chromatin accessibility followed globally consistent trends. Nevertheless, many individual genes underwent changes only in their gene expression (especially for genes with chromatin-accessible promoters already at baseline) or only in their chromatin accessibility profiles, underlining that chromatin accessibility is not a simple correlate of gene expression levels.

Quantitative analysis of gene expression and chromatin identifies shared and specific biological programs

To characterize the regulatory dynamics for each of the six stimuli, we identified all genes and genomic regions with pronounced changes over the time course, and we applied k-means clustering to their temporal profiles (Figures 2A and 2B). We observed the most pronounced changes in response to *Listeria* and LPS treatment, with more than 3,000 affected genes and more than 11,000 affected genomic regions per stimulus, which formed multiple clusters with distinct regulatory dynamics. The least pronounced responses were observed for *Candida* and LCMV, which affected several hundred genes and close to 2,000 genomic regions. Finally, interferon treatment caused responses of intermediate strength and complexity, which were generally more pronounced for IFN-β than for IFN-γ.

Over the time course (Figures 2C and 2D), *Candida* treatment caused rapid upregulation of one gene cluster and slower downregulation of a second cluster, both of which returned to homeostatic expression levels within 24 h. The effect of *Candida* treatment on chromatin accessibility comprised five clusters with distinct trajectories, which also returned to their homeostatic levels within 24 h. We thus conclude that UV-irradiated *Candida* triggers an acute response that is rapidly reigned in and does not leave an epigenetic or transcriptional memory among the affected macrophages. By contrast, treatment with IFN-β or IFN-γ caused changes in gene expression and chromatin accessibility that were established more slowly (typically reaching their most extreme levels after 6 to 8 h) but firmly persisted at the 24-h time point. The LCMV-induced response followed the least complex trajectory, with one cluster going down and one cluster (for gene expression) or two clusters (for chromatin accessibility) going up at the 24-h time point. Finally, treatment with *Listeria* and LPS induced diverse changes in both gene expression and chromatin accessibility, with some clusters showing a rapid response and subsequent return to homeostatic levels, while others peaked after 6 to 8 h and remained altered beyond the end of the time course.

To investigate the biological roles of the identified gene clusters, we annotated each cluster by gene set enrichment analysis (Figures 2E and 2G; Table S1). The enrichments fell into two main groups: immune signaling and basic cell functions. The first group of enrichments comprised genes involved in interleukin signaling, TNF signaling, and other immune signaling pathways. The corresponding gene clusters were strongly upregulated in response to LPS, LCMV, and *Listeria* but mostly returned to homeostatic levels within 24 h. The second group of enrichments comprised genes involved in cell cycle and metabolism. These gene clusters were downregulated in response to *Listeria* and LPS and upon treatment with IFN-β (but not IFN-γ). This temporary reduction of basic cell functions in macrophages thus appeared to be specific to the type-I IFN response triggered by IFN-β, *Listeria*, and LPS.

We performed a similar analysis also for genomic regions with differential chromatin accessibility over the time course (Figures 2F and 2H; Table S2), and we observed broad enrichment for putative regulatory regions associated with cellular immune responses, interferon signaling, and antigen presentation. The temporal dynamics varied widely, with an IFN-β cluster that peaked at 2 h and an LCMV cluster that peaked at 24 h. We also identified two very similar clusters for IFN-β and IFN-γ treatment that were characterized by rapid loss of chromatin accessibility within 2 h of stimulation, followed by swift recovery. These clusters did not show any distinctive enrichments, but both included regions associated with well-known immune genes such as *Ifitm10* (an ISG), the immune signaling receptor gene *Tgfbr1*, the transcriptional coactivator gene *Cited2* (modulating inflammatory responses), and *Cdk18* with its role in cell migration and adhesion crucial for immune cell trafficking.[32]

In summary, we identified diverse responses to the six immune stimuli, with characteristic temporal dynamics in gene expression and chromatin accessibility. A recurring theme was the rapid activation of immune-related programs accompanied by transcription-only downregulation of cell maintenance programs (which was more pronounced for IFN-β than for IFN-γ). We observed little loss of chromatin accessibility among the downregulated cell maintenance programs, suggesting that these genes preserve their potential for swift transcriptional reactivation.

Macrophages upregulate genes with pre-established epigenetic potential while repressing cell cycle genes

To dissect the interplay of epigenetic and transcriptional regulation in the pathogen response, we combined all RNA-seq and

Cell Systems
Methods

CellPress
OPEN ACCESS

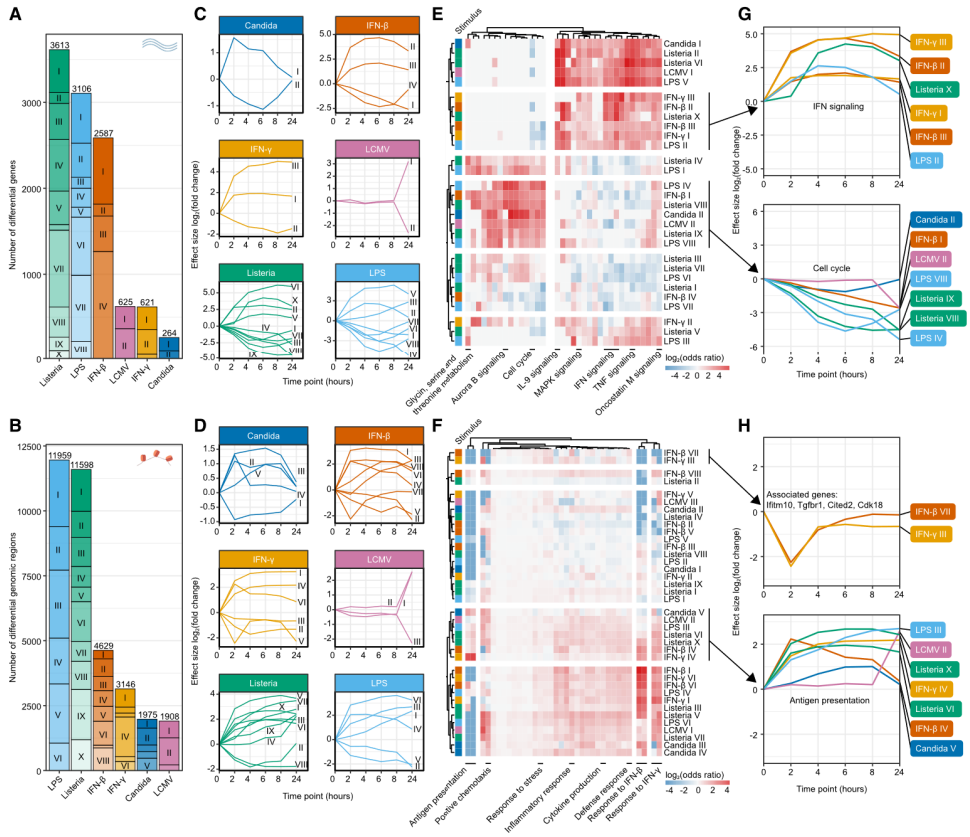

Figure 2. Quantitative analysis of gene expression (top) and chromatin accessibility (bottom) identifies shared and specific programs

(A and B) Bar plots showing the composition of time-series clusters for gene expression (A) and chromatin accessibility (B), ordered by the total number of differential genes or genomic regions per stimulus.

(C and D) Mean effect sizes of gene expression (C) and chromatin accessibility (D) for each cluster and stimulus over the time course.

(E and F) Hierarchically clustered heatmaps of enrichment analyses (based on the hypergeometric test) for clusters of genes (E) and genomic regions (F).

(G and H) Line plots showing mean effect sizes over the time course for clusters of genes (G) and genomic regions (H) with similar enrichments across stimuli.

ATAC-seq profiles in a gene-centric analysis (Figure 3A). This integrated dataset allowed us to test the hypothesis that rapid transcriptional upregulation exploits a pre-established "epigenetic potential" at certain genes (i.e., presence of open chromatin in excess of the gene's observed transcriptional activity[33]), as illustrated by *Prdm1* (Figure S1). By contrast, the upregulation proceeded more slowly for genes that lack such epigenetic potential. For example, *Tmem26* and *Ifnb1* peaked only after 4 h of stimulation with *Listeria* (Figure S3). Both LPS and *Listeria* led to increased promoter-associated chromatin accessibility (which is indicative of elevated epigenetic potential of their target genes), but often only *Listeria* induced transcriptional upregulation at those genes with open promoters (which is indicative of the realization of pre-established epigenetic potential for those genes).

To combine and compare gene expression and chromatin accessibility in a single analysis, for each gene, we quantified its expression level (based on RNA-seq) and the chromatin accessibility of its promoter region (based on ATAC-seq). We then performed normalization and batch effect correction to remove modality-specific differences. Unsupervised analysis of the resulting integrated time-series dataset confirmed the trends and trajectories observed in our separate analyses of gene expression and chromatin accessibility (Figure 3A). The first trajectory captured the response to interferon treatment, further segregating into two arms reflecting IFN-β and IFN-γ treatment,

CellPress OPEN ACCESS

Cell Systems
Methods

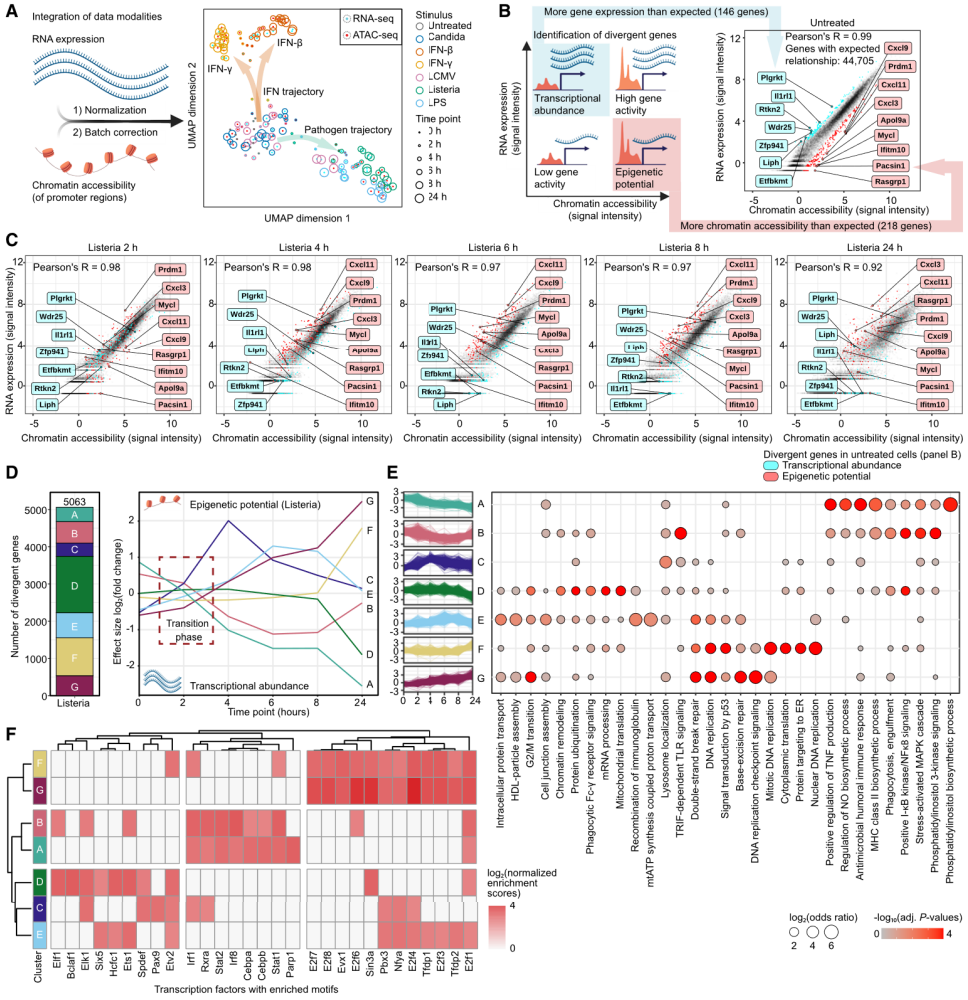

Figure 3. Macrophages upregulate genes with pre-established epigenetic potential while repressing cell cycle genes in response to *Listeria*

(A) Schematic outline (left) and unsupervised UMAP representation (right) of the integrated RNA-seq and ATAC-seq data after normalization and batch correction (142 samples). Stimuli are color-coded (outer circles), time points are denoted by circlesize, and data modality is indicated by red (chromatin accessibility) or blue (gene expression) central dots.

(B) Illustration of the concepts of epigenetic potential and relative transcriptional abundance (left) and scatterplot of gene expression (y axis) and chromatin accessibility (x axis) among the untreated controls (right). Genes identified as divergent (i.e., gene expression is substantially higher or lower than expected based on chromatin accessibility of the gene promoter) are highlighted in red (epigenetic potential) and blue (relative transcriptional abundance).

(C) Scatterplot of gene expression and chromatin accessibility across all time points in response to *Listeria* treatment, with labels highlighting divergent genes in the untreated controls (as shown in B).

(D) Bar plot showing the composition of time-series clusters (left) and mean temporal changes (right) in the relationship between gene expression and chromatin accessibility in response to *Listeria* treatment.

(E) Clustered temporal changes over the time series (left) and gene set enrichments (based on the hypergeometric test) for the identified clusters (right).

(F) Hierarchically clustered heatmap of the top five transcription factor motif enrichments of each cluster of divergent genes in response to *Listeria* treatment.

and the second trajectory corresponded to treatment with PAMPs and infectious pathogens.

While the time-series dynamics were generally consistent between the two modalities, we identified individual genes with gene expression levels that diverged from their promoter-associated chromatin accessibility. Some genes had higher chromatin accessibility than expected based on their gene expression, indicating an unrealized epigenetic potential for rapid transcriptional upregulation. Others exhibited higher gene expression than expected from their promoter-associated chromatin accessibility, suggesting a "relative transcriptional abundance," which we define as transcription levels that exceed those typically seen in genes with similar promoter accessibility (Figure 3B; Table S3). For example, *Listeria* treatment triggered rapid upregulation of gene expression well beyond the observed changes in chromatin accessibility for genes such as *Prdm1* (a negative regulator of ISG expression also known as BLIMP1), *Ifitm10* (encoding an interferon-inducible transmembrane protein), RAS family member *Rasgrp1*, proto-oncogene *Mycl*, and chemokine-encoding gene *Cxcl3* (Figure 3C). By contrast, we observed lower expression than expected based on chromatin accessibility for genes such as *Pacsin1* (a regulator of IFN-I response), apolipoprotein family member *Apol9a*, and chemokine-encoding genes *Cxcl9* and *Cxcl11*. These genes retained some epigenetic potential after 2 h of *Listeria* exposure but transitioned to relative transcriptional abundance at later time points. Similar analyses for the other stimuli are provided in the supplement (Figure S4; Table S3).

To investigate the temporal dynamics of divergent genes (i.e., gene expression is significantly higher or lower than expected based on the chromatin accessibility of the gene promoter) we quantified the effect sizes of these deviations such that positive values correspond to lower-than-expected gene expression (epigenetic potential) and negative values correspond to higher-than-expected gene expression (relative transcriptional abundance), while a value of zero indicates full consistency of gene expression and chromatin accessibility. When clustering these temporal profiles separately for each of the six stimuli, we identified up to seven gene clusters with different dynamics across the six stimuli (Figure S5; Table S3). The most diverse responses were observed for *Listeria* infection, prompting us to pursue an in-depth analysis of the corresponding time series.

For *Listeria* infection, two clusters of genes started the time course with unrealized epigenetic potential, while baseline transcriptional abundance was detected for three clusters, and for the remaining two clusters, gene expression and promoter chromatin accessibility were highly consistent with each other (Figure 3D). Within 2 h after treatment with infectious *Listeria*, all seven of these gene clusters transitioned through a short phase with high consistency between their gene expression and chromatin accessibility before proceeding to opposite regulatory states characterized by either high relative transcriptional abundance or strong unrealized epigenetic potential.

Genes in clusters A and B showed high epigenetic potential at baseline, which was rapidly realized upon *Listeria* infection and superseded by strong transcriptional abundance after 6 to 8 h. At the final time point, this transcriptional abundance had disappeared for cluster B (due to decreased gene expression), while it had become even stronger for cluster A (due to a further increase in gene expression and decreased chromatin accessibility) (Figures 3D and S5). Both clusters were enriched for classical immune response genes. Moreover, cluster B was enriched for genes involved in stress response, TLR signaling, and NF-κB signaling, while cluster A was enriched for genes related to TNF production, nitric oxide synthesis, and major histocompatibility complex (MHC) class II regulation, which are all relevant for a prolonged antimicrobial immune response (Figure 3E; Table S3). By contrast, genes in clusters C, E, and G started from modest transcriptional abundance that quickly evaporated due to decreased gene expression, followed by a phase with high epigenetic potential. For clusters C and E, we observed the return to a balanced state at the final time point, while cluster G, enriched for genes involved in DNA replication and repair, further increased its epigenetic potential (retaining its chromatin accessibility while decreasing transcription; Figure S5), which is indicative of a sustained memory response. Cluster F, which was enriched for DNA replication genes, built up epigenetic potential at the final time point. By contrast, cluster D, which was enriched for genes involved in phagocytic activity and NF-κB signaling, exhibited relative transcriptional abundance at the same time point.

To dissect the transcription-regulatory basis of the identified clusters, we performed enrichment analysis for transcription factor binding motifs in the corresponding gene promoters (Figure 3F). Both clusters A and B were enriched for binding motifs of the IRF, STAT, and CEBP transcription factors, which have well-established roles in immune gene regulation. By contrast, clusters F and G were enriched for binding sites of the E2F transcription factors, which are key regulators of cell cycle and have been linked to dynamic gene repression after immune stimulation.[8] Clusters C, D, and E displayed increased transcriptional activity at the later time points (Figures 3D and S5) and were enriched for genes involved in phagocytosis, lysosome localization, intracellular protein transport, mRNA translation, and NF-κB signaling (Figures 3E and 3F). The identified transcription factors are likely to interact with other regulatory mechanisms (e.g., mRNA stability and protein translation) in the establishment, maintenance, and realization of epigenetic potential and relative transcriptional abundance in the macrophage response to *Listeria*.

In summary, we observed a characteristic interplay of gene expression and chromatin accessibility upon *Listeria* treatment in macrophages. First, many immune genes initially had high chromatin accessibility but low expression, carrying an epigenetic potential that was rapidly realized upon stimulation. Second, cell cycle regulators were downregulated while their chromatin accessibility remained high, thus retaining epigenetic potential to restore their homeostatic expression levels after clearance of the infection. Third, we identified high relative transcriptional abundance and elevated expression of genes with moderate chromatin accessibility as an alternative and complementary path to the rapid upregulation of immune genes with pre-established, unrealized epigenetic potential.

Single-cell CRISPR sequencing functionally dissects gene regulation in response to *Listeria* treatment

To complement our time series of macrophage stimulation (Figures 1, 2, and 3) with a functional dissection of putative regulators, we performed pooled CRISPR screens using a

method that combines the single-cell whole-transcriptome readout of our CROP-seq technology[22] with a CITE-seq readout for 11 macrophage surface marker proteins.[34] We validated this integrated CROP-seq and CITE-seq assay in a targeted screen of 15 regulatory proteins over the course of *Listeria* treatment (Figure 4) and subsequently applied it to characterize the role of 135 transcription factors and chromatin regulators in the immune response of macrophages across several time points (Figures 5 and 6).

Screens were conducted in RAW 264.7 macrophages engineered to express Cas9 (Figure 4A). We delivered the CRISPR guide RNAs with a lentiviral vector at a multiplicity of infection of 0.1 to ensure that very few cells receive more than one guide RNA. Moreover, to mitigate potential autocrine and paracrine effects of individual CRISPR perturbations within the pooled screen, the guide RNA-expressing cells were co-cultured together with ~90% untransduced cells, which provide a consistent cellular context for the genetically engineerec cells throughout the screen. Consequently, our pooled screen focuses on cell-intrinsic effects of the perturbed transcriptional regulators while diluting out non-cell-intrinsic effects such as altered cytokine secretion. The cells were challenged with *Listeria* in the same way as in the time course experiments and collected at three time points: 0 (prior to *Listeria* treatment), 2, and 6 h. Successfully transduced cells were purified via fluorescence-activated cell sorting (FACS) (including those expressing non-targeting guide RNAs, which were used as controls) and subjected to single-cell RNA-seq with specific enrichment for the guide RNAs that identify the CRISPR perturbations as part of the single-cell transcriptomes (Figure S6A).

In this proof-of-concept screen, we knocked out regulatory genes involved in *Listeria* infection (*Rela*/*p65*), endogenous interferon response (*Jak1*, *Tyk2*, *Stat1*, *Stat2*, and *Irf9*), macrophage differentiation (*Spi1*, *Csf1r*, and *Irf8*), epigenetic regulation (*Ep300*, *Hdac6*, *Kdm1b*, and *Kdm6b*), and cell stress response (*Jun* and *Creb1*). Each gene was targeted with four different guide RNAs, and we included 10% non-targeting guide RNAs as controls (Table S4). In addition to the single-cell transcriptome readout and the sequencing of expressed guide RNAs, we quantified 11 cell-surface proteins using CITE-seq, which included the macrophage markers CD11b, CD14, CD115, CD163, and MAC2; activation markers CD64, CD69, CD80, and CD95; and immune checkpoints CD274/PD-L1 and CD172a/SIRPA.

The screen yielded 9,153 single-cell profiles passing quality control with one guide RNA per cell. This corresponds to a mean coverage exceeding 200 cells per target gene, which is sufficient for rigorous quantitative analysis. Confirming the efficiency of our gene targeting, we observed specific downregulation of the macrophage marker *Csf1r* (CD115) both at the RNA and surface protein level (Figure S6B). In an unsupervised analysis, the single-cell profiles generally grouped by time point (Figure 4B) or treatment (Figure S6C), suggesting that the gene perturbations modulate rather than abrogate the cells' response to *Listeria*. The notable exception was *Spi1*, which codes for the transcription factor PU.1. This gene knockout had dramatic and convergent effects on the transcriptomes at all three time points, consistent with the gene's central role in establishing the cellular identity of macrophages (Figure 4B).

We assessed the transcriptional response of genetically unperturbed macrophages using the cells that expressed non-targeting guide RNAs, thereby creating an internal reference against which we assessed the changes induced by the CRISPR knockouts (Figures 4C and S6D). Some of the control cells had elevated ISG expression already at the 0-h time point (including *Rsad2*, *Cmpk2*, *Ifih1*, *Oasl1*, *Isg15*, and *Ifit1*), which likely reflects tonic type-I interferon signaling consistent with prior research.[35] Following *Listeria* treatment, the CITE-seq readout detected a rapid decrease of CD115 (CSF1R) and MAC2 on the cell surface (both are markers of undifferentiated monocytes/macrophages and expected to be downregulated upon macrophage activation), together with slower downregulation of the checkpoint molecule CD172a (SIRPA) (Figure S6E). Conversely, we observed increased levels of CD274 (PD-L1), CD64, CD69, CD80, CD95, and CD14 proteins in response to *Listeria* infection, whereas the integrin subunit alpha M (CD11b) was upregulated upon infection but returned to its homeostatic levels already at the 6-h time point.

The *Spi1* (PU.1) knockout caused broad downregulation of genes and cell-surface markers relevant for macrophage biology, including CD14, CD115, and CD64 (Figure S6F), and for immune signaling pathways such as TLR, TNF-α, and JAK-STAT (Figure 4D), in accordance with its role as a master regulator and stimulus response factor.[11,12,36] The *Spi1* knockout cells also expressed increased levels of certain interferon response genes, including *Stat1*, *Usp18*, *Gbp2*, *Ifit3*, *Ifitm3*, and *Nos2* (Table S4), suggesting an altered but not entirely abrogated immune response in these knockouts. Given a recent study reporting that *Spi1*/PU.1 can act as transcriptional repressor,[37] *Spi1*/PU.1 may directly repress certain interferon response genes, in addition to its role as a lineage-determining transcription factor.

We quantified the transcriptional effects using the *Mixscape* method for CRISPR perturbation modeling[38] (Figures 4E–4H and S7A–S7C). This analysis uncovered strong co-clustering for knockouts of the JAK-STAT pathway genes *Jak1*, *Stat2*, and *Irf9* throughout the time course, while *Stat1* knockouts clustered separately. By contrast, many other effects were dynamic over the time course. For example, knockout of the NF-κB subunit *Rela* and the transcription factor *Irf8* led to strong transcriptional changes starting only after 2 and 6 h of *Listeria* infection, respectively.

Ep300 knockout had transcriptional consequences that differed from all other regulators, including upregulation of ISGs (*Irf7*, *Stat1*, *Ifit1*, *Ifit2*, *Ifit3*, and *Usp18*), ribosomal proteins, and genes involved in MHC class I cross-presentation (*Vamp8*, *Tap2*, *Psme1*, *Tap1*, *Psme2*, *Cyba*, *B2m*, *Psmb10*, *Psmb8*, *Tapbp*, and *Psmb9*) (Figure S8A). The *Ep300* knockout also led to increased surface expression of checkpoint proteins such as CD80 and PD-L1/CD274 (Figure S8B), and reduced expression of genes associated with neutrophil degranulation, MAPK signaling, and inflammatory response (Table S4), in accordance with *Ep300*'s role in NF-κB acetylation.[39] These results expand on a previous analysis of *Ep300* in macrophages[40] and indicate that *Ep300* regulates cell defense by promoting inflammation while restraining the interferon response, possibly via non-histone protein acetylation[41] and countering HDAC activity.[42]

In summary, we established a method for high-content CRISPR screening that combines CROP-seq and CITE-seq

Cell Systems
Methods

CellPress
OPEN ACCESS

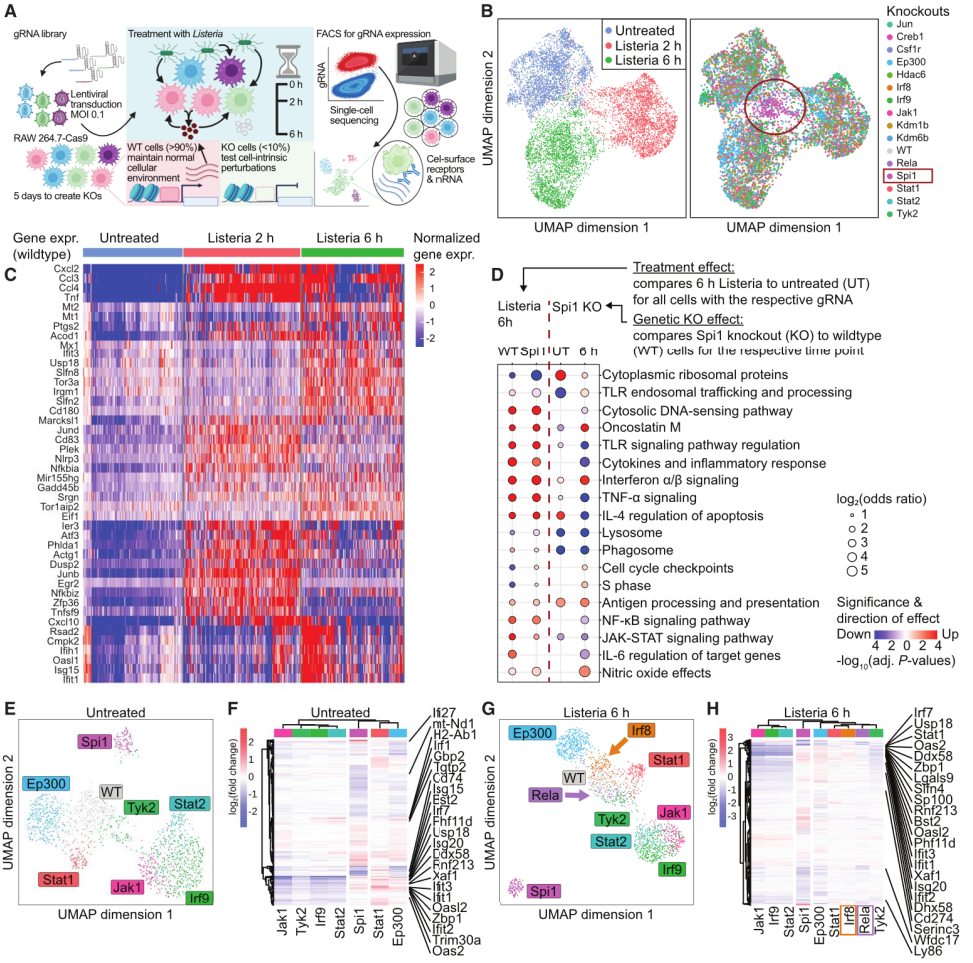

Figure 4. High-content CRISPR screening with transcriptome and cell-surface marker readout (combined CROP-seq and CITE-seq assay) functionally characterizes gene regulation in response to *Listeria* treatment

(A) Schematic outline of the CRISPR screen. Macrophages transduced with a CRISPR knockout library (10%) were cultured together with genetically unperturbed cells (90%, jointly referred to as "WT" together with those cells that were assigned to non-targeting guide RNAs). Transduced cells were subjected to single-cell sequencing at several time points, yielding gene expression profiles, cell-surface marker profiles, and guide RNA (gRNA) assignments.

(B) Unsupervised UMAP representation of single-cell transcriptomes (CROP-seq KO15; GEO: GSE263760; 9,153 cells) colored by time point (left) and genetic perturbation (right), respectively. Clustering of *Spi1* knockout cells across time points is highlighted by a circle.

(C) Hierarchically clustered heatmap of normalized gene expression for the most differentially expressed genes between time points in cells without genetic perturbation (i.e., those that were assigned non-targeting guide RNAs).

(D) Bubble plot of gene set enrichments (based on the hypergeometric test) after 6 h of *Listeria* treatment in cells without genetic perturbation (WT) and in cells with *Spi1* knockout (left), and for *Spi1* knockout cells that were untreated (UT) or treated with *Listeria* for 6 h (right).

(E and G) Unsupervised UMAP representation of LDA-transformed *Mixscape* genetic perturbation signatures, with cells colored by knockout (based on the assigned guide RNA) in untreated cells (E; 1,508 cells) and after 6 h of *Listeria* treatment (G; 1,828 cells). Arrows highlight the emergence of the *Irf8* and *Rela* knockout effects at the 6-h time point (G).

(F and H) Hierarchically clustered heatmap of effect sizes for knockout-induced differential gene expression in untreated cells (F) and after 6 h of *Listeria* treatment (H). Boxes highlight the emergence of the *Irf8* and *Rela* knockout effects at the 6-h time point (H).

CellPress OPEN ACCESS

Cell Systems
Methods

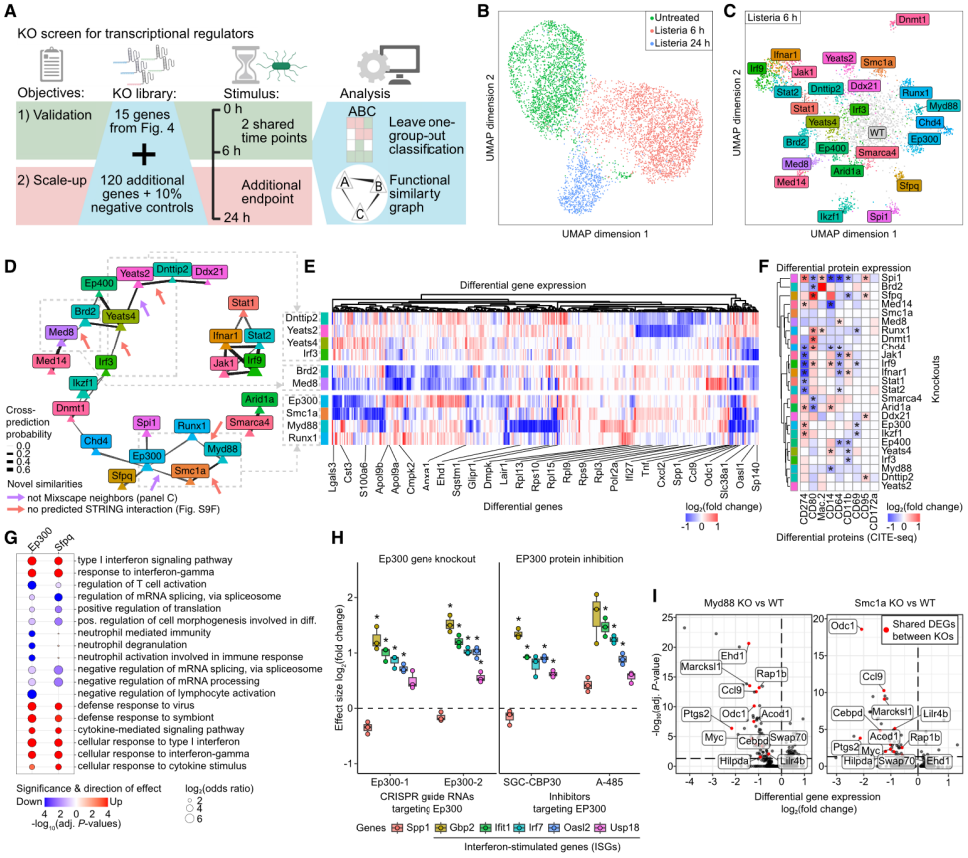

Figure 5. Upscaled high-content CRISPR screen with cross-prediction analysis uncovers transcriptional effects of epigenetic regulator knockouts in response to *Listeria* treatment

(A) Schematic overview of the upscaled CRISPR screen and the corresponding computational analysis. Compared with the proof-of-concept screen (Figure 4), the guide RNA library was extended with 120 additional target genes and with additional non-targeting guide RNAs to maintain ~10% genetically unperturbed control cells as controls, and a 24-h time point was added. In total, 28,303 single-cell profiles passed quality control. Cross-prediction between cell perturbation signatures was used to derive a functional similarity graph.

(B) Unsupervised UMAP representation of single-cell transcriptomes (CROP-seq KO150; GEO: GSE263761; 6,187 cells) following *Mixscape* genetic perturbation analysis, colored by time point.

(C) Unsupervised UMAP representation of LDA-transformed *Mixscape* genetic perturbation signatures (based on the assigned guide RNAs) after 6 h of *Listeria* treatment, with cells colored by their assigned guide RNAs (2,822 cells).

(D) Functional similarity graph derived by cross-prediction analysis for the 6-h time point of *Listeria* treatment. The 25 nodes represent gene knockouts, and edges denote average cross-prediction probabilities (pruned at a cutoff of 0.1). Node size corresponds to the square root of the number of cells for each knockout. Edges are visualized as trapezoids, where the width at the source node corresponds to the probability of cross-predicting the source node as the target node. Arrows highlight selected examples of similarities identified specifically by the cross-prediction analysis, which were either absent from protein-protein interaction analysis with STRING (red) or from the *Mixscape* analysis (purple).

(E) Hierarchically clustered heatmap of knockout-induced differential gene expression (fold changes; columns) compared with cells without genetic perturbation (i.e., those that were assigned non-targeting guide RNAs) at the 6-h time point of *Listeria* treatment, for selected groups of knockouts (rows, separated by white spacing) that were evident from the functional similarity graph but either absent from the STRING data or from the *Mixscape* analysis.

(F) Hierarchically clustered heatmap of knockout-induced differential cell-surface marker expression based on the CITE-seq readout (fold changes, columns) compared with cells without genetic perturbation at the 6-h time point of *Listeria* treatment. Statistical significance (adjusted p value < 0.05; Wilcoxon rank-sum test) is indicated by asterisks (*).

(legend continued on next page)

and applied it in a proof-of-concept screen over the *Listeria* time course. We uncovered immune-regulatory roles of JAK-STAT pathway members, of *Spi1* (PU.1), and of *Ep300* in the macrophage response to *Listeria* treatment.

Transcriptional effects of epigenetic regulator knockouts in homeostasis and response to *Listeria*

Using our CROP-seq and CITE-seq method, we performed an upscaled perturbation experiment targeting 135 genes at three time points of *Listeria* treatment: 0 (prior to treatment), 6, and 24 h (Figure 5A). We included known regulators of macrophage function and development, JAK-STAT pathway members, chromatin-modifying enzymes, and genes selected from our time course of pathogen response (Figures 1, 2, and 3). We obtained 28,303 single-cell profiles that passed stringent quality filtering, resulting in a mean coverage of 187 cells per target gene. Several analyses confirmed high data quality and established a baseline of *Listeria*-induced changes in gene expression and cell-surface marker expression over the time course (Figures 5B and S9A–S9D; Table S5).

Quantification of the transcriptional effects using *Mixscape* identified 28 genes whose knockout caused statistically significant changes over the time course of *Listeria* infection (Figures 5C, S9A, S10A, S10B, S11A, and S11B). We observed the most pronounced effects at 6 h, with strong clustering of the JAK-STAT pathway knockouts *Jak1*, *Stat1*, *Stat2*, *Irf9*, and *Ifnar1* (Figures S9A, S10A, S10B, S11A, and S11B). These knockouts caused more genes to be downregulated than upregulated, consistent with the pathway's role in rapid immune gene activation. By contrast, gene upregulation dominated for knockouts of *Ikzf1* (which codes for a hematopoietic transcription factor with both activating and repressive roles in macrophages[43]) and of the chromatin regulator genes *Chd4* and *Dnmt1* (Figures S9A, S9E, S10B, and S11B). Moreover, *Spi1* knockout caused pronounced loss of gene expression and cell-surface proteins characteristic of macrophage identity for all time points, consistent with our proof-of-concept screen (Figure S9C).

To integrate and compare transcriptional responses across gene knockouts, we performed cross-prediction between cell perturbation signatures, predicting for each single-cell RNA-seq profile what was the most likely gene knockout explaining this profile after removal of all cells of the correct class from the training set. The resulting cross-prediction probabilities provide a functional similarity measure based on which we constructed a global similarity graph, with thick edges indicating frequent cross-prediction between knockout pairs (Figures 5D, S10C, and S11C). This similarity graph uncovered strong connections at the 6-h time point between knockouts of *Med8* and *Med14*, which encode two components of the mediator complex, and between *Arid1a* and *Smarca4*, two members of SWI/SNF chromatin remodeling complexes. More than 80% (24 out of 29) of the edges in the functional similarity graph were supported by predicted protein-protein interactions in the STRING database, often with high interaction scores (Figures S9F, S10D, and S11D), suggesting that many of these regulator proteins with similar effects directly interact in the regulation of their target genes.

We also observed functional similarities between genes that were not connected by protein-protein interactions or by the *Mixscape* analysis (Figures 5D and 5E). This included knockouts of *Ep300*, *Smc1a*, *Myd88*, and *Runx1*, which all led to downregulation of the cytokine-encoding genes *Ccl2*, *Ccl3*, *Ccl9*, *Tnf*, *Il1a/b*, and *Spp1*, and knockouts of *Yeats2* and *Dnttip2*, which shared a characteristic downregulation of ribosomal genes. Moreover, knockouts of *Yeats4* and *Irf3* shared upregulation of immune and inflammatory genes, and knockouts of the transcription factor *Brd2* and the mediator gene *Med8* were associated with loss of expression for many immune genes, including the ISGs *Sp140*, *Apol9a/b*, *Ifi27*, and *Oasl1*. Transcriptional similarity was often reflected in the CITE-seq data of cell-surface proteins (for example, for *Dnttip2* and *Yeats2*, and for *Yeats4* and *Irf3*) (Figures 5F, S10E, and S11E). Several of these gene perturbations were also identified in a macrophage polarization screen,[40] supporting our claim that the single-cell transcriptome readout of CROP-seq captures many effects detected by screens with specialized readouts.

We further investigated knockouts with similar transcriptional effects. *Sfpq* and *Ep300* knockouts displayed some of the strongest effects among all tested perturbations, which included widespread upregulation of IFN-I response genes (Figures 5G and S10F). For *Sfpq*, an immune-regulatory role has previously been established.[44,45] By contrast, *Ep300* has not been widely studied in macrophages, prompting us to conduct validation experiments at the gene and protein level. We knocked out the *Ep300* gene in RAW 264.7 macrophages using CRISPR and, in separate experiments, interfered with EP300 protein function using the small-molecule inhibitors SGC-CBP30 (which targets the epigenetic reader domain of EP300) and A-485 (which targets the catalytic site of the epigenetic writer domain of EP300). We employed a qPCR-based readout comprising five ISGs (*Gbp2*, *Ifit1*, *Irf7*, *Oasl2*, and *Usp18*) and an inflammation marker (*Spp1*). Both knockout and inhibition resulted in the upregulation of the ISGs in cells that were treated with IFN-β for 2 h (Figure 5H) and in untreated cells (Figure S10G). *Spp1* levels decreased after *Ep300* knockout (Tables S4 and S5; Figure 5H), whereas pharmacological inhibition of the EP300 catalytic site via A-485

(G) Bubble plot of gene set enrichments for *Ep300* and *Sfpq* knockouts at the 6-h time point of *Listeria* treatment. Effect size (odds ratio) is indicated by bubble size, statistical significance (adjusted *p* value; hypergeometric test) by opacity, and effect directionality by color (red: higher expression in the knockouts; blue: lower expression in the knockouts).

(H) Boxplots of gene expression (fold changes compared with the respective controls) for *Spp1* and five interferon-stimulated genes (ISGs) upon interference with EP300 function at the DNA level (CRISPR knockout of *Ep300*, left) and at the protein level (treatment with small-molecule inhibitors of EP300, right). Gene expression was measured by qPCR in RAW 264.7 cells that were treated with IFN-β for 2 h. Three biological replicates were profiled and plotted, statistical significance was determined by paired t tests, and asterisks (*) indicate *p* values below 0.01.

(I) Volcano plots of differentially expressed genes for knockouts of *Myd88* (left) and *Smc1a* (right) compared with cells without genetic perturbation at the 6-h time point of *Listeria* treatment (Wilcoxon rank-sum test). Differentially expressed genes that are shared between the two comparisons are colored in red and individually labeled.

CellPress OPEN ACCESS

Cell Systems
Methods

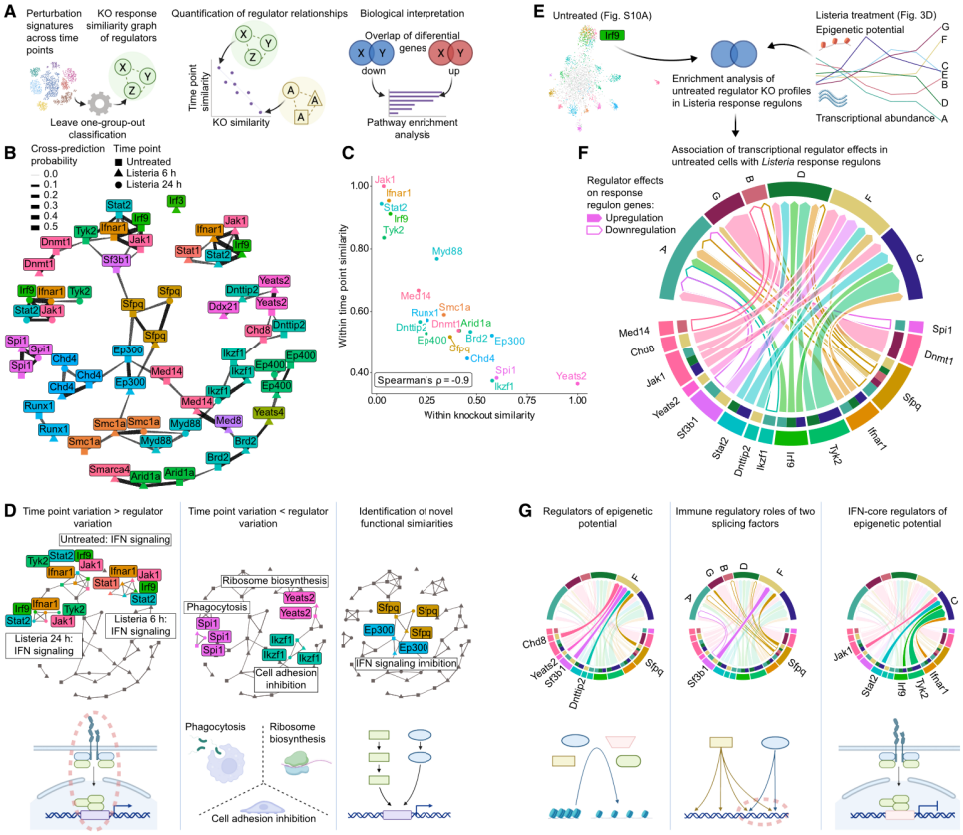

Figure 6. Integration of epigenome/transcriptome time series and genetic perturbations establishes temporal and functional dynamics of the macrophage response to *Listeria*

(A) Schematic outline of the cross-prediction analysis across time points, including differential gene expression and pathway enrichments for the resulting functional similarity graph.

(B) Functional similarity graph derived by cross-prediction analysis across three time points of *Listeria* treatment. The 58 nodes represent gene knockouts per time point (denoted by squares, triangles, and circles), and edges reflect average cross-prediction probabilities (pruned at a cutoff of 0.1). Edges are visualized as trapezoids, where the width at the source node corresponds to the probability of cross-predicting the source node as the target node.

(C) Scatterplot comparing the similarity within time points across knockouts (y axis) and the similarity within knockouts across time points (x axis), both derived from edge weights (i.e., average cross-prediction probabilities) between neighbors of the same knockout or time point in the unpruned functional similarity graph.

(D) Illustrative results of the cross-prediction analysis: (1) time point effects exceed genetic effects for interferon (IFN) signaling (left), (2) genetic effects exceed time point effects for *Spi1*, *Ikzf1*, and *Yeats2* (center), and (3) new functional similarities between knockouts for *Ep300* and *Sfpq* as negative regulators of IFN signaling (right).

(E) Schematic outline of the data integration between regulator effects determined by high-content CRISPR screening (left, from Figure S10A) and regulon dynamics derived from the integrated time series of gene expression and chromatin accessibility (right, from Figure 3D).

(F) Circos plot connecting regulator effects in untreated cells (bottom, from Figure S10A) with the regulons driving the response to *Listeria* treatment (top, from Figure 3D). Arrows indicate statistically significant enrichments (hypergeometric test; filled arrows: upregulation; outline-only arrows: downregulation), and arrow width denotes effect size ($\log_2$ odds ratio).

(G) Illustrative results of the integrative analysis: (1) regulators of genes with increased epigenetic potential 24 h after *Listeria* treatment (left), (2) immune-regulatory roles of splicing factors *Sf3b1* and *Sfpq* (center), and (3) core-IFN regulators that help establish an epigenetic potential that is realized during *Listeria* treatment (right).

resulted in elevated levels (Figures 5H and S10G). This suggests different mechanisms for the EP300-mediated regulation of ISGs and of other inflammation-linked genes such as *Spp1*.

Similar transcriptional effects were also observed for knockouts of the mediator genes *Med8* and *Med14*, both resulting in the downregulation of *Spp1*, of *Ccl3* (encoding the immune cell recruiting chemokine MIP-1α), of a myeloid immune checkpoint gene *Lilr4b*, of several IFIT genes (such as *Ifit3* and *Ifitm3*), and of the *Acod1* gene, which regulates TLR-mediated inflammatory responses (Figure S9G), consistent with observations for other mediator subunits.[46] Finally, knockouts of *Smc1a* (encoding a cohesin complex member) and *Myd88* (encoding a cytosolic adaptor protein and mediator of TLR signaling) both led to similar changes, including downregulation of the immune genes *Acod1*, *Cebpd*, *Ccl9*, and *Lilr4b* (Figure 5I). This observation is consistent with a previous report that linked the cohesin complex to TLR-induced stimulus response in macrophages.[47]

In summary, cross-prediction analysis for our CROP-seq screen identified regulators with similar effects in macrophage homeostasis and response to *Listeria*. Our results highlight the immune-regulatory roles of chromatin remodeling and the mediator complex and identify *Sfpq* and *Ep300* as modulators and constrainers of interferon signaling.

Integrative analysis of functional similarity quantifies regulon dynamics in response to *Listeria*

Toward a global map of the transcription-regulatory programs underlying the macrophage response to *Listeria*, we used cross-prediction analysis to integrate our upscaled CRISPR screening data simultaneously across perturbations and time points, and we annotated the resulting similarity graph using gene set enrichment analysis of the shared knockout effects for each pair of similarity-linked regulator genes (Figures 6A–6D and S12A; Table S5).

The JAK-STAT pathway members *Jak1*, *Stat2*, *Irf9*, *Ifnar1*, and *Tyk2* were closely connected throughout the time course, and their knockout effects were more similar to each other at a given time point than they were across time points for the same knockout (Figure 6C). In other words, the different JAK-STAT knockouts altered the macrophages in very similar ways, but they regulated different gene sets for each time point (Figure 6D, left). We also observed JAK-STAT knockout effects already at the 0-h time point (prior to treatment), which were similar to the knockout effect of the splicing regulator *Sf3b1* and the DNA methyltransferase *Dnmt1*, indicating homeostatic roles of JAK-STAT signaling that are partially distinct from the pathway's pathogen response to *Listeria* treatment.

By contrast, knockouts of *Ikzf1*, *Spi1*, and *Yeats2* each had highly distinct and characteristic transcriptional effects that showed little change over the time course (Figure 6C). Their differentially expressed genes were enriched for biological processes such as cell adhesion (*Ikzf1*), phagocytosis (*Spi1*), and ribosome biosynthesis (*Yeats2*)—constitutive cell functions that remained largely unaltered over the *Listeria* time course (Figure 6D, center). For a third group of genes, including *Sfpq* and *Ep300*, we observed knockout effects with similarities and differences both between genes and between time points (Figure 6D, right). The genes that were upregulated upon *Sfpq* and *Ep300* knockout shared an enrichment for interferon signaling at the 6- and 24-h time points, and to a lesser degree also at the 0-h time point (i.e., under homeostatic conditions), suggesting an inhibitory role of the two regulators on the interferon response. These observations illustrate how our cross-prediction analysis across time points helps dissect the functional similarity between gene knockouts in the time-resolved response to immune stimulation.

In a final analysis, we sought to connect the regulators identified in the CRISPR screens with the regulons inferred from the integrated RNA-seq and ATAC-seq time course of *Listeria* infection. To that end, we calculated pairwise enrichments between the differentially regulated gene sets for each regulator knockout at each time point on the one hand and the clusters of coregulated genes across the *Listeria* time course on the other hand (Figures 6E, 6F, and S12B). This analysis functionally confirmed the regulatory roles of *Spi1*, *Irf9*, *Stat1*, *Stat2*, *Ep300*, and *Irf3* that we predicted based on transcription factor binding site analysis in our time-series data (Table S3), while also mapping the epigenetic regulators in a similar manner (for which binding site enrichments are usually not possible).

Most *Listeria* response regulons (Figure 6F, top half) were linked to several regulator effects at homeostasis (Figure 6F, bottom half). For example, the splicing factor genes *Sfpq* and *Sf3b1*, as well as *Yeats2, Chd8*, and *Dnttip2*, showed evidence of positive regulation for regulon F of the time-series analysis, which captures the build-up of epigenetic potential at target genes associated with DNA replication and cytoplasmic translation (Figure 6G, left). At the same time, *Sfpq* and *Sf3b1* appeared as negative regulators of regulon A, which showed an opposite trend with high relative transcriptional abundance at the end of the *Listeria* time series (Figure 6G, center). We also identified a positive link of JAK-STAT pathway members under homeostatic conditions with regulons C and D, which were characterized by the rapid build-up and subsequent disposal of epigenetic potential at genes associated with lysozyme localization (regulon C) and with late relative transcriptional upregulation of phagocytic as well as NF-κB signaling (regulon D) (Figures 6G, right, and 3D–3F). These results indicate a regulatory interconnection between JAK-STAT signaling and the identified transcription factors in the macrophage response to *Listeria* infection.

In summary, our integrative analysis established an initial map of the regulators and gene-regulatory programs that underlie the macrophage response to *Listeria*. It also showcases the utility of combining and bioinformatically integrating multi-omics time series with high-content CRISPR screens using our CROP-seq and CITE-seq method as well as computational cross-prediction analysis.

DISCUSSION

This study combined epigenome and transcriptome time-series profiling with high-content CRISPR screening and integrative computational analysis in order to dissect the pathogen response in murine macrophages. We investigated six immune stimuli (*Listeria*, LCMV, *Candida*, LPS, IFN-β, and IFN-γ) over a dense multi-omics time course and performed high-throughput functional dissection of the macrophage response to *Listeria* using a combined CROP-seq and CITE-seq method.

We found that macrophages respond to these immune stimuli with a shift from cell cycle and maintenance programs to the activation of immune-related pathways, while retaining high chromatin accessibility among the promoters of the downregulated genes (Figures 1 and 2). The upregulation of immune genes was universal across all six stimuli, but downregulation of cell cycle genes differed widely. This downregulation was much more pronounced for stimulation of IFN-I signaling (IFN-β, *Listeria*, and LPS) than type II interferon signaling (IFN-γ). This finding contrasts with a previous study reporting stronger effects of IFN-γ in human PBMC-derived, M-CSF-differentiated macrophages,[7] which might reflect species-specific differences in macrophage regulation. We also observed different temporal dynamics across the six immune stimuli, ranging from the response to UV-inactivated *Candida*, which was almost resolved after 24 h, to the response to LCMV, which only started to unfold at that time point.

By epigenome and transcriptome data integration over the time series, we identified genes with unrealized epigenetic potential (i.e., higher chromatin accessibility than expected based on their gene expression) and genes with relative transcriptional abundance (i.e., transcription levels that exceed the typical expression levels of genes with similar chromatin accessibility in their promoter regions), constituting two ways how macrophages organize their response in a stimulus-specific manner (Figure 3). For example, stimulation with LPS (a PAMP but not an actual pathogen) was sufficient to broadly establish epigenetic potential at immune response genes, while *Listeria* (an infectious pathogen) in addition triggered broad transcriptional activation of immune response genes. For some genes, the increased RNA levels exceeded the typical gene expression predicted by chromatin accessibility, thus resulting in cases of relative transcriptional abundance.

Integrating the identified regulons (i.e., clusters of coregulated target genes) from the epigenome/transcriptome time series with perturbational data for key transcriptional regulators from the high-content CRISPR screens (Figures 4 and 5), we established a functional similarity graph of regulator effects on the macrophage response to *Listeria* (Figure 6). We found that gene regulation by JAK-STAT proteins was variable over the time course but similar across regulators. For example, our data support a switch from a STAT2/IRF9-dependent regulon under homeostatic conditions (possibly involving alternative ISGF3 complexes[48]) to a STAT1/STAT2/IRF9-dependent program that resembles canonical ISGF3 activity driven by IFN-β.[35] By contrast, knockout of SPI1/PU.1 (a master regulator of macrophage cell identity) led to consistently altered transcriptomes throughout the time course (without affecting recovered cell numbers as a direct measure for the survival of the perturbed cells), highlighting a constitutive role of this developmental transcription regulator in the macrophage response. Specifically, SPI1/PU.1 knockout cells exhibited broad loss of TLR, TNF-α, and JAK-STAT signaling activity as well as an unexpected increase in ISG activity.

Our analysis identified several chromatin-associated proteins as immune regulators in macrophages, including the mediator complex proteins MED8 and MED14, the cohesin subunit SMC1A, the splicing factors SFPQ and SF3B1, and the histone acetyltransferase EP300. For example, we observed EP300-mediated repression of ISGs, which we validated by CRISPR knockout and, independently, by small-molecule inhibition of EP300. Based on these results, we hypothesize that the histone acetyltransferase EP300 helps balance the regulatory role of histone deacetylases (HDACs), which are required for full transcriptional activity of ISGs.[41] It has been proposed that HDACs reduce global histone acetylation and thereby mitigate sequestration of the transcriptional co-factor BRD4 to chromatin, which ensures that enough BRD4 is available for efficient RNA polymerase II elongation.[42] EP300 may counteract this effect, underlining the importance of regulating global histone acetylation in macrophages. We further observed an unexpected similarity between EP300 knockout cells and knockouts for the splicing factor SFPQ, and our results suggest that SFPQ helps maintain the expression of similar genes at the post-transcriptional level as EP300 does at the transcriptional level, which establishes a case of simultaneous regulation across these two layers in macrophages.

Knockouts of JAK-STAT pathway members resulted in reduced ISG expression even in untreated macrophages (0-h time point), which is consistent with our recent study describing broad and diverse transcriptional effects of JAK-STAT signaling in homeostatic T cells and macrophages.[48] But we also observed an opposite effect: several regulator knockouts resulted in a pronounced upregulation of ISGs in untreated macrophages—most notably including the developmental transcription factor SPI1/PU.1, the histone acetyltransferase EP300, and the splicing factor SFPQ. These proteins may thus constitute negative regulators of immune signaling in untreated macrophages, supporting that baseline immune signaling in macrophage homeostasis is a tightly regulated process.

Combining the results of our study, we argue that the unrealized epigenetic potential, the ability to establish relative transcriptional abundance, and the baseline signaling through immune pathways in homeostatic immune cells all contribute to the macrophages' ability to maintain their preparedness for mounting rapid immune responses.

To our knowledge, this is the first study that combines epigenome/transcriptome time-series profiling with high-content CRISPR screening, demonstrated here for the dissection of gene regulation in mouse macrophages. Many of our results are confirmed by prior research, adding confidence to our approach. We also believe that combining these complementary methods in a single study holds the potential for a more integrated and quantitative understanding of gene regulation in mammalian cells. Our manuscript adds to a growing number of perturbational studies in innate immune cells, for example, investigating macrophage polarization,[40] phagocytosis,[49–51] programmed cell death,[15] RNA-binding proteins,[52] long noncoding RNAs,[53] Rab GTPases,[54] TLR-induced TNF alpha response,[55–57] and dendritic cell regulation.[9,58–60]

Potential limitations of our study include: (1) The epigenome/transcriptome time-series profiling covered only the first 24 h and was performed in two biological replicates, as we prioritized dense time points for computational modeling of the temporal dynamics; (2) Our analysis of the CROP-seq data used stringent thresholds across all time points to facilitate data integration, which resulted in the exclusion of many high-quality data points (raw data and source code are provided in the on the

supplementary website); (3) The combination of primary macrophages (for time-series analysis) and a macrophage cell line (for the CROP-seq analysis) comes with advantages as well as disadvantages. We found the cell line much easier to transduce with the CRISPR-Cas9 machinery, making it possible to obtain high cell coverage per perturbation, yet we expect differences, especially regarding their dependence on macrophage differentiation factors (*Spi1*/PU.1 and *Csf1r*/CD115); (4) The *Mixscape* method used for analyzing the CROP-seq experiments excludes perturbations that affect only a small number of genes. As a result, our current analysis (but not the raw data) omits certain knockouts, including the surface receptors *Csf1r*/CD115 and *Fcgr1*/CD64.

Finally, we would like to emphasize the practical utility of the presented experimental and computational approach. Dense epigenome/transcriptome time series can help identify key regulators of the macrophage response, high-content CRISPR screening can rapidly establish the causal effects of knocking out any of the identified regulators, and integrative computational analysis establishes functional similarity among regulators and regulons. We expect that this method will be useful also for cell types other than macrophages and for dissecting disease-associated mechanisms of gene regulation and therapeutic interventions that modulate the immune system.

RESOURCE AVAILABILITY

Lead contact

Further information and requests for resources should be directed to and will be fulfilled by the lead contact, Christoph Bock (cbock@cemm.oeaw.ac.at).

Materials availability

Plasmids generated in this study have been deposited at Addgene (CROFseq-3P5P: #219680).

Data and code availability

- The raw data (RNA-seq and ATAC-seq data as uBAM files and CROP-seq as FASTQ files) and the processed data (RNA-seq and ATAC-seq data as count matrices and CROP-seq data as H5 archives) are available from the NCBI GEO repository (GEO: GSE263763). Accession numbers are listed in the key resources table.
- The source code for data processing and analysis is available as a GitHub repository (https://github.com/epigen/macrophage-regulation) and in a Zenodo archive (https://doi.org/10.5281/zenodo.15262545).
- Any additional information required to reanalyze the data reported in this paper is available from the lead contact upon request.

ACKNOWLEDGMENTS

We thank the Biomedical Sequencing Facility at CeMM for assistance with next generation sequencing, Sophie Zahalka and Sylvia Knapp for providing RAW 264.7-Cas9 cells, Michael Riedelberger and Karl Kuchler for providing Candida albicans SC5314, and Alexander Lercher and Andreas Bergthaler for providing LCMV Clone 13. This study was co-funded by two Austrian Science Fund (FWF) Special Research Program grants (SFB F6102; SFB F7001). In addition, M.F. was supported by an Innovation Fund grant of the Austrian Academy of Sciences (IF_2015_36) and C.B. was supported by an ERC Consolidator Grant (grant agreement no. 101001971) of the European Union's Horizon 2020 research and innovation program.

AUTHOR CONTRIBUTIONS

P.T., S.R., F.H., M.F., and C.B. conceptualized the project with contributions from W.W. and T.D.; P.T. designed and conducted the experiments with contributions from L.S., V.F., A.N., D.P., and A.K.; P.T. and S.R. analyzed the data with contributions from L.F., D.B., N.F., A.F.R., and F.H.; M.F. and C.B. supervised the study; and P.T., S.R., M.F., and C.B. wrote the manuscript with input from all authors.

DECLARATION OF INTERESTS

C.B. is a cofounder and scientific advisor of Myllia Biotechnology and Neurolentech.

STAR★METHODS

Detailed methods are provided in the online version of this paper and include the following:

- KEY RESOURCES TABLE
- EXPERIMENTAL MODEL DETAILS
  - Isolation of cells from bone marrow
  - Cell culture
  - Listeria culture
- METHOD DETAILS
  - Stimulation time course and sampling
  - ATAC-seq
  - RNA-seq
  - Plasmid cloning
  - Library cloning
  - Lentivirus production
  - CROP-seq screening: Cell culture and treatment
  - CROP-seq screening: FACS purification
  - CROP-seq screening: Single-cell sequencing
  - Individual Ep300 knockout experiments
  - Small-molecule inhibition of EP300
  - qPCR measurement and analysis
- QUANTIFICATION AND STATISTICAL ANALYSIS
  - Bioinformatics and data visualization
  - RNA-seq data processing and analysis
  - ATAC-seq data processing and analysis
  - Genome browser tracks
  - Unsupervised time-series analysis
  - Differential gene expression and differential chromatin accessibility time-series analysis
  - Gene set enrichment analysis
  - Integrative analysis of gene expression and chromatin accessibility
  - CRISPR screening data processing and analysis
  - Single-cell perturbation analysis using Mixscape
  - Analysis of perturbation effects using differences in gene expression
  - Inference of functional similarity graphs
  - Enrichment of knockout signatures in temporal regulons of the Listeria response

SUPPLEMENTAL INFORMATION

Supplemental information can be found online at https://doi.org/10.1016/j.cels.2025.101346.

Received: July 2, 2024
Revised: March 17, 2025
Accepted: June 26, 2025
Published: August 8, 2025

REFERENCES

1. Sheu, K.M., and Hoffmann, A. (2022). Functional Hallmarks of Healthy Macrophage Responses: Their Regulatory Basis and Disease Relevance. Annu. Rev. Immunol. *40*, 295–321. https://doi.org/10.1146/annurev-immunol-101320-031555.

2. Rauch, I., Müller, M., and Decker, T. (2013). The regulation of inflammation by interferons and their STATs. JAK-STAT *2*, e23820. https://doi.org/10.4161/jkst.23820.

3. Xue, Q., Lu, Y., Eisele, M.R., Sulistijo, E.S., Khan, N., Fan, R., and Miller-Jensen, K. (2015). Analysis of single-cell cytokine secretion reveals a role for paracrine signaling in coordinating macrophage responses to TLR4 stimulation. Sci. Signal. *8*, ra59. https://doi.org/10.1126/scisignal.aaa2155.

4. Van Eyndhoven, L.C., Singh, A., and Tel, J. (2021). Decoding the dynamics of multilayered stochastic antiviral IFN-I responses. Trends Immunol. *42*, 824–839. https://doi.org/10.1016/j.it.2021.07.004.

5. Tong, A.-J., Liu, X., Thomas, B.J., Lissner, M.M., Baker, M.R., Senagolage, M.D., Allred, A.L., Barish, G.D., and Smale, S.T. (2016). A Stringent Systems Approach Uncovers Gene-Specific Mechanisms Regulating Inflammation. Cell *165*, 165–179. https://doi.org/10.1016/j.cell.2016.01.020.

6. Cheng, C.S., Behar, M.S., Suryawanshi, G.W., Feldman, K.E., Spreafico, R., and Hoffmann, A. (2017). Iterative Modeling Reveals Evidence of Sequential Transcriptional Control Mechanisms. Cell Syst. *4*, 330–343. e5. https://doi.org/10.1016/j.cels.2017.01.012.

7. Cheng, Q., Behzadi, F., Sen, S., Ohta, S., Spreafico, R., Teles, R., Modlin, R.L., and Hoffmann, A. (2019). Sequential conditioning-stimulation reveals distinct gene- and stimulus-specific effects of Type I and II IFN on human macrophage functions. Sci. Rep. *9*, 5288. https://doi.org/10.1038/s41598-019-40503-y.

8. Garber, M., Yosef, N., Goren, A., Raychowdhury, R., Thielke, A., Guttman, M., Robinson, J., Minie, B., Chevrier, N., Itzhaki, Z., et al. (2012). A High-Throughput Chromatin Immunoprecipitation Approach Reveals Principles of Dynamic Gene Regulation in Mammals. Mol. Cell *47*, 810–822. https://doi.org/10.1016/j.molcel.2012.07.030.

9. Amit, I., Garber, M., Chevrier, N., Leite, A.P., Donner, Y., Eisenhaure, T., Guttman, M., Grenier, J.K., Li, W., Zuk, O., et al. (2009). Unbiased Reconstruction of a Mammalian Transcriptional Network Mediating Pathogen Responses. Science *326*, 257–263. https://doi.org/10.1126/science.1179050.

10. Ramirez-Carrozzi, V.R., Braas, D., Bhatt, D.M., Cheng, C.S., Hong, C., Doty, K.R., Black, J.C., Hoffmann, A., Carey, M., and Smale, S.T. (2009). A Unifying Model for the Selective Regulation of Inducible Transcription by CpG Islands and Nucleosome Remodeling. Cell *138*, 114–128. https://doi.org/10.1016/j.cell.2009.04.020.

11. Kaikkonen, M.U., Spann, N.J., Heinz, S., Romanoski, C.E., Allison, K.A., Stender, J.D., Chun, H.B., Tough, D.F., Prinjha, R.K., Benner, C., et al. (2013). Remodeling of the Enhancer Landscape during Macrophage Activation Is Coupled to Enhancer Transcription. Mol. Cell *51*, 310–325. https://doi.org/10.1016/j.molcel.2013.07.010.

12. Ostuni, R., Piccolo, V., Barozzi, I., Polletti, S., Termanini, A., Bonifacio, S., Curina, A., Prosperini, E., Ghisletti, S., and Natoli, G. (2013). Latent Enhancers Activated by Stimulation in Differentiated Cells. Cell *152*, 157–171. https://doi.org/10.1016/j.cell.2012.12.018.

13. Hargreaves, D.C., Horng, T., and Medzhitov, R. (2009). Control of Inducible Gene Expression by Signal-Dependent Transcriptional Elongation. Cell *138*, 129–145. https://doi.org/10.1016/j.cell.2009.05.047.

14. Lin, D., Xu, W., Hong, P., Wu, C., Zhang, Z., Zhang, S., Xing, L., Yang, B., Zhou, W., Xiao, Q., et al. (2022). Decoding the spatial chromatin organization and dynamic epigenetic landscapes of macrophage cells during differentiation and immune activation. Nat. Commun. *13*, 5857. https://doi.org/10.1038/s41467-022-33558-5.

15. Malireddi, R.K.S., Bynigeri, R.R., Mall, R., Nadendla, E.K., Connelly, J.P., Pruett-Miller, S.M., and Kanneganti, T.-D. (2023). Whole-genome CRISPR screen identifies RAVER1 as a key regulator of RIPK1-mediated inflammatory cell death, PANoptosis. iScience *26*, 106938. https://doi.org/10.1016/j.isci.2023.106938.

16. Ramirez-Carrozzi, V.R., Nazarian, A.A., Li, C.C., Gore, S.L., Sridharan, R., Imbalzano, A.N., and Smale, S.T. (2006). Selective and antagonistic functions of SWI/SNF and Mi-2β nucleosome remodeling complexes during an inflammatory response. Genes Dev. *20*, 282–296. https://doi.org/10.1101/gad.1383206.

17. Nau, G.J., Richmond, J.F.L., Schlesinger, A., Jennings, E.G., Lander, E.S., and Young, R.A. (2002). Human macrophage activation programs induced by bacterial pathogens. Proc. Natl. Acad. Sci. USA *99*, 1503–1508. https://doi.org/10.1073/pnas.022649799.

18. Xue, J., Schmidt, S.V., Sander, J., Draffehn, A., Krebs, W., Quester, I., De Nardo, D., Gohel, T.D., Emde, M., Schmidleithner, L., et al. (2014). Transcriptome-Based Network Analysis Reveals a Spectrum Model of Human Macrophage Activation. Immunity *40*, 274–288. https://doi.org/10.1016/j.immuni.2014.01.006.

19. Singh, A., Sen, S., Iter, M., Adelaja, A., Luecke, S., Guo, X., and Hoffmann, A. (2024). Stimulus-response signaling dynamics characterize macrophage polarization states. Cell Syst. *15*, 563–577.e6. https://doi.org/10.1016/j.cels.2024.05.002.

20. Shalek, A.K., Satija, R., Shuga, J., Trombetta, J.J., Gennert, D., Lu, D., Chen, P., Gertner, R.S., Gaublomme, J.T., Yosef, N., et al. (2014). Single-cell RNA-seq reveals dynamic paracrine control of cellular variation. Nature *510*, 363–369. https://doi.org/10.1038/nature13437.

21. Bock, C., Datlinger, P., Chardon, F., Coelho, M.A., Dong, M.B., Lawson, K.A., Lu, T., Maroc, L., Norman, T.M., Song, B., et al. (2022). High-content CRISPR screening. Nat Rev Methods Prim. *2*, 8. https://doi.org/10.1038/s43586-021-00093-4.

22. Datlinger, P., Rendeiro, A.F., Schmidl, C., Krausgruber, T., Traxler, P., Klughammer, J., Schuster, L.C., Kuchler, A., Alpar, D., and Bock, C. (2017). Pooled CRISPR screening with single-cell transcriptome readout. Nat. Methods *14*, 297–301. https://doi.org/10.1038/nmeth.4177.

23. Moll, P., Ante, M., Seitz, A., and Reda, T. (2014). QuantSeq 3′ mRNA sequencing for RNA quantification. Nat. Methods *11*. i–iii. https://doi.org/10.1038/nmeth.f.376.

24. Buenrostro, J.D., Giresi, P.G., Zaba, L.C., Chang, H.Y., and Greenleaf, W.J. (2013). Transposition of native chromatin for fast and sensitive epigenomic profiling of open chromatin, DNA-binding proteins and nucleosome position. Nat. Methods *10*, 1213–1218. https://doi.org/10.1038/nmeth.2688.

25. Buenrostro, J.D., Wu, B., Chang, H.Y., and Greenleaf, W.J. (2015). ATAC-seq: A Method for Assaying Chromatin Accessibility Genome-Wide. Curr. Protoc. Mol. Biol. *109*, 21.29.1–21.29.9. https://doi.org/10.1002/0471142727.mb2129s109.

26. Eitel, J., Suttorp, N., and Opitz, B. (2010). Innate immune recognition and inflammasome activation in listeria monocytogenes infection. Front. Microbiol. *1*, 149. https://doi.org/10.3389/fmicb.2010.00149.

27. Takeuchi, O., and Akira, S. (2008). MDA5/RIG-I and virus recognition. Curr. Opin. Immunol. *20*, 17–22. https://doi.org/10.1016/j.coi.2008.01.002.

28. Ifrim, D.C., Quintin, J., Courjol, F., Verschueren, I., van Krieken, J.H., Koentgen, F., Fradin, C., Gow, N.A.R., Joosten, L.A.B., van der Meer, J.W.M., et al. (2016). The Role of Dectin-2 for Host Defense Against Disseminated Candidiasis. J. Interferon Cytokine Res. *36*, 267–276. https://doi.org/10.1089/jir.2015.0040.

29. Lu, Y.-C., Yeh, W.-C., and Ohashi, P.S. (2008). LPS/TLR4 signal transduction pathway. Cytokine *42*, 145–151. https://doi.org/10.1016/j.cyto.2008.01.006.

30. Platanias, L.C. (2005). Mechanisms of type-I- and type-II-interferon-mediated signalling. Nat. Rev. Immunol. *5*, 375–386. https://doi.org/10.1038/nri1604.

31. Russell, D.G., Huang, L., and VanderVen, B.C. (2019). Immunometabolism at the interface between macrophages and pathogens. Nat. Rev. Immunol. *19*, 291–304. https://doi.org/10.1038/s41577-019-0124-9.

32. Matsuda, S., Kawamoto, K., Miyamoto, K., Tsuji, A., and Yuasa, K. (2017). PCTK3/CDK18 regulates cell migration and adhesion by negatively modulating FAK activity. Sci. Rep. *7*, 45545. https://doi.org/10.1038/srep45545.

33. Krausgruber, T., Fortelny, N., Fife-Gernedl, V., Senekowitsch, M., Schuster, L.C., Lercher, A., Nemc, A., Schmidl, C., Rendeiro, A.F.,

Bergthaler, A., et al. (2020). Structural cells are key regulators of organ-specific immune responses. Nature *583*, 296–302. https://doi.org/10.1038/s41586-020-2424-4.

34. Mimitou, E.P., Cheng, A., Montalbano, A., Hao, S., Stoeckius, M., Legut, M., Roush, T., Herrera, A., Papalexi, E., Ouyang, Z., et al. (2019). Multiplexed detection of proteins, transcriptomes, clonotypes and CRISPR perturbations in single cells. Nat. Methods *16*, 409–412. https://doi.org/10.1038/s41592-019-0392-0.

35. Platanitis, E., Demiroz, D., Schneller, A., Fischer, K., Capelle, C., Hartl, M., Gossenreiter, T., Müller, M., Novatchkova, M., and Decker, T. (2019). A molecular switch from STAT2-IRF9 to ISGF3 underlies interferon-induced gene transcription. Nat. Commun. *10*, 2921. https://doi.org/10.1038/s41467-019-10970-y.

36. Karpurapu, M., Wang, X., Deng, J., Park, H., Xiao, L., Sadikot, R.T., Frey, R.S., Maus, U.A., Park, G.Y., Scott, E.W., et al. (2011). Functional PU.1 in macrophages has a pivotal role in NF-κB activation and neutrophilic lung inflammation during endotoxemia. Blood *118*, 5255–5266. https://doi.org/10.1182/blood-2011-03-341123.

37. Ueno, N., Nishimura, N., Ueno, S., Endo, S., Tatetsu, H., Hirata, S., Hata, H., Matsuoka, M., Mitsuya, H., and Okuno, Y. (2017). PU.1 acts as tumor suppressor for myeloma cells through direct transcriptional repression of IRF4. Oncogene *36*, 4481–4497. https://doi.org/10.1038/onc.2017.79.

38. Papalexi, E., Mimitou, E.P., Butler, A.W., Foster, S., Bracken, B., Mauck, W.M., III, Wessels, H.-H., Hao, Y., Yeung, B.Z., Smibert, P., et al. (2021). Characterizing the molecular regulation of inhibitory immune checkpoints with multimodal single-cell screens. Nat. Genet. *53*, 322–331. https://doi.org/10.1038/s41588-021-00778-2.

39. Wu, J., Han, Y., Xu, H., Sun, H., Wang, R., Ren, H., and Wang, G. (2023). Deficient chaperone-mediated autophagy facilitates LPS-induced microglial activation via regulation of the p300/NF-κB/NLRP3 pathway. Sci. Adv. *9*, eadi8343. https://doi.org/10.1126/sciadv.adi8343.

40. Surdziel, E., Clay, I., Nigsch, F., Thiemeyer, A., Allard, C., Hoffman, G., Reece-Hoyes, J.S., Phadke, T., Gambert, R., Keller, C.G., et al. (2017). Multidimensional pooled shRNA screens in human THP-1 cells identify candidate modulators of macrophage polarization. PLoS One *12*, e0183679. https://doi.org/10.1371/journal.pone.0183679.

41. Chang, H.-M., Paulson, M., Holko, M., Rice, C.M., Williams, B.R.G., Marié, I., and Levy, D.E. (2004). Induction of interferon-stimulated gene expression and antiviral responses require protein deacetylase activity. Proc. Natl. Acad. Sci. USA *101*, 9578–9583. https://doi.org/10.1073/pnas.0400567101.

42. Marié, I.J., Chang, H.-M., and Levy, D.E. (2018). HDAC stimulates gene expression through BRD4 availability in response to IFN and in interferonopathies. J. Exp. Med. *215*, 3194–3212. https://doi.org/10.1084/jem.20180520.

43. Oh, K.-S., Gottschalk, R.A., Lounsbury, N.W., Sun, J., Dorrington, M.G., Baek, S., Sun, G., Wang, Z., Krauss, K.S., Milner, J.D., et al. (2018). Dual Roles for Ikaros in Regulation of Macrophage Chromatin State and Inflammatory Gene Expression. J. Immunol. *201*, 757–771. https://doi.org/10.4049/jimmunol.1800158.

44. Ma, H., Han, P., Ye, W., Chen, H., Zheng, X., Cheng, L., Zhang, L., Yu, L., Wu, X., Xu, Z., et al. (2017). The Long Noncoding RNA NEAT1 Exerts Antihantaviral Effects by Acting as Positive Feedback for RIG-I Signaling. J. Virol. *91*, e02250-16. https://doi.org/10.1128/JVI.02250-16.

45. Imamura, K., Imamachi, N., Akizuki, G., Kumakura, M., Kawaguchi, A., Nagata, K., Kato, A., Kawaguchi, Y., Sato, H., Yoneda, M., et al. (2014). Long Noncoding RNA NEAT1-Dependent SFPQ Relocation from Promoter Region to Paraspeckle Mediates IL8 Expression upon Immune Stimuli. Mol. Cell *53*, 393–406. https://doi.org/10.1016/j.molcel.2014.01.009.

46. Wienerroither, S., Shukla, P., Farlik, M., Majoros, A., Stych, B., Vogl, C., Cheon, H., Stark, G.R., Strobl, B., Müller, M., et al. (2015). Cooperative Transcriptional Activation of Antimicrobial Genes by STAT and NF-κB Pathways by Concerted Recruitment of the Mediator Complex. Cell Rep. *12*, 300–312. https://doi.org/10.1016/j.celrep.2015.06.021.

47. Cuartero, S., Weiss, F.D., Dharmalingam, G., Guo, Y., Ing-Simmons, E., Masella, S., Robles-Rebollo, I., Xiao, X., Wang, Y.-F., Barozzi, I., et al. (2018). Control of inducible gene expression links cohesin to hematopoietic progenitor self-renewal and differentiation. Nat. Immunol. *19*, 932–941. https://doi.org/10.1038/s41590-018-0184-1.

48. Fortelny, N., Farlik, M., Fife, V., Gorki, A.-D., Lassnig, C., Maurer, B., Meissl, K., Dolezal, M., Boccuni, L., Ravi Sundar Jose Geetha, A., et al. (2024). JAK-STAT signaling maintains homeostasis in T cells and macrophages. Nat. Immunol. *25*, 847–859. https://doi.org/10.1038/s41590-024-01804-1.

49. Glover, R.C., Schwardt, N.H., Leano, S.E., Sanchez, M.E., Thomason, M.K., Olive, A.J., and Reniere, M.L. (2023). A genome-wide screen in macrophages identifies PTEN as required for myeloid restriction of Listeria monocytogenes infection. PLoS Pathog. *19*, e1011058. https://doi.org/10.1371/journal.ppat.1011058.

50. Haney, M.S., Bohlen, C.J., Morgens, D.W., Ousey, J.A., Barkal, A.A., Tsui, C.K., Ego, B.K., Levin, R., Kamber, R.A., Collins, H., et al. (2018). Identification of phagocytosis regulators using magnetic genome-wide CRISPR screens. Nat. Genet. *50*, 1716–1727. https://doi.org/10.1038/s41588-018-0254-1.

51. Shi, J., Wu, X., Wang, Z., Li, F., Meng, Y., Moore, R.M., Cui, J., Xue, C., Croce, K.R., Yurdagul, A., et al. (2022). A genome-wide CRISPR screen identifies WDFY3 as a regulator of macrophage efferocytosis. Nat. Commun. *13*, 7929. https://doi.org/10.1038/s41467-022-35604-8.

52. Tong, J., Wang, X., Liu, Y., Ren, X., Wang, A., Chen, Z., Yao, J., Mao, K., Liu, T., Meng, F.-L., et al. (2021). Pooled CRISPR screening identifies m^6A as a positive regulator of macrophage activation. Sci. Adv. *7*, eabd4742. https://doi.org/10.1126/sciadv.abd4742.

53. Halasz, H., Malekos, E., Covarrubias, S., Yitiz, S., Montano, C., Sudek, L., Katzman, S., Liu, S.J., Horlbeck, M.A., Namvar, L., et al. (2024). CRISPRi screens identify the lncRNA, *LOUP*, as a multifunctional locus regulating macrophage differentiation and inflammatory signaling. Proc. Natl. Acad. Sci. USA *121*, e2322524121. https://doi.org/10.1073/pnas.2322524121.

54. Solano-Collado, V., Colamarino, R.A., Calderwood, D.A., Baldassarre, M., and Spanò, S. (2021). A Small-Scale shRNA Screen in Primary Mouse Macrophages Identifies a Role for the Rab GTPase Rab1b in Controlling Salmonella Typhi Growth. Front. Cell. Infect. Microbiol. *11*, 660689. https://doi.org/10.3389/fcimb.2021.660689.

55. Sun, J., Katz, S., Dutta, B., Wang, Z., and Fraser, I.D.C. (2017). Genome-wide siRNA screen of genes regulating the LPS-induced TNF-α response in human macrophages. Sci. Data *4*, 170007. https://doi.org/10.1038/sdata.2017.7.

56. Sun, J., Li, N., Oh, K.-S., Dutta, B., Vayttaden, S.J., Lin, B., Ebert, T.S., De Nardo, D.D., Davis, J., Bagirzadeh, R., et al. (2016). Comprehensive RNAi-based screening of human and mouse TLR pathways identifies *species-specific preferences in signaling protein use*. Sci. Signal. *9*, ra3. https://doi.org/10.1126/scisignal.aab2191.

57. Li, N., Katz, S., Dutta, B., Benet, Z.L., Sun, J., and Fraser, I.D.C. (2017). Genome-wide siRNA screen of genes regulating the LPS-induced NF-κB and TNF-α responses in mouse macrophages. Sci. Data *4*, 170008. https://doi.org/10.1038/sdata.2017.8.

58. Jaitin, D.A., Weiner, A., Yofe, I., Lara-Astiaso, D., Keren-Shaul, H., David, E., Salame, T.M., Tanay, A., Van Oudenaarden, A., and Amit, I. (2016). Dissecting Immune Circuits by Linking CRISPR-Pooled Screens with Single-Cell RNA-Seq. Cell *167*, 1883–1896.e15. https://doi.org/10.1016/j.cell.2016.11.039.

59. Parnas, O., Jovanovic, M., Eisenhaure, T.M., Herbst, R.H., Dixit, A., Ye, C.J., Przybylski, D., Platt, R.J., Tirosh, I., Sanjana, N.E., et al. (2015). A Genome-wide CRISPR Screen in Primary Immune Cells to Dissect Regulatory Networks. Cell *162*, 675–686. https://doi.org/10.1016/j.cell.2015.06.059.

60. Geiger-Schuller, K., Eraslan, B., Kuksenko, O., Dey, K.K., Jagadeesh, K.A., Thakore, P.I., Karayel, O., Yung, A.R., Rajagopalan, A., Meireles, A.M., et al. (2023) Systematically Characterizing the Roles of E3-Ligase Family Members in Inflammatory Responses with Massively Parallel

Perturb-Seq. Preprint at bioRxiv. https://doi.org/10.1101/2023.01.23.525198.

61. Boccuni, L., Podgorschek, E., Schmiedeberg, M., Platanitis, E., Traxler, P., Fischer, P., Schirripa, A., Novoszel, P., Nebreda, A.R., Arthur, J.S.C., et al. (2022). Stress signaling boosts interferon-induced gene transcription in macrophages. Sci. Signal. *15*, eabq5389. https://doi.org/10.1126/scisignal.abq5389.
62. Reichl, S., Ergüner, B., Barreca, D., Folkman, L., Zhao, F., ter Horst, R., Dobnikar, L., and Bock, C. (2022) Ultimate ATAC-Seq Data Processing & Analysis Pipeline. https://doi.org/10.5281/zenodo.6323634.
63. Reichl, S., Romanovskaia, D., ter Horst, R., and Bock, C. (2024) Genomic Region Set & (Ranked) Gene Set Enrichment Analysis & Visualization Workflow for Human and Mouse Genomes. https://doi.org/10.5281/zenodo.7810621.
64. Reichl, S., Bednarsky, R., and Bock, C. (2024) Unsupervised Analysis Workflow. https://doi.org/10.5281/zenodo.8405360.
65. Reichl, S., and Bock, C. (2024) Genome Browser Track Visualization Workflow. https://doi.org/10.5281/zenodo.10849097.
66. Köster, J., Forster, J., Schmeier, S., Salazar, V., and matrs. (2021) Snakemake-Workflows/rna-seq-Star-deseq2, [Version 1.2.0]. https://doi.org/10.5281/zenodo.5245549.
67. Mölder, F., Jablonski, K.P., Letcher, B., Hall, M.B., Tomkins-Tinch, C.H., Sochat, V., Forster, J., Lee, S., Twardziok, S.O., Kanitz, A., et al. (2021). Sustainable data analysis with Snakemake. F1000Res *10*, 33. https://doi.org/10.12688/f1000research.29032.2.
68. Hao, Y., Hao, S., Andersen-Nissen, E., Mauck, W.M., III, Zheng, S., Butler, A., Lee, M.J., Wilk, A.J., Darby, C., Zager, M., et al. (2021). Integrated analysis of multimodal single-cell data. Cell *184*, 3573–3587. e29. https://doi.org/10.1016/j.cell.2021.04.048.
69. Ritchie, M.E., Phipson, B., Wu, D., Hu, Y., Law, C.W., Shi, W., and Smyth, G.K. (2015). limma powers differential expression analyses for RNA-sequencing and microarray studies. Nucleic Acids Res. *43*, e47. https://doi.org/10.1093/nar/gkv007.
70. Aibar, S., González-Blas, C.B., Moerman, T., Huynh-Thu, V.A., Imrichova, H., Hulselmans, G., Rambow, F., Marine, J.-C., Geurts, P., Aerts, J., et al. (2017). SCENIC: single-cell regulatory network inference and clustering. Nat. Methods *14*, 1083–1086. https://doi.org/10.1038/nmeth.4463.
71. Szklarczyk, D., Gable, A.L., Nastou, K.C., Lyon, D., Kirsch, R., Pyysalo, S., Doncheva, N.T., Legeay, M., Fang, T., Bork, P., et al. (2021). The STRING database in 2021: customizable protein–protein networks, and functional characterization of user-uploaded gene/measurement sets. Nucleic Acids Res. *49*, D605–D612. https://doi.org/10.1093/nar/gkaa1074.
72. McInnes, L., Healy, J., and Melville, J. (2018). UMAP: Uniform Manifold Approximation and Projection for Dimension Reduction. Preprint at arXiv. https://arxiv.org/abs/1802.03426.
73. Fang, Z., Liu, X., and Peltz, G. (2023). GSEApy: a comprehensive package for performing gene set enrichment analysis in Python. Bioinformatics *39*, btac757. https://doi.org/10.1093/bioinformatics/btac757.
74. Lopez-deLisle, L., Rabbani, L., Wolff, J., Bhardwaj, V., Backofen, R., Grüning, B., Ramírez, F., and Manke, T. (2021). pyGenomeTracks: reproducible plots for multivariate genomic datasets. Bioinformatics *37*, 422–423. https://doi.org/10.1093/bioinformatics/btaa692.
75. Guha, N., Baladandayuthapani, V., and Mallick, B.K. (2020). Quantile Graphical Models: Bayesian Approaches. J. Mach. Learn. Res. *21*, 1–47. https://github.com/tslearn-team/tslearn.
76. Pedregosa, F., Varoquaux, G., Gramfort, A., Michel, V., Thirion, B., Grisel, O., Blondel, M., Prettenhofer, P., Weiss, R., Dubourg, V., et al. (2011). Scikit-learn: Machine Learning in Python. J. Mach. Learn. Res. *12*, 2825–2830. http://jmlr.org/papers/v12/pedregosa11a.html.
77. Kolde, R. (2019). Pheatmap: Pretty Heatmaps. https://cran.r-project.org/web/packages/pheatmap/index.html.
78. Wickham, H. (2009). ggplot2: Elegant Graphics for Data Analysis (Springer-Verlag New York). https://doi.org/10.1007/978-0-387-98141-3.
79. Blighe, K., Rana, S., and Lewis, M. (2021). EnhancedVolcano: publication-ready volcano plots with enhanced colouring and labeling. https://bioconductor.org/packages/release/bioc/html/EnhancedVolcano.html.
80. Hansen, K.D., Irizarry, R.A., and Wu, Z. (2012). Removing technical variability in RNA-seq data using conditional quantile normalization. Biostatistics *13*, 204–216. https://doi.org/10.1093/biostatistics/kxr054.
81. Gu, Z., and Huebschmann, D. (2017). rGREAT. (Bioconductor). https://doi.org/10.18129/B9.bioc.rGREAT.
82. Gu, Z., Gu, L., Eils, R., Schlesner, M., and Brors, B. (2014). *circlize* implements and enhances circular visualization in R. Bioinformatics *30*, 2811–2812. https://doi.org/10.1093/bioinformatics/btu393.
83. Michlits, G., Jude, J., Hinterndorfer, M., de Almeida, M., Vainorius, G., Hubmann, M., Neumann, T., Schleiffer, A., Burkard, T.R., Fellner, M., et al. (2020). Multilayered VBC score predicts sgRNAs that efficiently generate loss-of-function alleles. Nat. Methods *17*, 708–716. https://doi.org/10.1038/s41592-020-0850-8.
84. Morgens, D.W., Wainberg, M., Boyle, E.A., Ursu, O., Araya, C.L., Tsui, C.K., Haney, M.S., Hess, G.T., Han, K., Jeng, E.E., et al. (2017). Genome-scale measurement of off-target activity using Cas9 toxicity in high-throughput screens. Nat. Commun. *8*, 15178. https://doi.org/10.1038/ncomms15178.
85. Ye, J., Coulouris, G., Zaretskaya, I., Cutcutache, I., Rozen, S., and Madden, T.L. (2012). Primer-BLAST: A tool to design target-specific primers for polymerase chain reaction. BMC Bioinformatics *13*, 134. https://doi.org/10.1186/1471-2105-13-134.
86. Sun, Y., Zuo, Z., and Kuang, Y. (2021). Prolactin-Releasing Peptide Differentially Regulates Gene Transcriptomic Profiles in Mouse Bone Marrow-Derived Macrophages. Int. J. Mol. Sci. *22*, 4456. https://doi.org/10.3390/ijms22094456.
87. Pfaffl, M.W. (2001). A new mathematical model for relative quantification in real-time RT-PCR. Nucleic Acids Res. *29*, e45. https://doi.org/10.1093/nar/29.9.e45.
88. R Core Team (2021). R: A Language and Environment for Statistical Computing (R Foundation for Statistical Computing). https://www.R-project.org/.
89. van Rossum, G. (1995). Python reference manual (Centrum voor Wiskunde en Informatica Amsterdam). https://ir.cwi.nl/pub/5008.
90. Reback, J., McKinney, W., jbrockmendel, Van den Bossche, J., Augspurger, T., Cloud, P., Gfyoung, Sinhrks, Hawkins, S., Klein, A., et al. (2020). pandas-dev/pandas: Pandas 1.1.3. Zenodo. https://doi.org/10.5281/zenodo.4067057.
91. Picard Toolkit (2019). Picard Toolkit [Version 2.19.2] (Broad Institute). https://broadinstitute.github.io/picard/.
92. Dobin, A., Davis, C.A., Schlesinger, F., Drenkow, J., Zaleski, C., Jha, S., Batut, P., Chaisson, M., and Gingeras, T.R. (2013). STAR: ultrafast universal RNA-seq aligner. Bioinformatics *29*, 15–21. https://doi.org/10.1093/bioinformatics/bts635.
93. Howe, K.L., Achuthan, P., Allen, J., Allen, J., Alvarez-Jarreta, J., Amode, M.R., Armean, I.M., Azov, A.G., Bennett, R., Bhai, J., et al. (2021). Ensembl 2021. Nucleic Acids Res. *49*, D884–D891. https://doi.org/10.1093/nar/gkaa942.
94. Ewels, P., Magnusson, M., Lundin, S., and Käller, M. (2016). MultiQC: summarize analysis results for multiple tools and samples in a single report. Bioinformatics *32*, 3047–3048. https://doi.org/10.1093/bioinformatics/btw354.
95. Robinson, M.D., McCarthy, D.J., and Smyth, G.K. (2010). edgeR: a Bioconductor package for differential expression analysis of digital gene expression data. Bioinformatics *26*, 139–140. https://doi.org/10.1093/bioinformatics/btp616.
96. Durinck, S., Spellman, P.T., Birney, E., and Huber, W. (2009). Mapping identifiers for the integration of genomic datasets with the R/Bioconductor package biomaRt. Nat. Protoc. *4*, 1184–1191. https://doi.org/10.1038/nprot.2009.97.

97. Chen, S., Zhou, Y., Chen, Y., and Gu, J. (2018). fastp: an ultra-fast all-in-one FASTQ preprocessor. Bioinformatics *34*, i884–i890. https://doi.org/10.1093/bioinformatics/bty560.

98. Langmead, B., and Salzberg, S.L. (2012). Fast gapped-read alignment with Bowtie 2. Nat. Methods *9*, 357–359. https://doi.org/10.1038/nmeth.1923.

99. Faust, G.G., and Hall, I.M. (2014). *SAMBLASTER*: fast duplicate marking and structural variant read extraction. Bioinformatics *30*, 2503–2505. https://doi.org/10.1093/bioinformatics/btu314.

100. Amemiya, H.M., Kundaje, A., and Boyle, A.P. (2019). The ENCODE Blacklist: Identification of Problematic Regions of the Genome. Sci. Rep. *9*, 9354. https://doi.org/10.1038/s41598-019-45839-z.

101. Li, H., Handsaker, B., Wysoker, A., Fennell, T., Ruan, J., Homer, N., Marth, G., Abecasis, G., and Durbin, R.; 1000 Genome Project Data Processing Subgroup (2009). The Sequence Alignment/Map format and SAMtools. Bioinformatics *25*, 2078–2079. https://doi.org/10.1093/bioinformatics/btp352.

102. Zhang, Y., Liu, T., Meyer, C.A., Eeckhoute, J., Johnson, D.S., Bernstein, B.E., Nusbaum, C., Myers, R.M., Brown, M., Li, W., et al. (2008). Model-based Analysis of ChIP-Seq (MACS). Genome Biol. *9*, R137. https://doi.org/10.1186/gb-2008-9-9-r137.

103. Quinlan, A.R., and Hall, I.M. (2010). BEDTools: a flexible suite of utilities for comparing genomic features. Bioinformatics *26*, 841–842. https://doi.org/10.1093/bioinformatics/btq033.

104. Dale, R.K., Pedersen, B.S., and Quinlan, A.R. (2011). Pybedtools: a flexible Python library for manipulating genomic datasets and annotations. Bioinformatics *27*, 3423–3424. https://doi.org/10.1093/bioinformatics/btr539.

105. Heinz, S., Benner, C., Spann, N., Bertolino, E., Lin, Y.C., Laslo, P., Cheng, J.X., Murre, C., Singh, H., and Glass, C.K. (2010). Simple combinations of lineage-determining transcription factors prime cis-regulatory elements required for macrophage and B cell identities. Mol. Cell *38*, 576–589. https://doi.org/10.1016/j.molcel.2010.05.004.

106. Ramírez, F., Ryan, D.P., Grüning, B., Bhardwaj, V., Kilpert, F., Richter, A.S., Heyne, S., Dündar, F., and Manke, T. (2016). deepTools2: a next generation web server for deep-sequencing data analysis. Nucleic Acids Res. *44*, W160–W165. https://doi.org/10.1093/nar/gkw257.

107. Pearson, K. (1901). LIII. On lines and planes of closest fit to systems of points in space. Lond. Edinb. Dublin Philos. Mag. J. Sci. *2*, 559–572. https://doi.org/10.1080/14786440109462720.

108. Smyth, G.K. (2005). limma: Linear Models for Microarray Data. In Bioinformatics and Computational Biology Solutions Using R and Bioconductor, R. Gentleman, V.J. Carey, W. Huber, R.A. Irizarry, and S. Dudoit, eds. (Springer-Verlag), pp. 397–420. https://doi.org/10.1007/0-387-29362-0_23.

109. Kuleshov, M.V., Jones, M.R., Rouillard, A.D., Fernandez, N.F., Duan, Q., Wang, Z., Koplev, S., Jenkins, S.L., Jagodnik, K.M., Lachmann, A., et al. (2016). Enrichr: a comprehensive gene set enrichment analysis web server 2016 update. Nucleic Acids Res. *44*, W90–W97. https://doi.org/10.1093/nar/gkw377.

110. McLean, C.Y., Bristor, D., Hiller, M., Clarke, S.L., Schaar, B.T., Lowe, C.B., Wenger, A.M., and Bejerano, G. (2010). GREAT improves functional interpretation of cis-regulatory regions. Nat. Biotechnol. *28*, 495–501. https://doi.org/10.1038/nbt.1630.

111. Lawrence, M., Huber, W., Pagès, H., Aboyoun, P., Carlson, M., Gentleman, R., Morgan, M.T., and Carey, V.J. (2013). Software for Computing and Annotating Genomic Ranges. PLoS Comp. Biol. *9*, e1003118. https://doi.org/10.1371/journal.pcbi.1003118.

112. Hafemeister, C., and Satija, R. (2019). Normalization and variance stabilization of single-cell RNA-seq data using regularized negative binomial regression. Genome Biol. *20*, 296. https://doi.org/10.1186/s13059-019-1874-1.

113. Blake, J.A., Baldarelli, R., Kadin, J.A., Richardson, J.E., Smith, C.L., and Bult, C.J.; Mouse Genome Database Group (2021). Mouse Genome Database (MGD): Knowledgebase for mouse–human comparative biology. Nucleic Acids Res. *49*, D981–D987. https://doi.org/10.1093/nar/gkaa1083.

114. Butts, C.T. (2008). Social Network Analysis with sna. J. Stat. Software *24*. https://doi.org/10.18637/jss.v024.i06.

CellPress OPEN ACCESS

Cell Systems
Methods

STAR★METHODS

KEY RESOURCES TABLE

REAGENT or RESOURCE	SOURCE	IDENTIFIER
Antibodies		
TotalSeq-C antibodies	BioLegend	See Table S6 -Antibodies
Bacterial and virus strains		
Listeria monocytogenes (LO28)	Thomas Decker Lab	N/A
Candida albicans (SC5314, UV-killed)	Karl Kuchler Lab	N/A
Lymphocytic choriomeningitis virus (Clone 13)	Andreas Bergthaler Lab	N/A
Chemicals, peptides, and recombinant proteins		
SGC-CBP30	MedChemExpress	Cat #: HY-15826
A-485	MedChemExpress	Cat #: HY-107455
Murine M-CSF	Peprotech	Cat #: 315-02
LPS	Merck	Cat #: L4641
IFN-beta	PBL Assay Science	Cat #: 12401-1
IFN-gamma	Peprotech	Cat #: 315-05
Critical commercial assays		
QuantSeq	Lexogen	Cat #: 015.96
scRNA-seq (Chromium Next GEM Single Cell 5′ v2 Dual Indexing Kit with Feature Barcoding)	10x Genomics	Cat #:1000263
Deposited data		
SuperSeries containing all data described below	This paper	GEO: GSE263763
Epigenome ATAC-seq time series	This paper	GEO: GSE263758
Transcriptome RNA-seq time series	This paper	GEO: GSE263759
Proof-of-concept CROP-seq KO15 screen	This paper	GEO: GSE263760
Upscaled CROP-seq KO150 screen	This paper	GEO: GSE263761
Experimental models: Cell lines		
Murine: RAW 264.7-Cas9 (transduced with Addgene plasmid #52962)	Sylvia Knapp Lab	N/A
Human: Lenti-X 293T	Takara	Cat #: 632180
Experimental models: Organisms/strains		
Mice (STOCK Gt(ROSA)26Sortm1.1 (CAG-cas9*,-EGFP)Fezh/J)	Jackson Laboratory	Strain #:024858 RRID: IMSR_JAX:024858
Oligonucleotides		
Sequencing primers	This paper	See Table S6 Sequencing_primer
Cloning components for CROPseq-3P5P	This paper	See Table S6 CROPseq-3P5P_cloning
gRNA sequences for cloning into CROPseq-3P5P	This paper	See Table S6 KO15/KO150/Individual_gRNAs
qPCR primers	This paper	See Table S6 qPCR_primer
Recombinant DNA		
Plasmid: CROPseq-Guide-Puro-mCherry2	Boccuni et al.[61]	Addgene: #219679; RRID: Addgene_219679
Plasmid: CROPseq-3P5P	This paper	Addgene: #219680; RRID: Addgene_219680
Software and algorithms		
Source code and software specifications to reproduce results and figures (as Zenodo archive)	This paper	https://doi.org/10.5281/zenodo.15262545
ATAC-seq Snakemake workflow (v0.1.0)	Reichl et al.[62]	https://doi.org/10.5281/zenodo.6323634
Enrichment analysis Snakemake workflow	Reichl et al.[63]	https://doi.org/10.5281/zenodo.7810621
Unsupervised Analysis Snakemake workflow (v0.2.0)	Reichl et al.[64]	https://doi.org/10.5281/zenodo.8405360
Genome Tracks Snakemake workflow (v2.0.1)	Reichl et al.[65]	https://doi.org/10.5281/zenodo.10849097

(*Continued on next page*)

Continued

REAGENT or RESOURCE	SOURCE	IDENTIFIER
RNA-seq STAR DeSeq2 Snakemake workflow (v1.2.0)	Köster et al.[66]	https://doi.org/10.5281/zenodo.4737358
Snakemake (v6.4.1)	Mölder et al.[67]	https://snakemake.github.io/
Seurat (v4.0.1)	Hao et al.[68]	https://satijalab.org/seurat/
Mixscape	Papalexi et al.[38]	https://satijalab.org/seurat/articles/mixscape_vignette
limma (v3.46.0)	Ritchie et al.[69]	https://doi.org/10.18129/B9.bioc.limma
Rcistarget (v1.14.0)	Aribar et al.[70]	https://doi.org/10.18129/B9.bioc.RcisTarget
STRINGdb (v2.10.0)	Szklarczyk et al.[71]	https://doi.org/10.18129/B9.bioc.STRINGdb
umap-learn (v0.5.0)	McInnes et al.[72]	https://umap-learn.readthedocs.io/
GSEApy (v0.10.5)	Fang et al.[73]	https://gseapy.readthedocs.io
pyGenomeTracks (v3.8)	Lopez-Delisle et al.[74]	https://pygenometracks.readthedocs.io/
tslearn (v0.5.1.0)	Tavenard et al.[75]	https://tslearn.readthedocs.io/
scikit-learn (v1.0.2)	Pedregosa et al.[76]	https://scikit-learn.org/
pheatmap (v1.0.12)	Kolde et al.[77]	https://CRAN.R-project.org/package=pheatmap
ggplot2 (v3.5.0)	Wickham et al.[78]	https://ggplot2.tidyverse.org/
EnhancedVolcano (v1.12.0)	Blighe et al.[79]	https://doi.org/10.18129/B9.bioc.EnhancedVolcano
CQN (v1.34.0)	Hansen et al.[80]	https://doi.org/10.18129/B9.bioc.cqn
rGREAT (v1.24.0)	Zuguang et al.[81]	https://doi.org/10.18129/B9.bioc.rGREAT
circlize (v0.4.16)	Gu et al.[82]	https://CRAN.R-project.org/package=circlize
Other		
Supplementary website (including UCSC Genome Browser Tracks for interactive viewing)	This paper	http://macrophage-regulation.bocklab.org

EXPERIMENTAL MODEL DETAILS

Isolation of cells from bone marrow

Femurs and tibias were obtained from 8-12 week old female Cas9 mice (Jackson Laboratory cat. No. 024858) and washed with PBS. Bones were crushed in PBS with a sterile mortar and pestle. Bone marrow containing supernatant was filtered through 100 μm and 45 μm cell strainers. Cells were counted, centrifuged at 4 °C for 5 minutes at 400 rcf and resuspended in DMEM-GlutaMAX (Gibco cat. No. 31966047) with 40% FBS. The cell suspension was mixed with an equal volume of DMEM GlutaMAX with 40% FBS and 30% DMSO (Sigma cat. No. 1019001000), frozen at 50 million cells/ml, and aliquots were stored at -80 °C (short-term) or in liquid nitrogen (long-term storage).

Cell culture

Bone marrow derived macrophages (BMDMs) and cell lines (Lenti-X, HEK293T, and RAW 264.7 transduced with Cas9 using Addgene plasmid #52962) were cultivated in standard media (DMEM-GlutaMAX (Gibco cat. No. 31966047) with 10% FBS and 1x penicillin-streptomycin (Gibco cat. No. 15140122)). RAW 264.7-Cas9 media was supplemented with 20 μg/ml blasticidin (InvivoGen cat. No. ant-bl-1). Cell lines were passaged every 3-4 days and kept at low passage number. To detach the cells, supernatant was removed, cells were washed with DPBS (Thermo Fisher cat. No. 14190144) and incubated with 0.05% Trypsin-EDTA (Thermo Fisher cat. No. 25300054) for 3-5 minutes following the manufacturer's recommendations. All cells were grown at 37 °C and 5% CO_2, and regularly tested for mycoplasma contamination (Lonza cat. No. LT07-318). The cell line authenticity of RAW 264.7-Cas9 was not verified by genotyping but the RNA-seq data confirmed their identity as murine macrophage-like cells.

Listeria culture

Listeria monocytogenes bacteria (strain LO28) were inoculated in 5 ml BHI media (VWR cat. No. 84626.0500; 37g/l in water) and incubated at 37 °C in a shaking incubator overnight. The concentration was determined by measuring the OD_{600}, with an OD_{600} of 1 corresponding to one billion bacteria per milliliter.

METHOD DETAILS

Stimulation time course and sampling

Experiments were performed in two biological replicates using independently harvested bone marrow samples from different mouse litters. Per replicate, seven bone marrow aliquots were thawed, washed once with media to remove excess DMSO, and seeded on three 15 cm cell culture dishes (non-treated, VWR cat. No. 734-2797) in 20 ml standard media supplemented with 200 ng/ml murine

M-CSF (Peprotech cat. No. 315-02). After four days, 5 ml of the media was exchanged with fresh media supplemented with murine M-CSF to reach a total concentration of 100 ng/ml in the dish, and the media substitution was repeated after an additional 3 days. On day 9, cells were scraped, counted, and seeded into 6-well plates (non-treated, Fisher Scientific cat. No. 10284901) with fresh standard media (without penicillin-streptomycin antibiotic) supplemented with 100 ng/ml M-CSF, at 1-2 million cells per well. The following day, wells were treated in a staggered manner by adding the respective stimulus for the stated duration, such that all treatments (except the 24 hour time point) could be stopped and harvested at the same time to minimize technical variability. The pathogens and infection-linked stimuli were applied at concentrations that were chosen based on pilot experiments as well as common practices in the field (as documented in the scientific literature). UV-killed *Candida albicans* SC5314 were added at a multiplicity of infection (MOI) of 2, LCMV Cl13 at an MOI of 3, *Listeria monocytogenes* LO28 at an MOI of 20, LPS (Merck cat. No. L4641) at a final concentration of 10 ng/ml, IFN-β (PBL Assay Science cat. No. 12401-1) at a final concentration of 500 U/ml, and IFN-γ (Peprotech cat. No. 315-05) at a final concentration of 240 U/ml. Gentamicin (MP Biomedicals cat. No. 1676045) was added at a final concentration of 50 μg/ml to *Listeria monocytogenes LO28* treated wells after one hour to eliminate any remaining extracellular bacteria. Two hours after infection, the media was exchanged with standard media without antibiotics supplemented with 100 ng/ml M-CSF and 5 μg/ml gentamicin.

At the end of the treatment period, cells were washed with PBS and then scraped in 0.5 ml PBS per million cells. The cell number was determined, and 50,000 cells were directly used for ATAC-seq. For RNA-seq, 300,000 to 500,000 cells were centrifuged for 5 minutes at 4 °C at 500 rcf, resuspended in 150 μl RLT lysis buffer (RNeasy Kit, Qiagen cat. No. 74181) with β-mercaptoethanol, vortexed for 1 minute, and frozen at -80 °C.

ATAC-seq

Cells were centrifuged at 4 °C and 500 rcf for 5 minutes. Supernatant was removed, and cells were lysed and tagmented at 37 °C for 30 minutes in the following mixture (per sample): 9.75 μl water, 2x transposase buffer (Illumina cat. No. 20034197), 0.5 μl PIC (Roche cat. No. 11873580001), 2 μl TDE1 Tagment DNA Enzyme (Illumina cat. No. 20034197), and 0.25 μl 1% Digitonin (Promega cat. No. G9441). The DNA was cleaned using the MinElute PCR Purification Kit (Qiagen cat. No. 28006) according to the manufacturer's recommendations and eluted in 12 μl EB buffer. To estimate the enrichment cycle number, a qPCR was set up using 2.9 μl water, 0.5 μl index primer 1 noMX and Index primer 2.1 barcode, respectively, 0.1 μl 100x SYBR green (Invitrogen cat. No. S7563), 5 μl NEBNext HF 2x MM (NEB cat. No. M0541L), and 1 μl eluted sample, and run as follows: 5 minutes at 72 °C, 30 seconds at 98 °C, 25x cycles of (10 seconds at 98 °C, 30 seconds at 63 °C and 1 minutes at 72 °C). The cycle number was determined based on the amplification entering the early exponential phase. Subsequently, an enrichment PCR was set up with 10 μl water, 2.5 μl Index primer 1 noMX and Index primer 2 barcode, respectively, 25 μl NEBNext HF 2x MM (NEB cat. No. M0541L), and 10 μl eluted sample, using standard ATAC-seq primer sequences.[24] A 1.6x left-sided clean-up was performed using AMPure XP beads (Beckman Coulter cat. No. A63881). To that end, 80 μl beads were added and the sample incubated for 10 minutes at room temperature, followed by 10 minutes on a magnetic rack at room temperature. The beads were washed twice with 80% EtOH, air-dried for 2 minutes and the DNA was eluted in 50 μl EB buffer. A second 0.5/1.4 double-sided clean-up was performed. 25 μl beads were added and the sample incubated 10 minutes at room temperature followed by 10 minutes on a magnetic rack as before. The supernatant was transferred to a new well and mixed with additional 45 μl beads, incubated for 10 minutes at room temperature followed by 10 minutes on a magnetic rack at room temperature. The beads were washed twice with 80% EtOH, air-dried for 2 minutes. The DNA was eluted in 15 μl EB buffer, the concentration measured using the Qubit dsDNA HS Kit (Thermo Fisher cat. No. Q32854), and the molarity estimated from a Bioanalyzer HS DNA chip (Agilent 5067-4626) profile. The ATAC-seq libraries were pooled and sequenced using the Illumina HiSeq 3000/4000 platform with 50 bp single-read configuration in the Biomedical Sequencing Facility at CeMM.

RNA-seq

RNA was extracted using the RNeasy Kit (Qiagen cat. No. 74181) following the manufacturer's recommendations. RNA was eluted in two rounds, with 45 μl and 20 μl RNase-free water, respectively. Concentration was measured using the Qubit HS RNA Kit (Thermo Fisher cat. No. Q32854). 5 μl eluted RNA was processed with the QuantSeq 3' mRNA-Seq Kit (Lexogen cat. No. 015.96) according to the manufacturer's recommendations, using 16 PCR cycles for the amplification. The RNA-seq libraries were pooled and sequenced using the Illumina HiSeq 3000/4000 platform with 50 bp single-read configuration in the Biomedical Sequencing Facility at CeMM.

Plasmid cloning

The CROPseq-3P5P plasmid (Addgene #219680) was designed for compatibility with both 3' (3P) and 5' (5P) single-cell RNA-seq assays. It was cloned from the CROPseq-Guide-Puro-mCherry2 plasmid (Addgene #219679)[61] using NEB HiFi assembly of DpnI treated PCR fragments and a gBlock (IDT) containing base changes of the guide RNA (gRNA) constant part and the 10x Genomics capture sequence 1 (which provides compatibility with the 10x Genomics 3' CRISPR assay protocol). Primer and gBlock sequences as well as annealing temperature and elongation times are provided in Table S6. PCR amplification was performed by mixing 25 μl Q5 Hot Start High-Fidelity 2x Master Mix (NEB cat. No. M0494L) with 2 μl of 10 μM fwd/rev primer, 1-10 ng of plasmid template, and nuclease-free water to 50 μl. The mixture was incubated as follows: 30 seconds at 98 °C, 25 cycles of (98 °C for 10 seconds, annealing temperature for 30 seconds, 72 °C for ~25 seconds per kb product length, see Table S6), 72 °C for 30 seconds, and held at 4 °C. PCR reactions were cleaned following the QIAquick PCR Purification Kit (Qiagen cat. No. 28104) and eluted in 30 μl EB buffer. DNA concentration was measured using the Qubit dsDNA HS Assay (Thermo Fisher cat. No. Q32854). 8 μl of the PCR product were mixed

with 1 µl CutSmart Buffer and 1 µl DpnI (NEB cat. No. R0176S) and incubated at 37 °C for 30 minutes followed by heat inactivation for 20 minutes at 80 °C. 0.02 pmol of each PCR fragment were mixed with 0.1 pmol gBlock, water added to reach 10 µl, and subsequently mixed with 10 µl NEBuilder HiFi DNA Assembly Master Mix (NEB cat. No. E2621S). The reaction was incubated at 50 °C for 60 minutes, after which 2.5 µl of the reaction were transformed into NEB Stable Competent *E. coli* (NEB cat. No. C3040H) following the manufacturer's recommendations (*High Efficiency Transformation Protocol*). Colonies were further incubated at 32 °C, shaken at 200 rpm in 2 ml LB broth (Merck cat. No. L3522-1kg) and checked for correct assembly using Sanger sequencing.

Library cloning

All CRISPR target genes and guide RNA sequences are listed in Table S6. The proof-of-concept (KO15) library includes 15 target genes involved in *Listeria* infection such as NFκB subunit (*Rela/p65*), endogenous interferon response (*Jak1*, *Tyk2*, *Stat1*, *Stat2*, *Irf9*), macrophage differentiation (*Spi1*, *Csf1r*, *Irf8*), epigenetic regulation (*Ep300*, *Hdac6*, *Kdm1b*, *Kdm6b*), and cell stress response (*Jun*, *Creb1*). The upscaled screening (KO150) library includes the same 15 target genes plus 120 additional target genes focusing on epigenetic and transcription factors, while taking into account their expression levels in macrophages and differential expression in the time series data.

Guide RNAs for the selected target genes were designed using VBC-Score.[83] Non-targeting guide RNAs were selected from a previous publication.[84] The guide RNAs were ordered as a single-stranded oligo pool (IDT oPools, Table S6). A total of 6 to 10 reactions were performed in parallel. Per reaction, 1 µg of CROPseq-3P5P plasmid was cut by mixing it with 1 µl BsmBI-v2 (NEB cat. No. R0739L), 5 µl NEB buffer 3.2, and water to a total of 50 µl. The reactions were incubated at 55 °C for 60 minutes after which 2.5 µl rSAP (NEB cat. No. M0371L) were added and the samples further incubated at 37 °C for 60 minutes, followed by 20 minutes heat inactivation at 80 °C. The linearized plasmids were loaded onto a 0.7% agarose gel prepared with a 1:1000 dilution of a 0.16% crystal violet stock in 1x TAE buffer (Invitrogen cat. No. 24710030). Linearized plasmids from two reactions were cut out from the gel and DNA isolated using the QIAquick Gel Extraction Kit (Qiagen cat. No. 28704) following the manufacturer's recommendations. 100 ng (35 fmol) of vector were mixed with 4.329 ng (175 fmol) single-stranded oligo pool (IDT oPools, resuspended in 40 µl EB, further diluted in water), 10 µl HiFi DNA Assembly Master Mix (NEB cat. No. E2621S), and water to 20 µl. The reaction was incubated at 50 °C for 60 minutes, and then pipetted on a filter (Merck cat. No. VMWP04700) floating on water and incubated for 30 minutes. The remaining drop was carefully recovered. 10 µl of the remaining desalted solution were mixed with 25 µl Lucigen Endura *E. coli* cells (Lucigen cat. No. 60242-2) and electroporated and amplified as described previously.[22] The DNA was extracted from the recovered bacterial colonies with the Plasmid Maxi Kit (Qiagen cat. No. 12163) following the manufacturer's protocol. Correct guide RNA insertion and distribution was validated by Sanger sequencing of individual colonies using Primer_465 and by next-generation sequencing after PCR amplification of 10 ng plasmid library with 2.5 µl of a 10 µM fwd/rev primer (CROPseq_libQC_i5, CROPseq-3P5P_amplicon_i7, Table S6), 25 µl Q5 Hot Start High-Fidelity 2x Master Mix (NEB cat. No. M0494L), 0.5 µl SYBR green of a 100x stock (Invitrogen cat. No. S7563), and water to 50 µl. The reaction was incubated at the following settings: 98 °C for 30 seconds, 12 cycles of (98 °C for 10 seconds, 72 °C for 25 seconds). The number of amplification cycles was determined by inspecting the fluorescence signal. The reaction was stopped once the amplification has reached the early exponential phase. Libraries were pooled to 4 nM and sequenced using the Illumina MiSeq platform in the Biomedical Sequencing Facility at CeMM.

Lentivirus production

Lenti-X cells (Takara cat. No. 632180) were seeded in 15 cm dishes (19.3 million cells in total) with lentivirus production media consisting of Opti-MEM-GlutaMAX (Thermo Fisher cat. No. 51985026), 5% FBS, and 200 µM sodium pyruvate (Gibco cat. No. 11360-070). After at least three hours, cells were transfected with 28.2 µg of the guide RNA plasmid library (KO15 or KO150) and 14.9 µg of each packaging plasmid pMDLg/pRRE (Addgene #12251), pRSV-Rev (Addgene #12253), and pMD2.G (Addgene #12259), using Lipofectamine 3000 (Invitrogen cat. No. L3000075) following the manufacturer's recommendations. Media exchange with fresh lentivirus production media was performed 4 to 6 hours thereafter. Supernatant was harvested after 24 and 48 hours, with a top-up with fresh lentivirus production media after the first harvest. The supernatant was filtered through a 0.45 µm filter, and the virus was concentrated 100x using the Lenti-X Concentrator (Takara cat. No. 631232) according to the manufacturer's protocol. The concentrated virus was resuspended in PBS and frozen at -80 °C in single-use aliquots.

CROP-seq screening: Cell culture and treatment

RAW 264.7-Cas9 macrophages (12 million cells) were seeded per 10 cm dish in triplicates at least three hours before transduction start. For the KO150 screen we used cells from three frozen vials independently thawed on different days. To transduce the cells, polybrene at a final concentration of 8 µg/ml (Sigma Aldrich, cat. No. H9268-5G) and virus dilutions were added to obtain a multiplicity of infection (MOI) of 0.1. The remaining 90% of untransduced cells were retained (i.e., not selected against) to provide a consistent background of paracrine signaling (they were removed via FACS after cell harvest, as described in the next section below). After 24 hours, the cells were detached, and 95% of these cells were seeded in fresh media without polybrene on 15 cm dishes. The remaining 5% of cells were seeded in a 6-well plate and kept for MOI assessment via flow cytometry after three days, for which cells were scraped in FACS buffer containing 1x DAPI stain (BioLegend, cat. No. 422801). The mCherry signal (i.e., guide RNA positive) among DAPI negative cells (live cells) was measured to estimate the MOI. For the KO15 library, we selected plates with 10% mCherry positive cells, counted and expanded them, and exchanged media. Five days after transduction, cells were detached and single-cell filtered through a 45 µm filter, and 25-30 million cells per treatment condition were seeded in standard media without antibiotics

(no penicillin/streptomycin and blasticidin). Three hours after cell seeding, *Listeria monocytogenes* (strain LO28) were added for the 24 hour time point with an MOI of 20, while the other time points were started the next day, in order to finish at a single shared time point. Gentamicin (MP Biomedicals cat. No. 1676045) was added at a final concentration of 50 μg/ml to *Listeria* treated wells 1 hour after infection. Two hours later, the media was exchanged to standard media without antibiotics supplemented with 5 μg/ml gentamicin. All treatments were harvested at the same time at 6 days after transduction.

CROP-seq screening: FACS purification

To stop the treatment, cells were washed with ice cold FACS buffer, scraped without trypsin, and centrifuged at 4 °C for 5 minutes at 500 rcf. The cells were resuspended in 100 μl FACS buffer containing 1 μg TrueStain FcX PLUS (Biozym cat. No. 156604) per 1 million cells and incubated on ice for 10 minutes. Afterward, 100 μl FACS buffer containing CITE-seq antibodies (Table S6; 1 μl per antibody per 10 million cells for KO15; 0.33 μl per 10 million cells for KO150) as well as TotalSeq-C hashing antibodies (BioLegend; 1 μl antibody per 10 million cells) were added, and the incubation was continued at 4 °C for 30 minutes. Cells were washed twice with FACS buffer and resuspended in fresh FACS buffer with Zombie NIR viability staining (BioLegend cat. No. 423105) at a 1:1000 dilution. Cells were sorted on a FACS Aria by selecting for NIR negative and mCherry positive cells, which effectively removes dead and untransduced cells. For the KO15 transduced cells, two tubes with 50,000 cells per condition were sorted. The replicates of the same condition for the KO150 library were sorted, with 50,000 cells each going into three tubes.

CROP-seq screening: Single-cell sequencing

Excess supernatant was reduced using the VR NxT instrument (Menarini Silicon Biosystems) and processed using the Chromium Next GEM Single Cell 5' v2 Dual Indexing Kit with Feature Barcoding (10x Genomics cat. No. 1000263), with the following modifications. During Step 1.1 of the GEM generation process, 0.5 μl of a 10 μM stock CROPseq-3P5P_gRNA_RT primer (Table S6) were added additionally to the master mix. The cDNA amplification was performed for 11 cycles, and during the SPRI select clean-up, the remaining 80 μl supernatant was mixed with 30 μl beads to perform a 1.2x clean-up of the gRNA fraction, otherwise following the 2.3B Cell Surface Protein protocol. 5 μl of the guide RNA fraction were amplified with the following PCR mix: 3 μl of a 10 μM fwd/rev CROPseq-3P5P i7/i5 primer mix (Table S6), 2x KAPA HiFi HotStart Ready Mix (Roche cat. No. 7958935001), 0.5 μl SYBR green (Thermo Fisher cat. No. S7563), and 16.5 μl water. The PCR was run for 30 seconds at 98 °C, 7 to 8 cycles of (10 seconds at 98 °C, 30 seconds at 70 °C and 20 seconds at 72 °C), followed by 1 minutes at 72 °C. The number of amplification cycles was determined by inspecting the fluorescence signal. The reaction was stopped once the amplification has reached the early exponential phase. A 0.9x left-sided SPRI bead clean-up was performed, and the DNA eluted in 15 μl EB buffer. Correct amplification was determined using a Bioanalyzer HS DNA chip (Agilent 5067-4626), confirming a peak at ~272 bp for the guide RNA library. For the KO15 and KO150 experiments, cell surface and guide RNA libraries were added to the gene expression library at 10% and 15% of the final concentration, respectively. Final libraries were pooled to 4 nM and sequenced using the Illumina NovaSeq platform with 100 bp paired-end configuration in the Biomedical Sequencing Facility at CeMM.

Individual Ep300 knockout experiments

CROPseq-3P5P plasmid was cut by mixing 1 μg of the plasmid with 1 μl BsmBI-v2 (NEB cat. No. R0739L), 5 μl NEB buffer 3.2, and water to a total of 50 μl. The reactions were incubated at 55 °C for 60 minutes, after which 2.5 μl rSAP (NEB cat. No. M0371L) were added and the samples further incubated at 37 °C for 60 minutes, followed by 20 minutes heat inactivation at 80 °C. The individual guide RNAs were ordered as homologous oligo pairs (Table S6), and the respective fwd/rev pair was diluted with water to 100 μM. 1 μl of the oligo pair was mixed with 1 μl T4 DNA Ligase Buffer (NEB cat. No. B0202S), 7.5 μl water, and 0.5 μl T4 PNK enzyme (NEB cat. No. M0201S). The reaction was incubated for 30 minutes at 37 °C, 5 minutes at 95 °C, and ramped from 90 °C to 25 °C at 5 °C/min. The phosphorylated and annealed oligo duplex was diluted 1:200 with water, and 1 μl of the product was mixed with 1.6 μl rSAP treated CROPseq-3P5P backbone, 1 μl T4 DNA Ligase Buffer, 5.9 μl water, and 0.5 μl T4 DNA Ligase (NEB cat. No. M0202S). The reaction was incubated for 15 minutes at 25 °C, and 2 μl of the product were transformed into 10 μl NEB Stable Competent E. coli (NEB cat. No. C3040H) using the manufacturer's recommendations (*5 Minute Transformation Protocol*). Bacterial colonies were grown on LB-agar plates prepared from 15 g/l agar (Millipore cat. No. 05040-100G) with LB broth (Sigma cat. No. L3522-250G) containing 100 μg/ml ampicillin (Sigma cat. No. A9518-5G) for up to 24 hours at 30 °C, after which colonies were picked and expanded for up to 24 hours at 30 °C while shaking in 3 ml liquid LB broth containing 100 μg/ml ampicillin. Plasmid DNA was extracted from 2 ml of bacterial culture using the QIAprep Spin Miniprep Kit (Qiagen cat. No. 27104), and correct guide RNA insertion was validated by Sanger sequencing of individual colonies using Primer_465 (Table S6). The remaining 1 ml bacterial culture was topped up with 150 ml LB broth and expanded for another 24 hours, after which plasmid DNA was extracted using the HiSpeed Plasmid Maxi Kit (Qiagen cat. No. 12663).

Lenti-X cells (Takara cat. No. 632180) were grown in 10 cm dishes to confluency (around 8 million cells). The cells were transfected with 10.15 μg of the guide RNA plasmid and 5.37 μg of each packaging plasmid pMDLg/pRRE (Addgene #12251), pRSV-Rev (Addgene #12253), and pMD2.G (Addgene #12259), using Lipofectamine 3000 (Invitrogen cat. No. L3000075) following the manufacturer's recommendations. Media exchange with fresh lentivirus production media was performed 4 thereafter. Supernatant was harvested after 24 hours and filtered through a 0.45 μm filter for direct addition to macrophages.

RAW 264.7-Cas9 macrophages (8 million cells) were seeded in 9 ml media per 10 cm dish three hours before transduction. Thereafter, 1 ml filtered but unconcentrated viral supernatant was added, and polybrene was supplemented up to a final concentration of

8 μg/ml (Sigma Aldrich, cat. No. H9268-5G). After 24 hours, the cells were detached by trypsinization, seeded in two 10 cm dishes in fresh media, and expanded. Three days after transduction, fresh media supplemented with 5 μg/ml puromycin (Sigma cat. No. P8833-10MG) was added. Six days after the transduction, the media was replaced and puromycin reduced to 1 μg/ml for continuous culture. The expression of mCherry as a marker of successful transduction was confirmed by fluorescent microscopy. Cells were expanded and subsequently frozen in DMEM-GlutaMAX (Gibco cat. No. 31966047) containing 20% FBS and 10% DMSO (Sigma cat. No. 1019001000).

Finally, RAW 264.7-Cas9 macrophages (1 million cells per well, three replicates per condition) were seeded in 6-well plates in 2 ml media supplemented with 1 μg/ml puromycin. After 22 hours, the respective wells were treated with IFN-β (PBL Assay Science cat. No. 12401-1) at a final concentration of 500 U/ml for a total of 2 hours. 24 hours after seeding, cells were harvested via trypsinization, and 200,000 cells were centrifuged for 5 minutes at 300 rcf at 4 °C. The supernatant was discarded, and the cell pellet was resuspended in 350 μl RLT lysis buffer (RNeasy Kit, Qiagen cat. No. 74181) containing β-mercaptoethanol, vortexed for 1 minute, and frozen at -80 °C.

Small-molecule inhibition of EP300

RAW 264.7-Cas9 macrophages (1 million cells) from three separate thaws were seeded in each well of a 6-well culture plate in 2 ml media. The experiment was started three hours after cell seeding. Cells were treated for 24 hours with 1 μg/ml SGC-CBP30, 1 μg/ml A-485, or an equivalent volume of DMSO (as a control). 2 hours before harvest, IFN-β (PBL Assay Science cat. No. 12401-1) was added to half of the wells at a final concentration of 500 U/ml. 27 hours after cell seeding, all cells were harvested via trypsinization, and 1 million cells were centrifuged for 5 minutes at 300 rcf at 4 °C. The supernatant was discarded and the cell pellet resuspended in 350 μl RLT lysis buffer (RNeasy Kit, Qiagen cat. No. 74181) with β-mercaptoethanol following the manufacturer's recommendations, vortexed for 1 minute, and frozen at -80 °C.

qPCR measurement and analysis

RNA was extracted using the RNeasy Mini Kit (Qiagen cat. No. 74104) following the manufacturer's recommendations. RNA was eluted in one round with 30 μl RNase-free water. Concentration was measured using a NanoDrop instrument (Thermo Fisher) and 200 ng RNA was used for reverse-transcription with LunaScript RT SuperMix (NEB cat. No. E3010) following the manufacturer's recommendations. A 4x dilution was created by adding 60 μl RNase-free water to the resulting 20 μl sample, of which 2 μl were used as input cDNA template for each qPCR reaction, together with 2 μl of a 20 μM fwd/rev primer stock, 6 μl water and 10 μl GoTaq qPCR Master Mix (Promega cat. No. A6002). Primers were designed using the Primer-BLAST tool[85] with PCR product range 50-250 bp and requirement to span an exon-junction, or taken from the literature[86] (Table S6). The qPCR reaction was run in duplicate on a Bio-Rad CFX Opus 96 machine with the following settings: 2 minutes activation at 95 °C followed by 40 cycles of (5 seconds at 95 °C, 30 seconds at 56 °C) and a melt curve. Cq values were determined using the default settings of the Bio-Rad CFX Maestro software version 2.3 (5.3.022.1030).

Primer efficiencies were determined from standard curves and used as efficiency values in the Pfaffl method.[87] *Actb* served as the reference gene for all experiments except for the untreated CRISPR knockout, where *Gapdh* was used. For each sample, Cq values were averaged per replicate, normalized to the reference gene (ΔCq), and further normalized to the matched control (non-targeting guide RNA or DMSO control), resulting in ΔΔCq values. Fold changes were computed using the Pfaffl method as Efficiency$^{-\Delta\Delta Cq}$. Paired t-tests were used for the comparisons.

QUANTIFICATION AND STATISTICAL ANALYSIS

Bioinformatics and data visualization

Bioinformatic analyses were performed using command line tools, *R*,[88] and *Python*.[89] In the following sections, the term "features" denotes both genes (for RNA-seq and scRNA-seq) and genomic regions (for ATAC-seq). The GRCm38 (mm10) assembly of the mouse genome was used as reference. If not stated otherwise, default parameters and random seed 42 were used. Dataframe operations in *Python* used the *pandas* library (1.1.3).[90] Heatmaps and dot plots were hierarchically clustered with the *R* function *hclust*; heatmaps were plotted with the R package *pheatmap* (1.0.12).[77] Plots were generated with the R package *ggplot2* (3.3.5).[78] Illustrations were drawn in BioRender (Figure 1A: q79m361; Figure 3A and 3B: t27m528; Figure 4A: t75h912; Figures 5A, 6A, 6D, and 6G: j58b598).

RNA-seq data processing and analysis

Base calling was performed using the *Illumina Real Time Analysis* (2.7.7) software. Base calls were converted to reads using the *IlluminaBasecallsToSam* tool from the *Picard* software (2.19.2).[91] Sequencing reads were mapped, and gene counts were generated with *STAR* (2.7.8a)[92] using the GRCm38 (mm10) assembly of the mouse genome and its Ensembl annotations.[93] Quality control metrics were aggregated and reported using *MultiQC* version 1.10.[94] These processing steps were performed with a widely used *Snakemake* (6.4.1)[67] workflow (1.2.0).[66] We identified and removed two outlier samples, based on the number of total reads, principal component analysis (PCA), and an expression correlation heatmap, resulting in 64 samples for downstream analyses. Genes were filtered to 12,729 genes by applying the function *filterByExpr* from the package *edgeR* (3.32.1)[95] with "group" parameter set to *stimulus and time point*, to protect group-specific expression patterns from being removed. Conditional quantile normalization *cqn* (1.36.0)[80] was performed using the filtered expression matrix together with the exon length and GC-content as conditions. These

values were obtained from *Biomart* (2.46.3)[96] using a version of the function *getGeneLengthAndGCContent* from the package *EDASeq* (2.24.0) that was adapted to the relevant Ensembl annotations.

ATAC-seq data processing and analysis

Base calling was performed using the *Illumina Real Time Analysis* (2.7.7) software. Base calls were converted to reads using the *IlluminaBasecallsToSam* tool from the *Picard* software (2.19.2).[91] Sequencing adapters were removed using the *fastp* software (0.20.1).[97] *Bowtie2* (2.4.4)[98] was used for aligning the reads (representing locations of transposition events) to the GRCm38 (mm10) assembly of the mouse genome using the "–very-sensitive" parameter. PCR duplicates were marked using *samblaster* (0.1.24).[99] Aligned BAM files were then sorted, filtered using ENCODE blacklisted regions,[100] and indexed using *samtools* (1.12).[101] To detect the open chromatin regions, peak calling was performed using *MACS2* (2.2.7.1)[102] using the "–nomodel", "–keep-dup auto" and "–extsize 147" options on each sample. Quality control metrics were aggregated and reported using *MultiQC* (1.9).[94] No samples needed to be removed due to quality concerns, and all 78 samples were included in the downstream analyses. A consensus region set was generated by merging the identified peak summits, extended by 250 bp on both sides using the *slop* function from *bedtools* (2.27.1)[103] and *pybedtools* (0.8.1),[104] across all samples while again discarding peaks overlapping blacklisted features as defined by the ENCODE project.[100] A total of 142,831 genomic regions were obtained and were annotated using the *annotatePeaks* function from *Homer* (4.11).[105] This consensus region set was used to quantify the chromatin accessibility in each sample by summing the number of reads overlapping each consensus region. Sample-wise quantification of chromatin accessibility was performed using *bedtools* (2.27.1)[103] and *pybedtools* (0.8.1).[104] For all downstream analyses, we filtered the 142,831 consensus regions to 136,735 regions that had reads in at least 3 samples and were covered by at least 10 reads in total (normalized by median library size) across at least 6 samples and by at least 15 total reads across all samples. Conditional quantile normalization *cqn* (1.36.0)[80] was performed on the filtered accessibility matrix using the region length and GC-content of the consensus regions as conditions, quantified using *bedtools* (2.27.1)[103] and *pybedtools* (0.8.1).[104] The data processing was performed using a dedicated *Snakemake* workflow (0.1.0).[62]

Genome browser tracks

Aligned BAM files for the same data modality (RNA-seq or ATAC-seq), stimulus, and time point were merged and indexed using *samtools* (1.14).[101] BigWig files were created using the *deepTools* (3.5.1)[106] function *bamCoverage*. Genome browser track plots were generated using the *gtracks* (1.8.1) wrapper for the *pyGenomeTracks* (3.6)[74] *Python* package. Data processing and visualization was performed using a dedicated *Snakemake* workflow (2.0.1).[65]

Unsupervised time-series analysis

We applied two dimensionality reduction methods to the normalized RNA-seq and ATAC-seq data. We used PCA[107] from *scikit-learn* (0.24.2)[76] as a linear approach and uniform manifold approximation and projection (UMAP) from *umap-learn* (0.5.1)[72] with the correlation metric as a non-linear approach. The *ggplot2::geom_jitter* method with parameter width 2 was used for the ATAC-seq UMAP visualization to reduce the sample overlap in two dimensions.

Differential gene expression and differential chromatin accessibility time-series analysis

For differential analyses, the filtered raw counts were used in a *limma* (3.46.0)[69,108] workflow fitting a linear model: *feature* ~ *group* + *batch*, where *group* denotes the combination of stimulus (e.g., *Listeria*) and time point (e.g., 2 hours), to identify features with statistically significant changes according to stimulus and time point compared to the untreated control (intercept). We applied *voom* to prepare the data for linear modelling, *lmFit* to fit the model to the data, and *eBayes* to compute moderated t-statistics. For all downstream analyses, we used the extracted feature-wise effect sizes as $\log_2$ fold change and their adjusted statistical significance as p-values (determined using the Benjamini-Hochberg method) from each comparison defined by *group*. Next, the results were filtered for *differential features* if in at least one of the investigated comparisons they fulfilled the following criteria: statistical significance (adjusted p-value < 0.05), sizeable change (absolute $\log_2$ fold change > 2), and at least moderate gene expression levels (average gene expression > 1) in case of RNA-seq or at least moderate chromatin accessibility (mean chromatin accessibility > 0) in case of ATAC-seq. Finally, hierarchical clustering on the *differential features* and *groups* found four *group* clusters in each modality and eight gene / nine genomic region clusters, respectively.

To analyze the temporal dynamics of changes in gene expression and chromatin accessibility, the stimulus-specific filtered results of the differential analyses were used to construct a time course of $\log_2$ fold changes for each *differential feature* using the function *to_time_series_dataset* from the package *tslearn* (0.5.1.0).[75] For *C. albicans* stimulus, the filtering criteria for absolute $\log_2$ fold changes were loosened (>1) to include more features in the analysis. The constructed stimulus-specific time courses were clustered using *tslearn::TimeSeriesKMeans* into *k* groups of similarly behaving features over time. To represent the mean temporal pattern of the identified temporal clusters, the respective cluster centers, determined by the arithmetic mean, were used in the time course visualizations.

Gene set enrichment analysis

Gene set enrichment analysis was performed on feature sets from the hierarchically clustered *group*-wise differential analysis results, and from the temporal clustering per stimulus. For RNA-seq we used *Enrichr*[109] through the *Python* wrapper *GSEApy* (0.10.6).[73] As background feature sets, we used the filtered set of features from the respective differential analysis. For ATAC-seq, region sets were

analyzed with *GREAT*[110] via *rGREAT* (1.24)[81] using a dedicated *Snakemake* workflow.[63] For the enrichment summary heatmaps of the time-series analyses, we identified the union of the top two most significantly enriched terms per temporal cluster across all stimuli and used the effect sizes of each term in all temporal clusters in the hierarchical clustering. Two databases were used across all analyses: GO Biological Process 2021 (Figures 1D, 2G, 3E, 5I, S6D, and S10F) and BioPlanet 2019 (Figures 2E, 4D, and 6D).

Integrative analysis of gene expression and chromatin accessibility

For data integration of the RNA-seq and ATAC-seq profiles into a shared feature space, gene promoter regions were identified using *promoters* from the package *GenomicRanges* (1.42.0),[111] and their chromatin accessibility was quantified by adding up the overlapping ATAC-seq reads for a given sample. Genes (for RNA-seq) and matched promoters (for ATAC-seq) were separately filtered by gene expression levels using *edgeR::filterByExpr*. The union of filtered genes and their matched promoters was used as the shared gene-centric feature space. Finally, the raw count matrices of both modalities were concatenated into a matrix of $N1 + N2$ samples by M features, where $N1$ is the number of RNA-seq samples, $N2$ is the number of ATAC-seq samples, and M is the number of selected gene-promoter pairs. The resulting count matrix was normalized using the function *limma::voom* (with method *quantile*). Next, *limma::removeBatchEffect* was used to remove systematic differences between the two data modalities, while protecting the *group* (stimulus and time point) and (processing) *batch* covariates. Unsupervised analysis (UMAP with correlation metric) was used for validation and interpretation of the computational integration into a shared feature space. Finally, we tested for differential gene-promoter pairs using *limma::lmfit*, followed by *limma::eBayes* and the following model: *gene-promoter pair* ~ 0 + *group* + *group:library* + *batch*, where *library* represents either RNA-seq or ATAC-seq.

Downstream analysis focused on the fitted coefficients of the ATAC-seq interaction term versus RNA-seq (*group:library*) in the linear model. The results were filtered for the most divergent gene-promoter pairs by statistical significance (adjusted p-value < 0.05), sizeable change (absolute log2 fold change > 1), and at least moderate signal intensity (average expression > 1). Gene-promoter pairs exhibiting relative transcriptional abundance were identified by negative effect sizes ($\log_2$ fold changes < 0), while gene-promoter pairs exhibiting epigenetic potential (calculated in the same way as in our previous study[33]) were identified by positive effect-sizes ($\log_2$ fold changes > 0). The most divergent gene-promoter pairs per *group* were highlighted in scatterplots comparing the mean signal intensities for RNA-seq and ATAC-seq. Time series clustering and enrichment analyses of these gene-promoter pairs were performed separately for each stimulus, describing the changing relationship between gene expression and chromatin accessibility over time within a stimulus. Transcription factor binding motif enrichments were identified using *Rcistarget* (1.14.0)[70] for each temporal cluster within a stimulus. The enrichment results for each stimulus' clustering were summarized by retaining only the maximum normalized enrichment scores (NES) of each transcription factor annotated to the respective enriched motif with high confidence. This resulted in a transcription factor by cluster matrix for each stimulus, containing the highest NES for the respective transcription factor binding motif.

CRISPR screening data processing and analysis

The data for the combined CROP-seq and CITE-seq assay were processed using the *10x Genomics Cell Ranger* software (3.0.2) and the R package *Seurat* (4.0.1).[68] Raw sequencing data were demultiplexed and converted to FASTQ format using the *Cell Ranger* command *mkfastq*. FASTQ files were then aligned to the mouse reference genome assembly GRCm38 (mm10), and count matrices were generated for each sample based on genome annotation v93 using the *Cell Ranger* command *count*. Cells were assigned to time points within each sample based on hashtag oligonucleotide antibody counts using a Gaussian mixture model that infers the probability with which a given antibody count constitutes true signal or background noise. Quality control was performed individually for each time point within each sample, based on the following parameters: (i) threshold on the minimum number of detected genes, (ii) fraction of mitochondrial counts, and (iii) fraction of ribosomal counts. The thresholds were determined for each time point within each sample upon inspection of the distribution of the quality control metrics.

The preprocessed samples were merged using the function *merge* that concatenates the individual samples and their metadata into one *Seurat* object. Guide RNA assignment was performed based on the protospacer call information provided by the CRISPR functionality of *10x Genomics Cell Ranger* (3.0.2). To minimize the effects of multiple gene knockouts in the same cell, only cells with exactly one called protospacer were considered. Cells were filtered based on the quality control metrics, assignment of time point, and unique guide RNA assignment, resulting in 9,153 (Figure 4) and 28,303 (Figures 5 and 6) high-quality cell profiles with confident time point and guide RNA assignment.

The filtered count data were normalized using *Seurat::SCTransform*,[112] with the method parameter *glmGamPoi* to increase computational efficiency, and simultaneously scaled and corrected using mitochondrial percentage and cell cycle scores as covariates. The cell cycle scores were determined using the function *Seurat::CellCycleScoring* with gene lists for *M* and *G2M* phase provided by *Seurat::cc.genes* and mapped to the mouse genome using MGI mouse homology mappings.[113] Unsupervised analysis of the scaled and corrected data was performed using the PCA and UMAP methods from *Seurat* and a dedicated *Snakemake* workflow (0.2.0).[64]

To visualize the effect of *Listeria* treatment in cells without genetic perturbations, we calculated the gene expression profiles of the cells that were confidently assigned to non-targeting guide RNAs and plotted the expression of the top-100 genes that significantly changed between time points as well as manually selected immune genes using the function *Seurat::DoHeatmap*. Similarly, we plotted the average CITE-seq protein expression per time point using the function *Seurat::DotPlot*, normalized with *Seurat::NormalizeData* method *CLR* and margin 2.

Single-cell perturbation analysis using Mixscape

We applied the *Mixscape*[38] workflow in *Seurat* to each time point separately and to all time points simultaneously, identifying genetically perturbed cells in comparison with genetically unperturbed controls (i.e., cells that were confidently assigned to non-targeting guide RNAs). Cell perturbation signatures were calculated with *Seurat::CalcPerturbSig* by subtracting the average gene expression profile of the 30 closest unperturbed control cells in a 40-dimensional PCA space. Using *Seurat::RunMixscape*, with a $\log_2$ fold change threshold of 0.1, cells were classified as perturbed or unperturbed using posterior probabilities of an expectation-maximization (EM) algorithm for mixtures of univariate Gaussian distributions, assuming that each target gene group is a mixture of two Gaussian distributions (perturbed signal and unperturbed background). Linear discriminant analysis (LDA) was applied on the perturbation signatures of all cells using *Seurat::MixscapeLDA* to find the most discriminative subspace given the labeled cells. To visualize the LDA-transformed data in two dimensions, UMAP with *Seurat::RunUMAP* was used.

Analysis of perturbation effects using differences in gene expression

Differential gene expression analysis between genetically perturbed and control cells within time points, and within knockouts across time points, was performed using *Seurat::FindMarkers*, with a $\log_2$ fold change threshold of 0.1 and the Wilcoxon rank-sum test. The same approach was used to analyze differential surface protein expression. These analyses were performed separately for all cells and only for the perturbed cells identified by *Mixscape*. The results were visualized by volcano plots using the R package *EnhancedVolcano* (1.12.0),[79] plotting the average $\log_2$ fold change and adjusted p-values per gene and protein for each comparison. To visually summarize the results for one type of analysis (e.g., all knockout effects within a time point), clustered heatmaps of average $\log_2$ fold changes were plotted for genes that were significantly differentially expressed at least in one comparison. Gene set enrichment analysis was performed on the differentially expressed genes.

Inference of functional similarity graphs

To quantify the similarity between gene knockouts, we conducted a cross-prediction analysis where a multi-class logistic regression model was used to predict for each cell perturbation signature which knockout class was the most fitting when all cells with the actual knockout class were removed from the training set. The cross-prediction models were trained and evaluated using *LogisticRegression* from *scikit-learn* (0.24.2)[76] with elastic-net penalization, l1-ratio of 0.5, and saga solver, in combination with *model_selection.cross_val_predict* using the cross-validation scheme *LeaveOneGroupOut* and the method *predict_proba*. Prediction probabilities for each knockout were averaged to get a confusion matrix consisting of average probabilities of cross-prediction (the diagonal was empty because correct predictions were impossible due to the leave-one-group-out cross-validation setup). All averaged prediction probabilities below 0.1 were pruned (i.e., set to 0). The resulting matrix was used as an adjacency matrix to plot a directed graph, with edge pairs for each pair of nodes visualized as trapezoids in which the widths at the target and source node correspond to the average probabilities of the cross-predictions, using *gplot* from *sna* (2.6)[114] with the Fruchterman-Reingold algorithm option. Then the resulting functional similarity graph was compared to prior knowledge using the STRING database (11.5),[71] queried via the R package *STRINGdb* (2.10). The same threshold of an interaction confidence of 0.1 was used to prune the protein interaction graph. To test if overlapping edges were significantly enriched in higher interaction confidence scores from STRING, the Mann-Whitney U test was used.

To identify functional similarity relationships between gene knockouts across all three time points, the same approach was applied to the results of the *Mixscape* perturbation analysis across all time points. Here, each class was defined as the combination of a time point and a knockout. Two scores were determined to quantify the relationship of within-knockout similarity to within-time-point similarity for all target genes. The scores for each target gene were determined by adding up each node's edge weights of its direct neighbors by the same knockout or time point, respectively. To that end, the unpruned graph (i.e., the full adjacency matrix) was used, which represents all averaged cross-prediction probabilities. Scores were scaled by the total number of nodes with the knockout. To propose a biological interpretation of the identified perturbation relationships of the similarity graph across all time points, we selected the overlap of statistically significant genes split by directionality (upregulated versus downregulated) of the respective differential expression results for the connected nodes (perturbation effect within a time point). Gene set enrichment analysis was performed on these overlapping genes.

Enrichment of knockout signatures in temporal regulons of the Listeria response

To identify regulators of macrophage homeostasis and *Listeria* response, we analyzed the enrichment of knockout-induced differentially expressed genes among the temporal regulons (Figure 3). We used the significantly upregulated or downregulated genes for each knockout and time point as our query gene sets. These genes were tested for enrichment among the temporal clusters of divergent genes upon *Listeria* treatment. Enrichment analysis was conducted using *Enrichr*[109] through the *Python* wrapper *GSEApy* (0.10.6).[73] The odds ratios of the statistically significant results were visualized using the *chordDiagram* function from the *circlize* package (0.4.15).[82]

Cell Systems, Volume *16*

Supplemental information

Integrated time-series analysis and high-content CRISPR screening delineate the dynamics of macrophage immune regulation

Peter Traxler, Stephan Reichl, Lukas Folkman, Lisa Shaw, Victoria Fife, Amelie Nemc, Djurdja Pasajlic, Anna Kusienicka, Daniele Barreca, Nikolaus Fortelny, André F. Rendeiro, Florian Halbritter, Wolfgang Weninger, Thomas Decker, Matthias Farlik, and Christoph Bock

SUPPLEMENTARY FIGURES

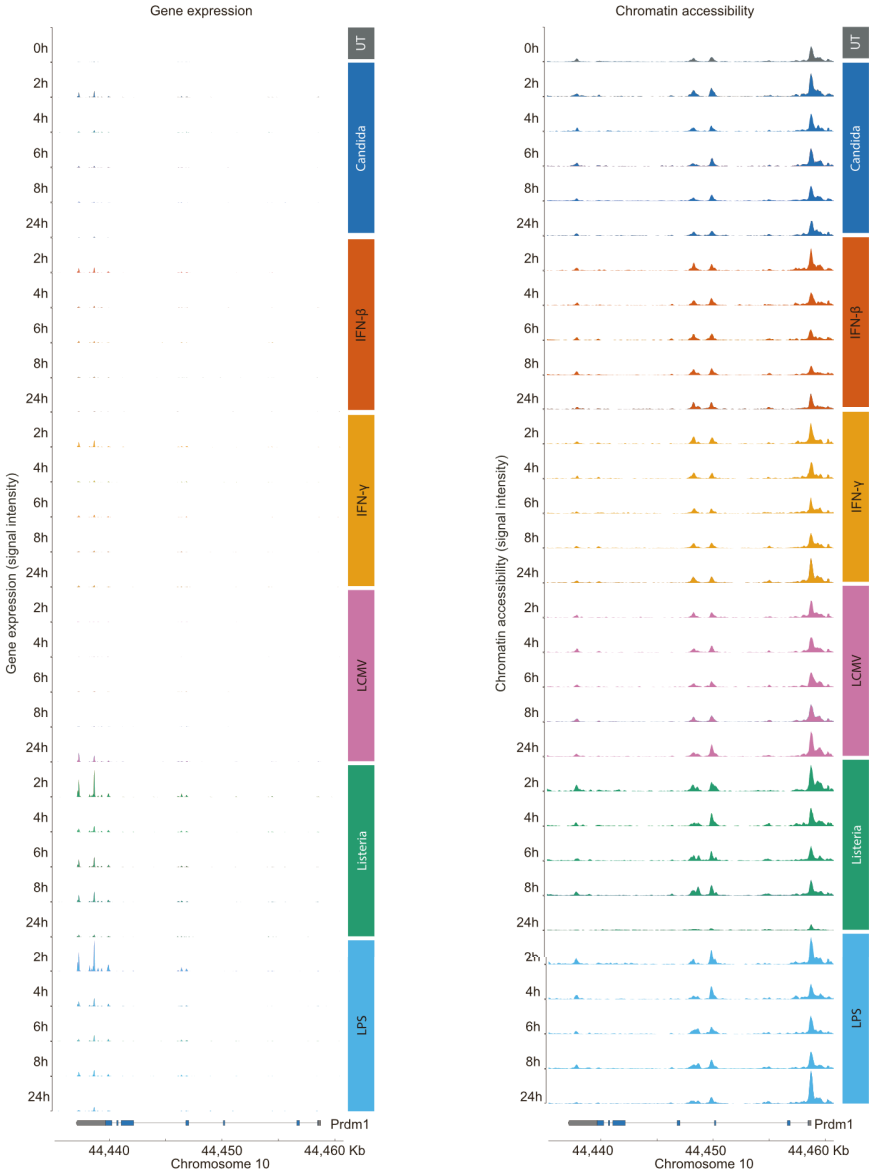

Figure S1 (related to Figure 1). Time series of transcriptome and epigenome profiles for the *Prdm1* locus in macrophages responding to six immune stimuli

Genome browser tracks depicting gene expression (left) and chromatin accessibility (right) at the *Prdm1* locus (the direction of transcription is from right to left) over time across stimuli (colored) and for untreated controls (grey).

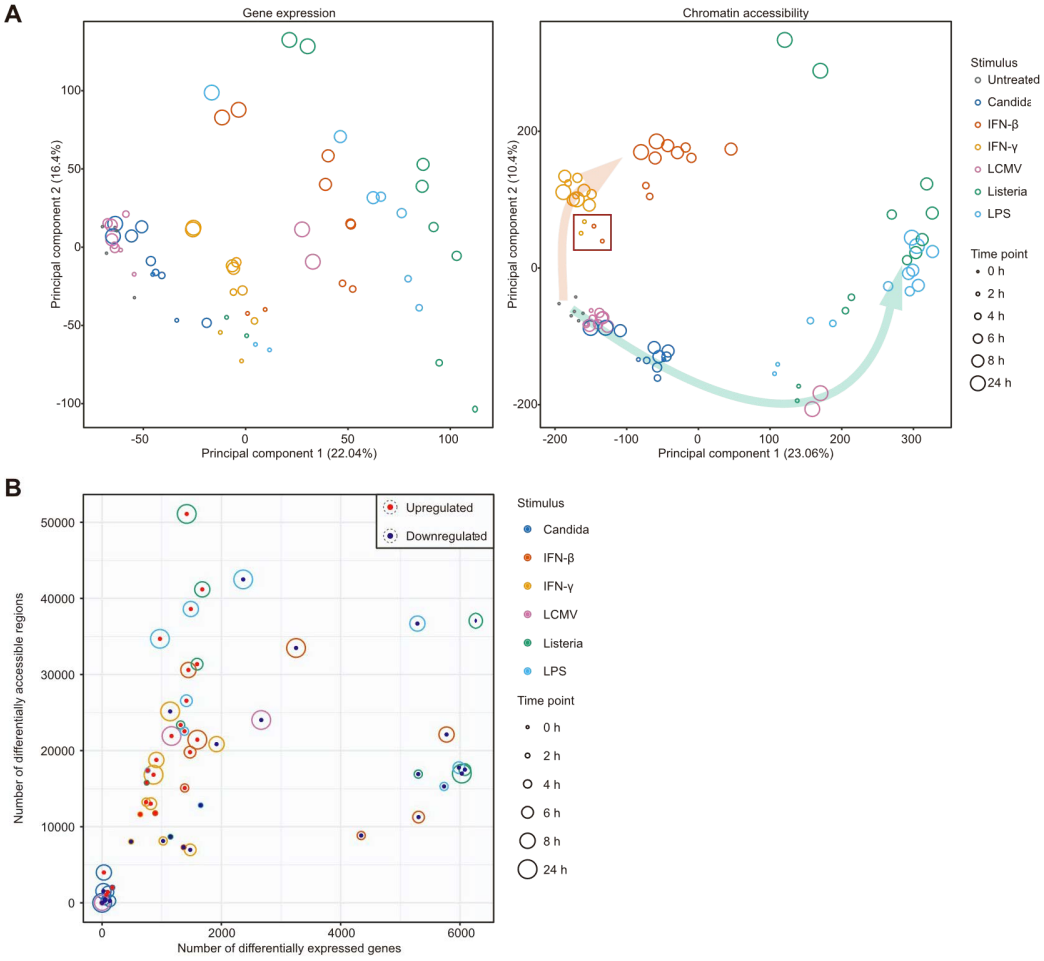

Figure S2 (related to Figure 1). Overview of gene expression and chromatin accessibility dynamics in macrophages responding to six immune stimuli

(A) Scatterplot of first and second principal components for all gene expression (left, RNA-seq: GSE263759; 64 samples) and chromatin accessibility profiles (right, ATAC-seq: GSE263758; 78 samples). Stimuli are color-coded, time points are denoted by circle size, and arrows indicate shared trends. The red box highlights the similarity of the IFN-β and IFN-γ response at the 2 hours' time point.

(B) Scatterplot comparing the number of significant differentially expressed genes (x-axis) and differentially accessible genomic regions (y-axis) for each stimulus compared to untreated controls. Stimuli are color-coded, time points are denoted by circle size and direction of change by red (upregulation) or blue (downregulation) central dots.

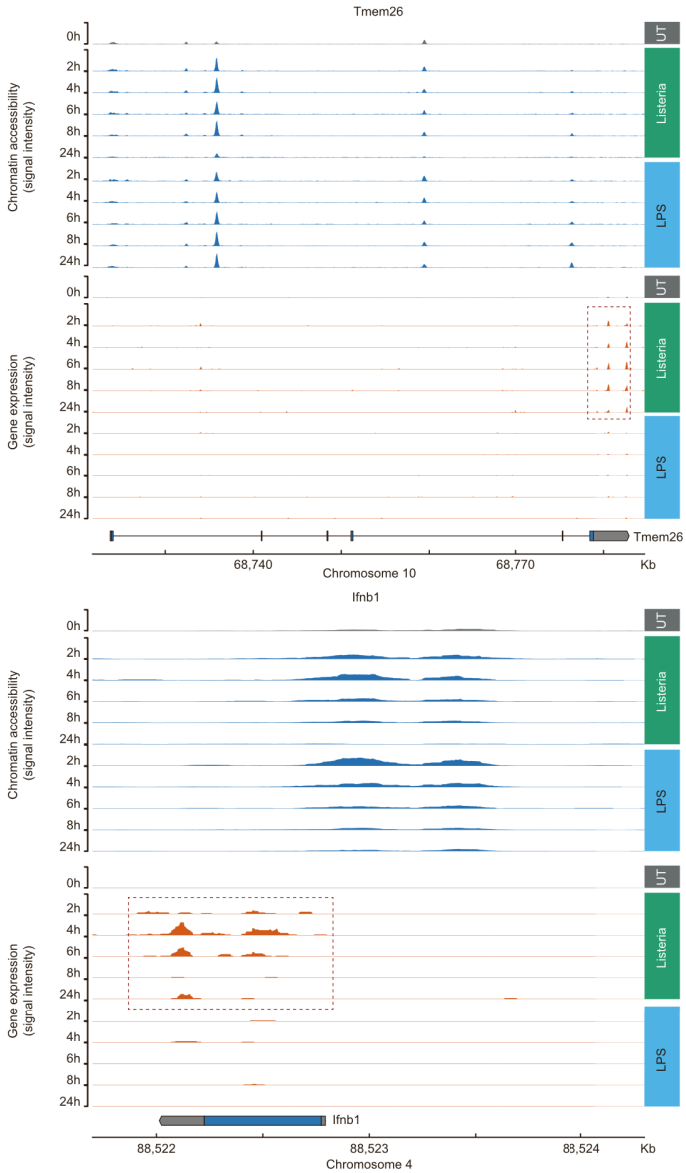

Figure S3 (related to Figure 3). Example of established epigenetic potential and its transcriptional realization for *Tmem26* and *Ifnb1* in macrophages responding to LPS and *Listeria*

Genome browser tracks depicting gene expression (orange) and chromatin accessibility (blue) at the *Tmem26* (top, direction of transcription from left to right) and *Ifnb1* (bottom, direction of transcription from right to left) gene loci over time for LPS and *Listeria* treatments (colored) and untreatec controls (grey). Dashed boxes highlight the realization of the established epigenetic potential as part of the response to *Listeria* treatment but not for LPS treatment.

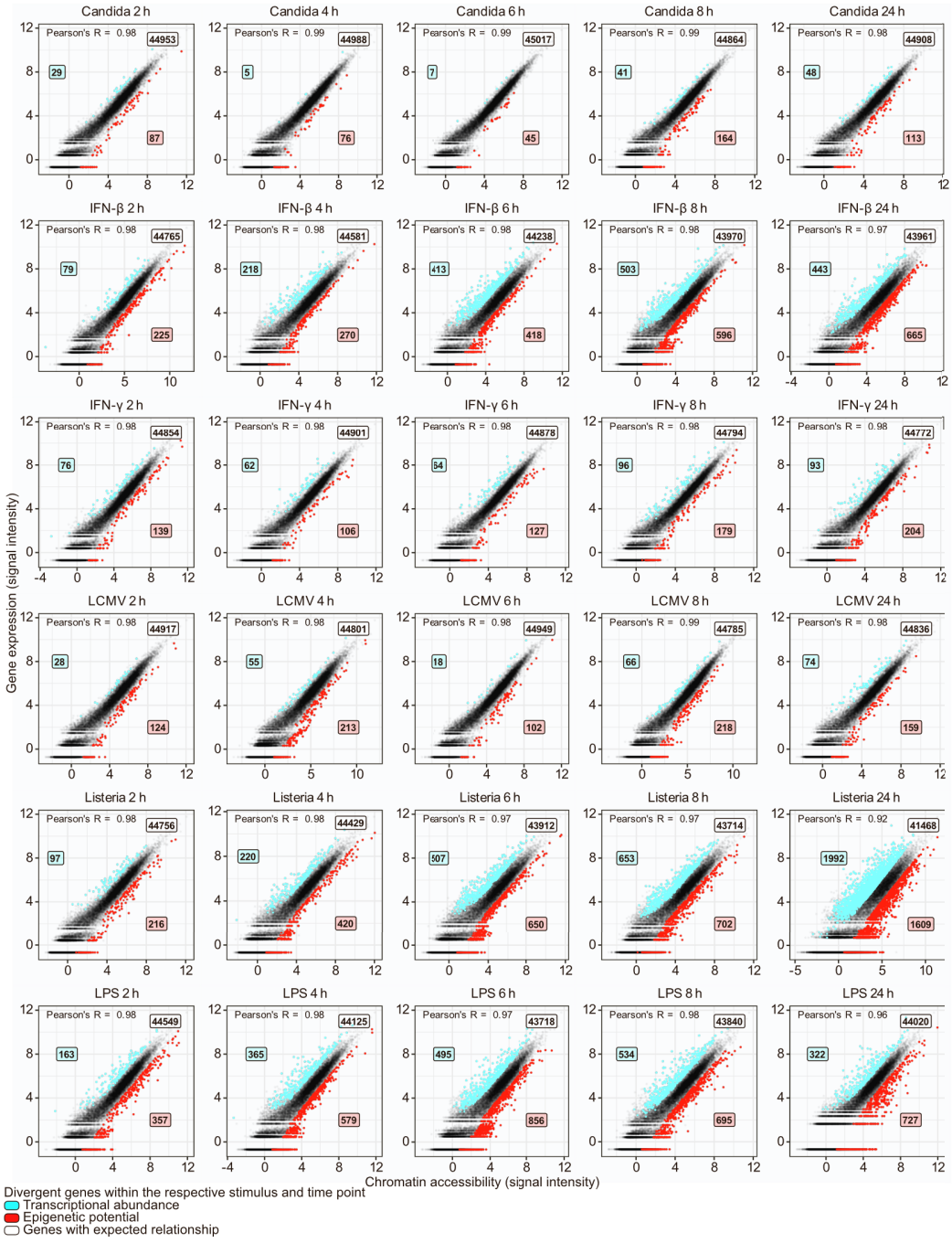
Candida 2 h
Pearson's R = 0.98
44953
29
87
Candida 4 h
Pearson's R = 0.99
44988
5
76
Candida 6 h
Pearson's R = 0.99
45017
7
45
Candida 8 h
Pearson's R = 0.99
44864
41
164
Candida 24 h
Pearson's R = 0.98
44908
48
113
IFN-β 2 h
Pearson's R = 0.98
44765
79
225
IFN-β 4 h
Pearson's R = 0.98
44581
218
270
IFN-β 6 h
Pearson's R = 0.98
44238
413
418
IFN-β 8 h
Pearson's R = 0.98
43970
503
596
IFN-β 24 h
Pearson's R = 0.97
43961
443
665
IFN-γ 2 h
Pearson's R = 0.98
44854
76
139
IFN-γ 4 h
Pearson's R = 0.98
44901
62
106
IFN-γ 6 h
Pearson's R = 0.98
44878
54
127
IFN-γ 8 h
Pearson's R = 0.98
44794
96
179
IFN-γ 24 h
Pearson's R = 0.98
44772
93
204
LCMV 2 h
Pearson's R = 0.98
44917
28
124
LCMV 4 h
Pearson's R = 0.98
44801
55
213
LCMV 6 h
Pearson's R = 0.98
44949
18
102
LCMV 8 h
Pearson's R = 0.99
44785
66
218
LCMV 24 h
Pearson's R = 0.98
44836
74
159
Listeria 2 h
Pearson's R = 0.98
44756
97
216
Listeria 4 h
Pearson's R = 0.98
44429
220
420
Listeria 6 h
Pearson's R = 0.97
43912
507
650
Listeria 8 h
Pearson's R = 0.97
43714
653
702
Listeria 24 h
Pearson's R = 0.92
41468
1992
1609
LPS 2 h
Pearson's R = 0.98
44549
163
357
LPS 4 h
Pearson's R = 0.98
44125
365
579
LPS 6 h
Pearson's R = 0.97
43718
495
856
LPS 8 h
Pearson's R = 0.98
43840
534
695
LPS 24 h
Pearson's R = 0.96
44020
322
727
Gene expression (signal intensity)
Chromatin accessibility (signal intensity)
Divergent genes within the respective stimulus and time point
Transcriptional abundance
Epigenetic potential
Genes with expected relationship

Figure S4 (related to Figure 3). Epigenetic potential and relative transcriptional abundance in macrophages responding to six immune stimuli and in untreated controls

Scatterplots of gene expression and chromatin accessibility for each stimulus and time point, with genes colored as carriers of epigenetic potential (red), relative transcriptional abundance (blue), or expected relationship of expression and chromatin (black), separately for each time point and stimulus. The number of genes per category is indicated.

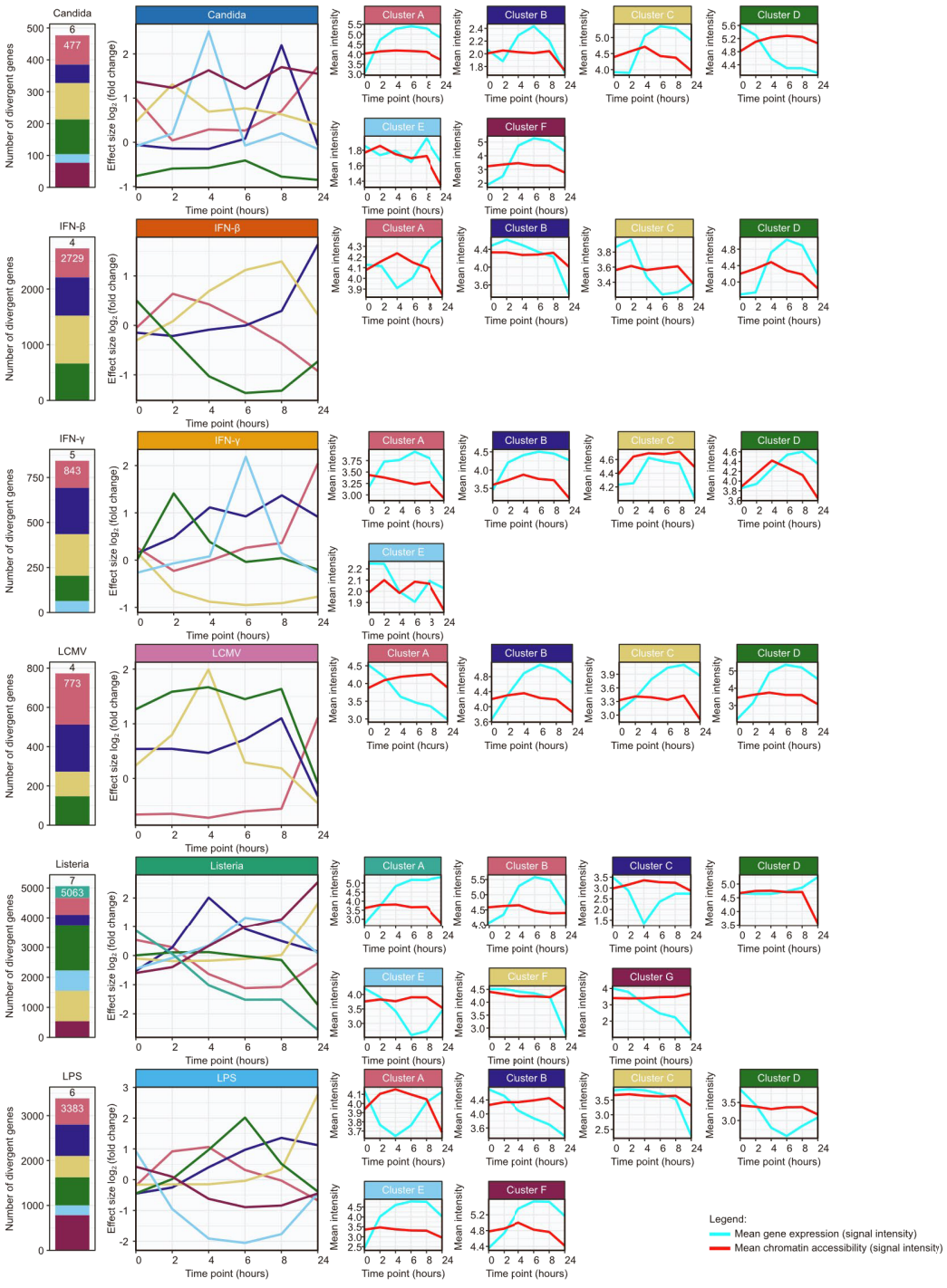
Candida
IFN-β
IFN-γ
LCMV
Listeria
LPS
Number of divergent genes
Effect size log2 (fold change)
Time point (hours)
Mean intensity
Cluster A
Cluster B
Cluster C
Cluster D
Cluster E
Cluster F
Cluster G
Legend:
Mean gene expression (signal intensity)
Mean chromatin accessibility (signal intensity)

Figure S5 (related to Figure 3). Cluster analysis of gene-promoter pairs over the time series of macrophages responding to six immune stimuli

Bar plots showing the composition of time-series clusters (left), mean temporal changes (center), and mean signal intensities (red: chromatin accessibility; blue: gene expression) per cluster (right) in the relationship between gene expression and chromatin accessibility over the time series in response to six immune stimuli (rows).

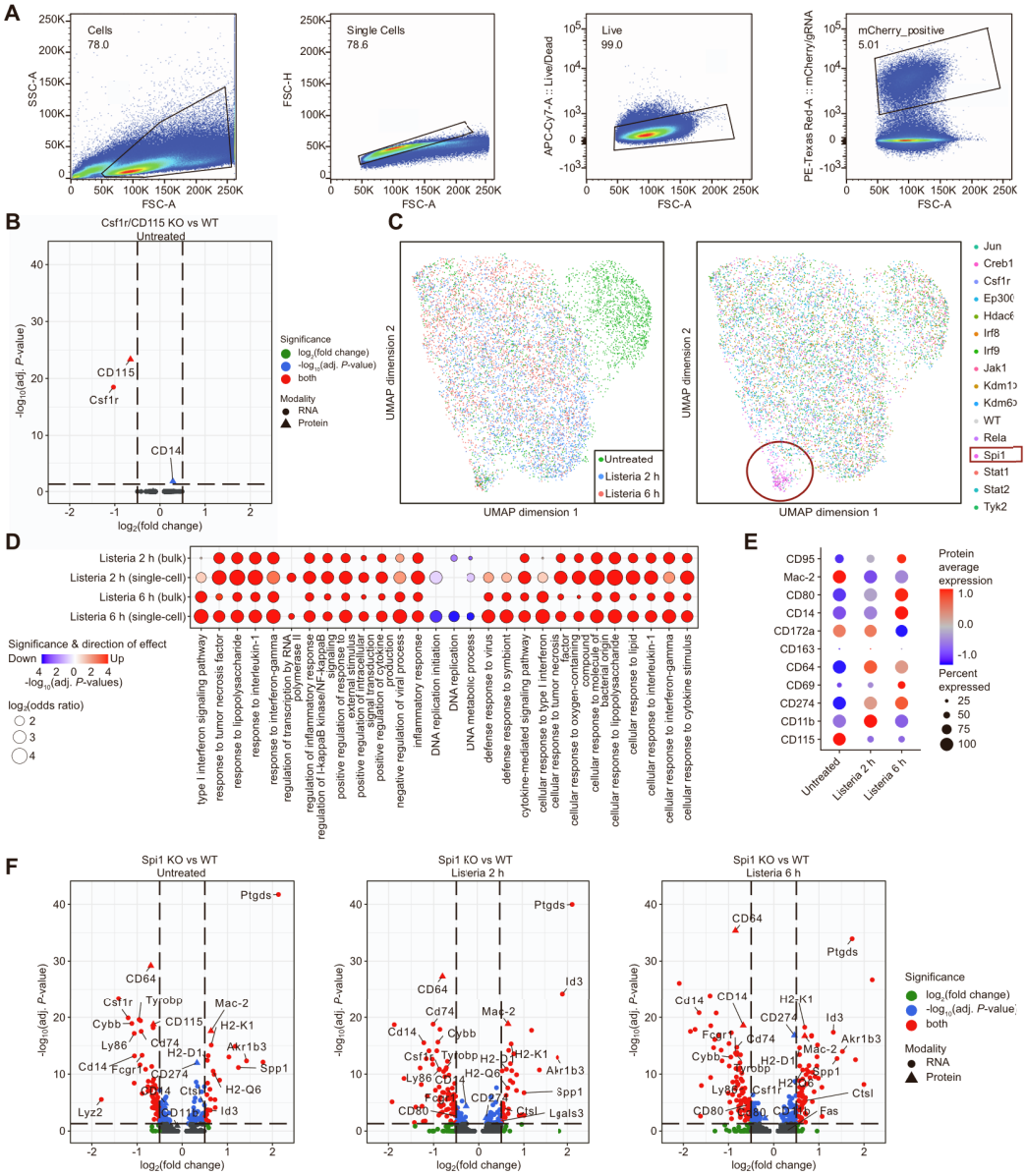

Figure S6 (related to Figure 4). High-content CRISPR screens with a combined CROP-seq and CITE-seq method in macrophages treated with *Listeria*

(A) Representative scatterplots of the FACS gating strategy (left to right) for selecting live cells that have been successfully transduced with a CRISPR guide RNA construct according to mCherry expression.

(B) Volcano plot of differentially expressed genes (circles) and differentially expressed surface proteins (triangles) for knockout (KO) of *Csf1r*/CD115 at the untreated time point, compared to cells without genetic perturbation (WT), based on the Wilcoxon rank-sum test.

(C) Unsupervised UMAP representation of single-cell surface protein expression data (CITE-seq of CROP-seq KO15: GSE263760; 9,153 cells) colored by time point (left) and genetic perturbation (right), respectively. Clustering of *Spi1* knockout cells is highlighted by a circle.

(D) Bubble plot of overlapping gene set enrichments after two and six hours of *Listeria* treatment according to bulk RNA-seq profiles (corresponding to **Figure 1, 2**) and single-cell RNA-seq profiles based on the CROP-seq data in cells without genetic perturbation (WT; corresponding to **Figure 4C**). Effect size (odds ratio) is indicated by bubble size, statistical significance (adjusted *P*-value; hypergeometric test) by opacity, and effect directionality by color (red: higher expression after treatment; blue: lower expression after treatment).

(E) Dot plot of normalized average surface protein expression (based on the CITE-seq readout) in cells without genetic perturbation (WT) across time points. The percentage of cells expressing the protein is indicated by circle size.

(F) Volcano plots of differentially expressed genes (circles) and differentially expressed surface proteins (triangles) for knockout (KO) *Spi1* across time points, compared to cells without genetic perturbation (WT), based on the Wilcoxon rank-sum test.

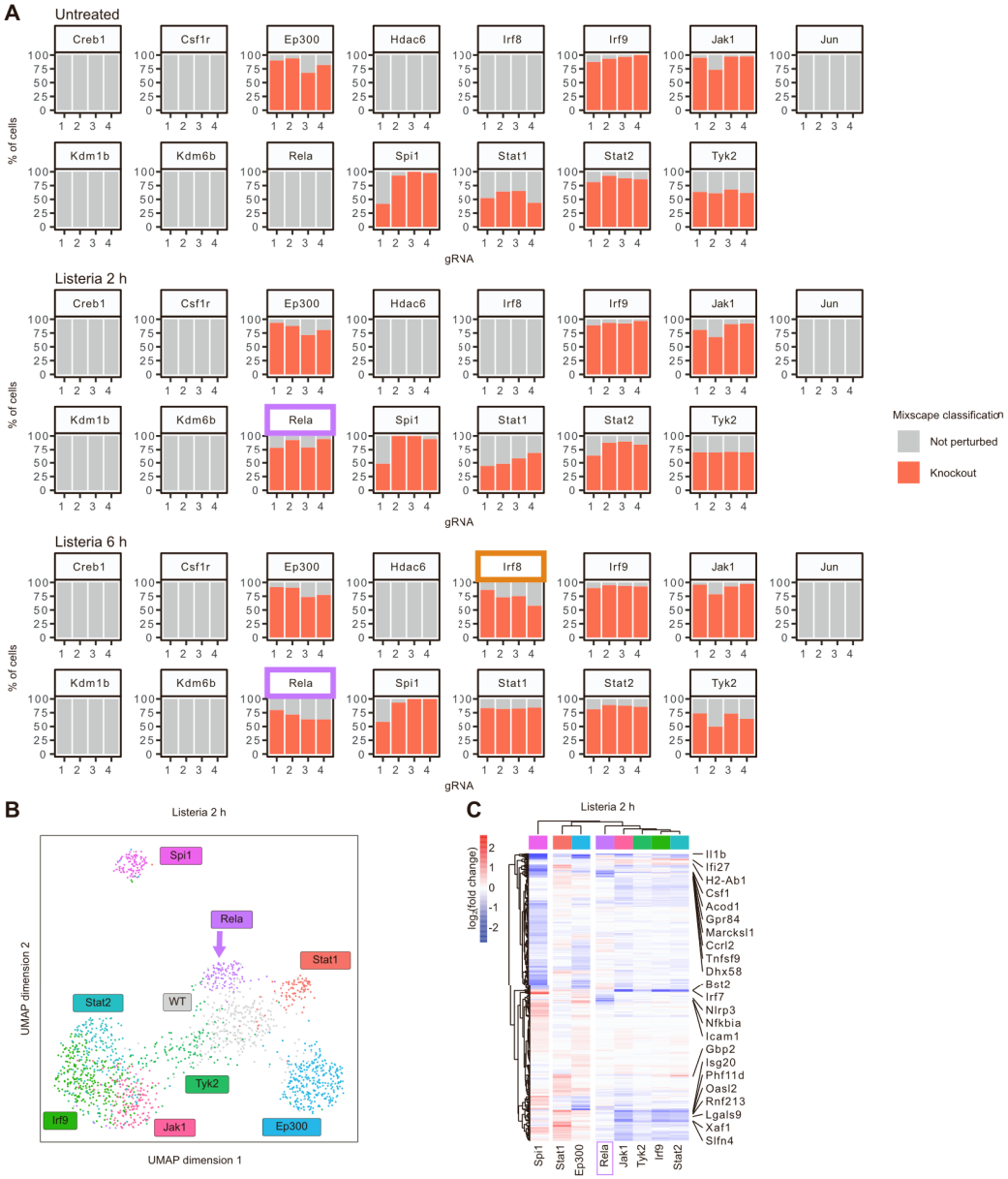

Figure S7 (related to Figure 4). *Mixscape* classification of genetic perturbations for high-content CRISPR screens in macrophages treated with *Listeria*

(A) Bar plots of perturbed cells as the percentage of total cells as determined by *Mixscape* analysis, separately for each target gene, guide RNA, and time point. Boxes highlight the emergence of the *Rela* and *Irf8* knockout effects after two and six hours of *Listeria* treatment, respectively.

(B) Unsupervised UMAP representation of LDA-transformed *Mixscape* genetic perturbation signatures (based on the assigned guide RNAs) after two hours of *Listeria* treatment, with cells colored by their assigned guide RNAs (1,642 cells). The arrow highlights the emergence of the *Rela* knockout effect at the 2 hours' time point.

(C) Hierarchically clustered heatmap of effect sizes for knockout-induced differential gene expression after two hours of *Listeria* treatment. The box highlights the emergence of the *Rela* knockout effect at the 2 hours' time point.

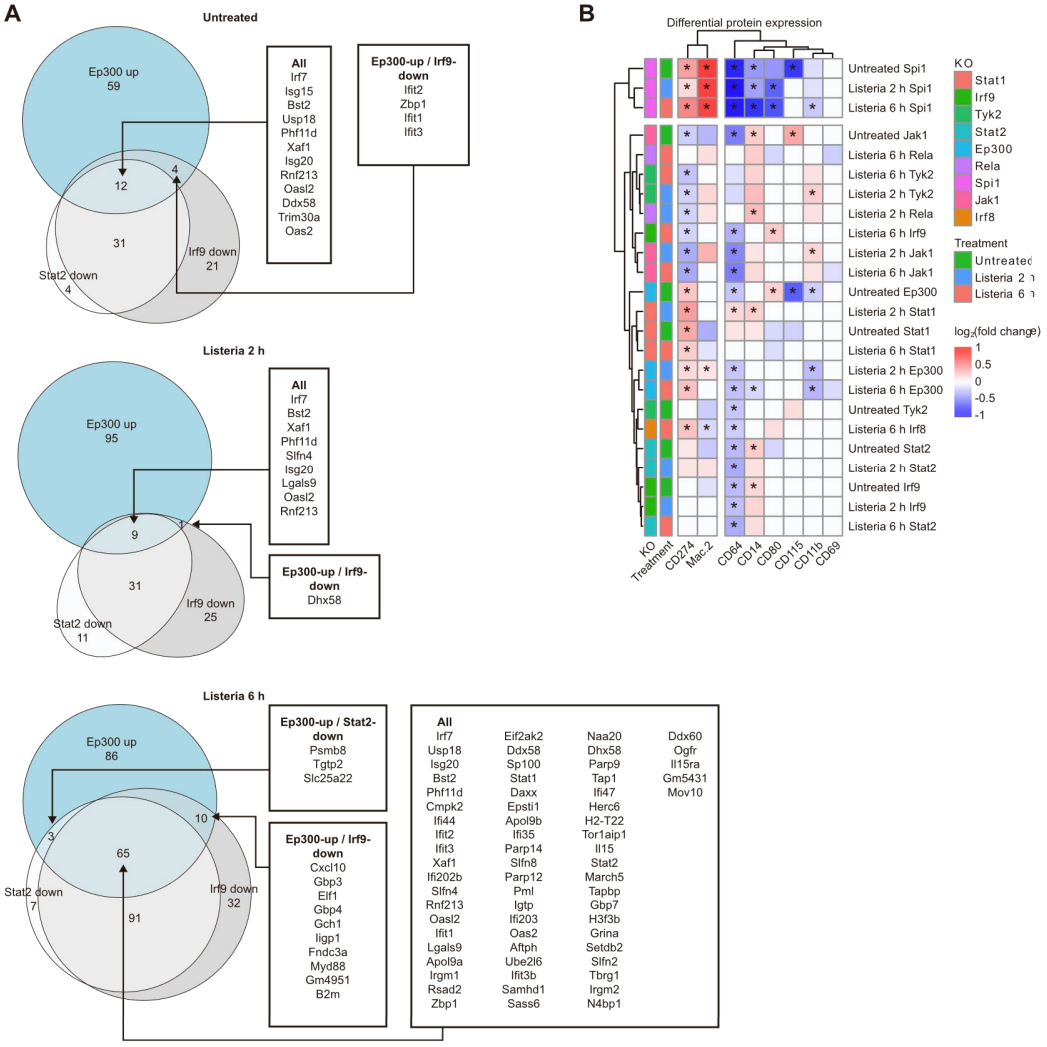

Figure S8 (related to Figure 4). Regulators of ISG expression and differential cell surface protein expression

(A) Euler plots of downregulated genes for the *Irf9* and *Stat2* knockouts and upregulated genes for the *Ep300* knockout at each time point of *Listeria* treatment (left). Overlapping genes are annotated in boxes (right).

(B) Hierarchically clustered heatmap of knockout-induced differential cell surface marker expression based on CITE-seq (fold changes, columns) compared to cells without genetic perturbation, across all time points. Statistical significance (adjusted *P*-value < 0.05; Wilcoxon rank-sum test) is indicated by asterisks (*).

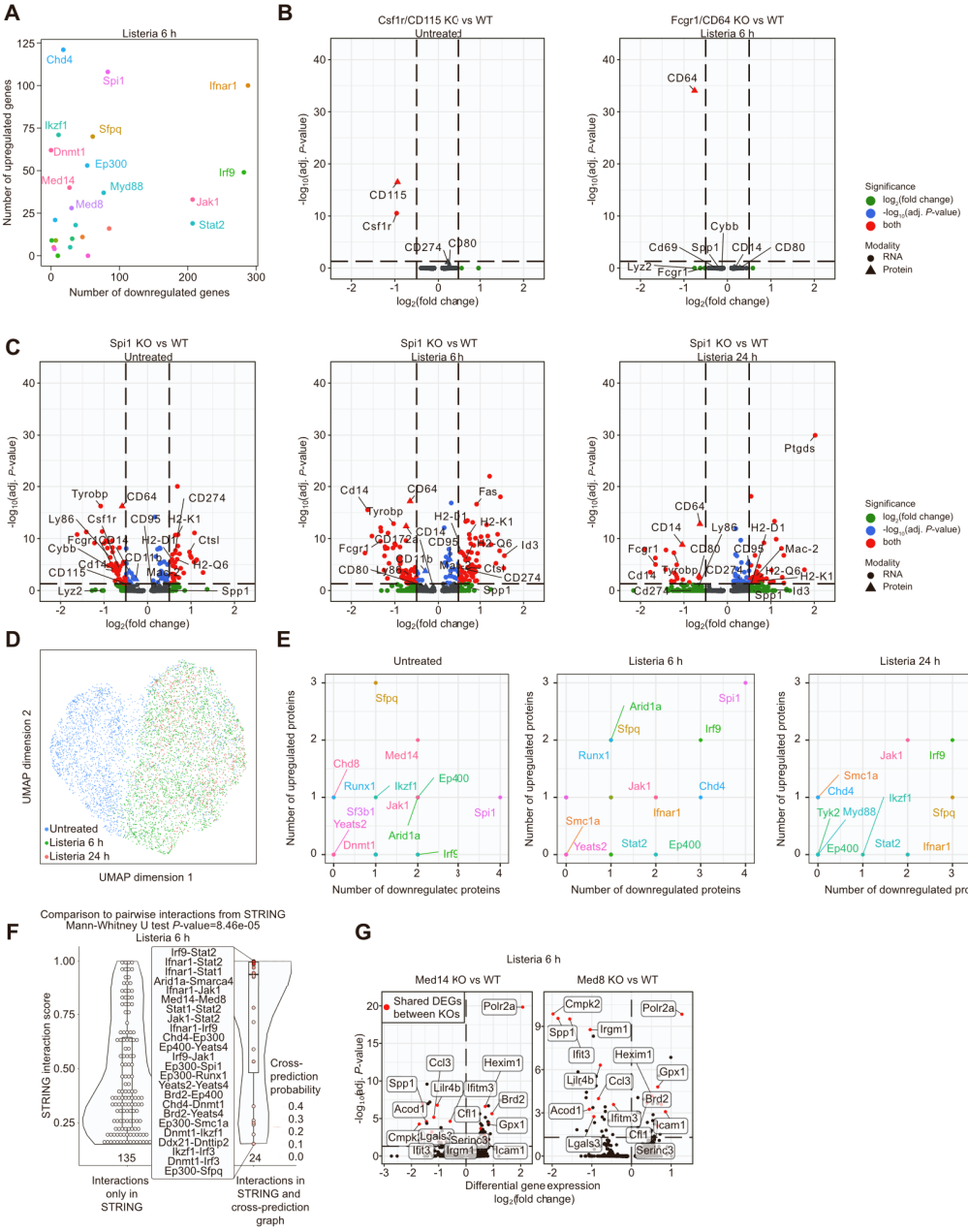
A
Listeria 6 h
Number of upregulated genes
Number of downregulated genes
Chd4
Spi1
Ifnar1
Ikzf1
Sfpq
Dnmt1
Ep300
Irf9
Med14
Myd88
Med8
Jak1
Stat2
B
Csf1r/CD115 KO vs WT
Untreated
Fcgr1/CD64 KO vs WT
Listeria 6 h
-log10(adj. P-value)
log2(fold change)
CD115
Csf1r
CD274
CD80
CD64
Cybb
Cd69
Spp1
CD14
Lyz2
Fcgr1
Significance
log2(fold change)
-log10(adj. P-value)
both
Modality
RNA
Protein
C
Spi1 KO vs WT
Untreated
Listeria 6 h
Listeria 24 h
Tyrobp
CD64
CD274
Ly86
Csf1r
CD95
H2-K1
Fcgr1
CD14
H2-D1
Ctsl
Cybb
CD11b
Cd14
H2-Q6
CD115
Mac-2
Lyz2
Spp1
Fas
Cfs1
Id3
Ptgds
D
UMAP dimension 2
UMAP dimension 1
Untreated
Listeria 6 h
Listeria 24 h
E
Untreated
Listeria 6 h
Listeria 24 h
Number of upregulated proteins
Number of downregulated proteins
Sfpq
Med14
Chd8
Runx1
Ikzf1
Ep400
Sf3b1
Jak1
Spi1
Yeats2
Arid1a
Dnmt1
Irf9
Arid1a
Sfpq
Irf9
Runx1
Jak1
Chd4
Ifnar1
Smc1a
Yeats2
Stat2
Ep400
Jak1
Irf9
Smc1a
Chd4
Ikzf1
Tyk2
Myd88
Sfpq
Ep400
Stat2
Ifnar1
F
Comparison to pairwise interactions from STRING
Mann-Whitney U test P-value=8.46e-05
Listeria 6 h
STRING interaction score
Irf9-Stat2
Ifnar1-Stat2
Ifnar1-Stat1
Arid1a-Smarca4
Ifnar1-Jak1
Med14-Med8
Stat1-Stat2
Jak1-Stat2
Ifnar1-Irf9
Chd4-Ep300
Ep400-Yeats4
Irf9-Jak1
Ep300-Spi1
Ep300-Runx1
Yeats2-Yeats4
Brd2-Ep400
Chd4-Dnmt1
Brd2-Yeats4
Ep300-Smc1a
Dnmt1-Ikzf1
Ddx21-Dnttip2
Ikzf1-Irf3
Dnmt1-Irf3
Ep300-Sfpq
135
24
Cross-prediction probability
Interactions only in STRING
Interactions in STRING and cross-prediction graph
G
Listeria 6 h
Med14 KO vs WT
Med8 KO vs WT
Shared DEGs between KOs
-log10(adj. P-value)
Differential gene expression
log2(fold change)
Polr2a
Cmpk2
Irgm1
Ccl3
Hexim1
Spp1
Lilr4b
Ifitm3
Ifit3
Gpx1
Acod1
Cfl1
Brd2
Lgals3
Serinc3
Icam1

Figure S9 (related to Figure 5). Quality control, differential protein expression, and protein-protein interactions for the upscaled CROP-seq screen

(A) Scatterplot comparing the number of significantly upregulated genes (y-axis) and significantly downregulated genes (x-axis) for each knockout based on the *Mixscape* genetic perturbation analysis for the 6 hours' time point, based on the Wilcoxon rank-sum test.

(B) Volcano plots of differentially expressed genes (circles) and differentially expressed surface proteins (triangles) for knockouts (KO) *Csf1r*/CD115 (left) and *Fcgr1*/CD64 (right) in the untreated and the 6 hours' time point, respectively, compared to cells without genetic perturbation (WT), based on the Wilcoxon rank-sum test.

(C) Volcano plots of differentially expressed genes (circles) and differentially expressed surface proteins (triangles) for the knockout (KO) of *Spi1* across time points, compared to cells without genetic perturbation (WT), based on the Wilcoxon rank-sum test.

(D) Unsupervised UMAP representation of single-cell surface protein expression (CITE-seq of CROP-seq KO150: GSE263761; 6,187 cells) following *Mixscape* genetic perturbation analysis, colored by time point.

(E) Scatterplots comparing the number of significantly upregulated (y-axis) and downregulated (x-axis) surface proteins (CITE-seq) for each knockout based on *Mixscape* genetic perturbation analysis across all time points, based on the Wilcoxon rank-sum test.

(F) Distribution of protein-protein interaction scores from the STRING database for regulators with significant knockout effects based on *Mixscape* genetic perturbation analysis after six hours of Listeria treatment, shown separately for regulator pairs that were (right) or were not (left) connected in the functional similarity graph (**Figure 5D**). Regulator pairs were colored based on the average prediction probability connecting the two knockouts, and score distributions were compared by Mann-Whitney U test.

(G) Volcano plots of differentially expressed genes for the mediator complex knockouts *Med14* (left) and *Med8* (right) after six hours of *Listeria* treatment, compared to cells without genetic perturbation (WT). Differentially expressed genes that are shared between the two comparisons are colored in red and individually labeled, based on the Wilcoxon rank-sum test.

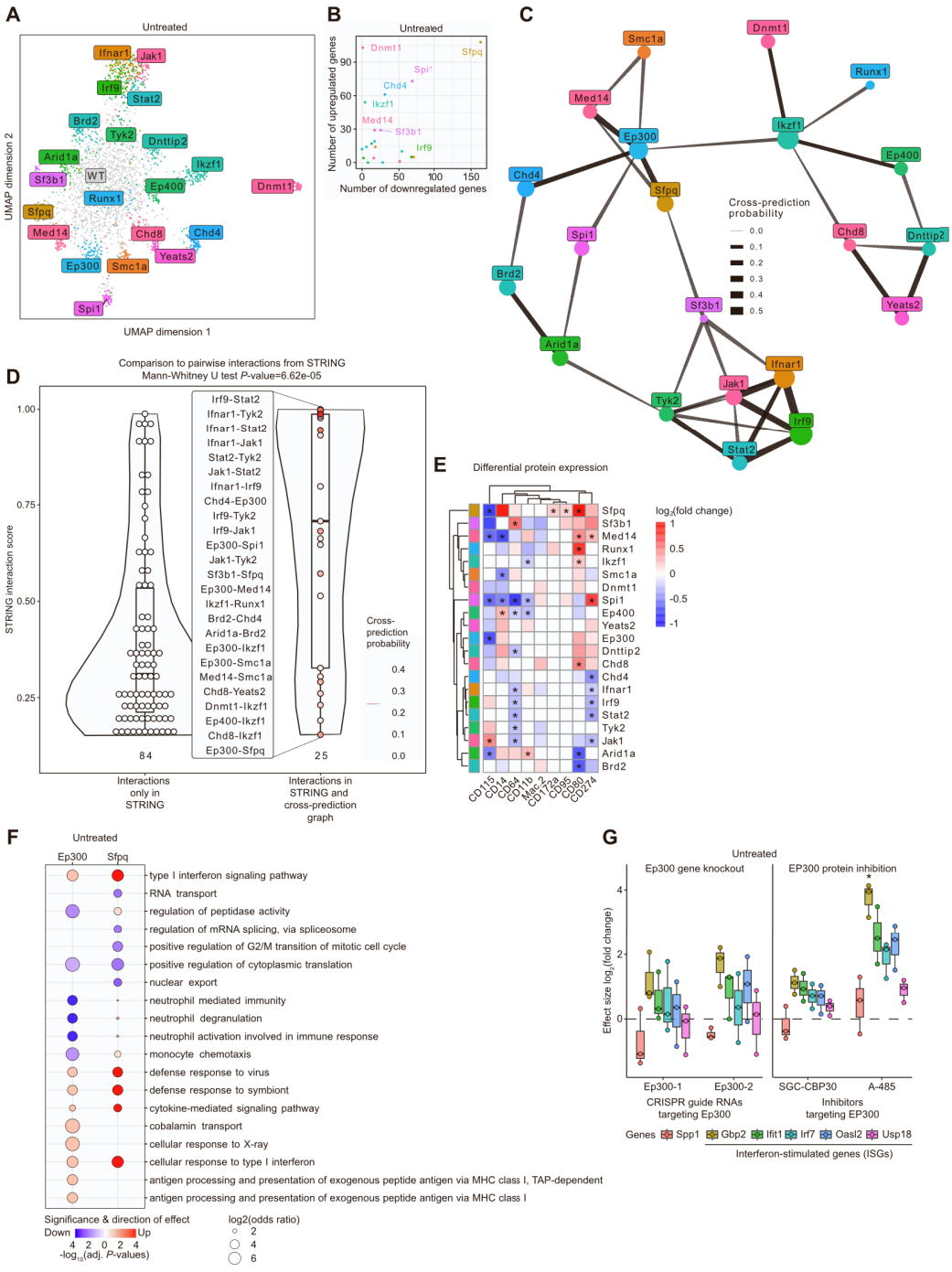
A
Untreated
UMAP dimension 2
UMAP dimension 1
Ifnar1
Jak1
Irf9
Stat2
Brd2
Tyk2
Dnttip2
Arid1a
Ikzf1
Sf3b1
WT
Ep400
Dnmt1
Runx1
Sfpq
Med14
Chd8
Chd4
Yeats2
Ep300
Smc1a
Spi1
B
Untreated
Number of upregulated genes
Number of downregulated genes
C
Smc1a
Dnmt1
Runx1
Med14
Ikzf1
Ep300
Ep400
Chd4
Sfpq
Cross-prediction probability
Spi1
Chd8
Dnttip2
Brd2
Sf3b1
Yeats2
Arid1a
Ifnar1
Jak1
Tyk2
Irf9
Stat2
D
Comparison to pairwise interactions from STRING
Mann-Whitney U test P-value=6.62e-05
STRING interaction score
Irf9-Stat2
Ifnar1-Tyk2
Ifnar1-Stat2
Ifnar1-Jak1
Stat2-Tyk2
Jak1-Stat2
Ifnar1-Irf9
Chd4-Ep300
Irf9-Tyk2
Irf9-Jak1
Ep300-Spi1
Jak1-Tyk2
Sf3b1-Sfpq
Ep300-Med14
Ikzf1-Runx1
Brd2-Chd4
Arid1a-Brd2
Ep300-Ikzf1
Ep300-Smc1a
Med14-Smc1a
Chd8-Yeats2
Dnmt1-Ikzf1
Ep400-Ikzf1
Chd8-Ikzf1
Ep300-Sfpq
Cross-prediction probability
84
25
Interactions only in STRING
Interactions in STRING and cross-prediction graph
E
Differential protein expression
log2(fold change)
Sfpq
Sf3b1
Med14
Runx1
Ikzf1
Smc1a
Dnmt1
Spi1
Ep400
Yeats2
Ep300
Dnttip2
Chd8
Chd4
Ifnar1
Irf9
Stat2
Tyk2
Jak1
Arid1a
Brd2
CD115
CD14
CD64
CD11b
Mac-2
CD172a
CD95
CD80
CD274
F
Untreated
Ep300
Sfpq
type I interferon signaling pathway
RNA transport
regulation of peptidase activity
regulation of mRNA splicing, via spliceosome
positive regulation of G2/M transition of mitotic cell cycle
positive regulation of cytoplasmic translation
nuclear export
neutrophil mediated immunity
neutrophil degranulation
neutrophil activation involved in immune response
monocyte chemotaxis
defense response to virus
defense response to symbiont
cytokine-mediated signaling pathway
cobalamin transport
cellular response to X-ray
cellular response to type I interferon
antigen processing and presentation of exogenous peptide antigen via MHC class I, TAP-dependent
antigen processing and presentation of exogenous peptide antigen via MHC class I
Significance & direction of effect
Down
Up
-log10(adj. P-values)
log2(odds ratio)
G
Untreated
Ep300 gene knockout
EP300 protein inhibition
Effect size log2(fold change)
Ep300-1
Ep300-2
SGC-CBP30
A-485
CRISPR guide RNAs targeting Ep300
Inhibitors targeting EP300
Genes
Spp1
Gbp2
Ifit1
Irf7
Oasl2
Usp18
Interferon-stimulated genes (ISGs)

Figure S10 (related to Figure 5). Analysis of the upscaled CROP-seq screen for untreated macrophages

(A) Unsupervised UMAP representation of LDA-transformed *Mixscape* genetic perturbation signatures (based on the assigned guide RNAs) in untreated cells, with cells colored by their assigned guide RNAs (2,485 cells).

(B) Scatterplot comparing the number of significantly upregulated genes (y-axis) and significantly downregulated genes (x-axis) for each knockout based on *Mixscape* genetic perturbation analysis in untreated cells, based on the Wilcoxon rank-sum test.

(C) Functional similarity graph derived by cross-prediction analysis in untreated cells. The 21 nodes represent gene knockouts and edges denote average cross-prediction probabilities (pruned at a cutoff of 0.1). Node size corresponds to the square root of the number of cells for each knockout. Edges are visualized as trapezoids, where the width at the source node corresponds to the probability of cross-predicting the source node as the target node.

(D) Distribution of protein-protein interaction scores from the STRING database for regulators with significant knockout effects based on *Mixscape* genetic perturbation analysis in untreated cells, shown separately for regulator pairs that were (right) or were not (left) connected in the functional similarity graph (**Figure S10C**). Regulator pairs were colored based on the average prediction probability connecting the two knockouts, and score distributions were compared by Mann-Whitney U test.

(E) Hierarchically clustered heatmap of knockout-induced differential cell surface marker expression based on CITE-seq (fold changes, columns) compared to cells without genetic perturbation, in untreated cells. Statistical significance (adjusted *P*-value < 0.05; Wilcoxon rank-sum test) is indicated by asterisks (*).

(F) Bubble plot of gene set enrichments for *Ep300* and *Sfpq* knockouts in untreated cells. Effect size (odds ratio) is indicated by bubble size, statistical significance (adjusted *P*-value; hypergeometric test) by opacity, and effect directionality by color (red: higher expression in the knockouts; blue: lower expression in the knockouts).

(G) Boxplots of gene expression (fold changes compared to the respective controls) for *Spp1* and five interferon stimulated genes (ISGs) upon interference with EP300 function at the DNA level (CRISPR knockout of *Ep300*, left) and at the protein level (treatment with small-molecule inhibitors of EP300, right). Gene expression was measured by qPCR in untreated RAW 264.7 cells. Three biological replicates were profiled and plotted, statistical significance was determined by paired t-tests, and asterisks (*) indicate *P*-values below 0.01.

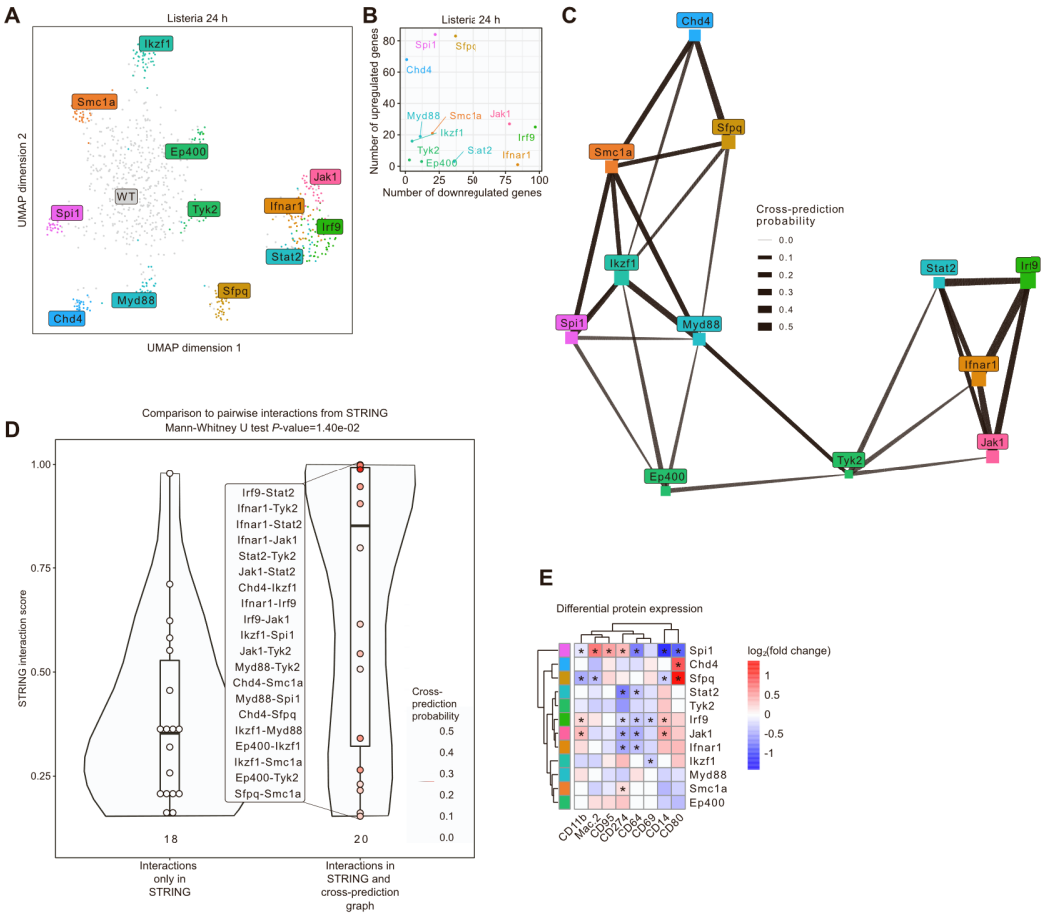

Figure S11 (related to Figure 5). Analysis of the upscaled CROP-seq screen for macrophages after 24 hours of *Listeria* treatment

(A) Unsupervised UMAP representation of LDA-transformed *Mixscape* genetic perturbation signatures (based on the assigned guide RNAs) after 24 hours of *Listeria* treatment, with cells colored by their assigned guide RNAs (880 cells).

(B) Scatterplot comparing the number of significantly upregulated genes (y-axis) and significantly downregulated genes (x-axis) for each knockout based on *Mixscape* genetic perturbation analysis at the 24 hours' time point, based on the Wilcoxon rank-sum test.

(C) Functional similarity graph derived by cross-prediction analysis for the 24 hours' time point. The 12 nodes represent gene knockouts and edges denote average cross-prediction probabilities (pruned at a cutoff of 0.1). Node size corresponds to the square root of the number of cells for each knockout. Edges are visualized as trapezoids, where the width at the source node corresponds to the probability of cross-predicting the source node as the target node.

(D) Distribution of protein-protein interaction scores from the STRING database for regulators with significant knockout effects based on *Mixscape* genetic perturbation analysis after 24 hours of Listeria treatment, shown separately for regulator pairs that were (right) or were not (left) connected in the functional similarity graph (**Figure S11C**). Regulator pairs were colored based on the average prediction probability connecting the two knockouts, and score distributions were compared by Mann-Whitney U test.

(E) Hierarchically clustered heatmap of knockout-induced differential cell surface marker expression based on CITE-seq (fold changes, columns) compared to cells without genetic perturbation, for the 24 hours' time point. Statistical significance (adjusted *P*-value < 0.05; Wilcoxon rank-sum test) is indicated by asterisks (*).

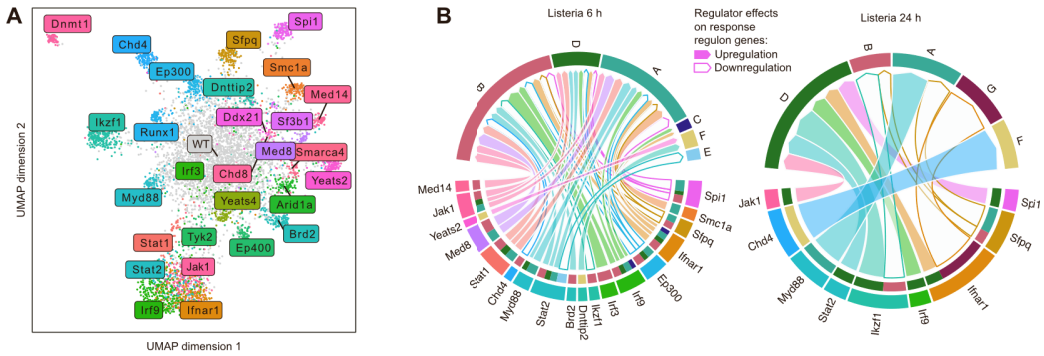

Figure S12 (related to Figure 6). Analysis of *Listeria* response regulators linked to *Listeria* response regulons

(A) Unsupervised UMAP representation of LDA-transformed *Mixscape* genetic perturbation signatures (based on the assigned guide RNAs) across all time points, with cells colored by their assigned guide RNAs (6,198 cells).

(B) Circos plots connecting the regulator effects after six hours (left diagram: bottom, from **Figure 5C**) and 24 hours (right diagram: bottom, from **Figure S11A**) of *Listeria* treatment with the regulons driving the response to *Listeria* (both diagrams: top, from **Figure 3D**). Arrows indicate statistically significant enrichments (hypergeometric test; filled arrows: upregulation; outline-only arrows: downregulation); arrow width denotes effect size (log_2 odds ratio).

CHAPTER THREE: Discussion

3.1 General discussion:

A holistic view of cell biology and the underlying molecular pathways will benefit from high-throughput analysis of gene functions in robust experiments covering a range of conditions, timepoints and readout modalities. In the course of this thesis, we explored novel screening technology based on CRISPR-Cas9 mediated genetic perturbations targeting over a hundred individual genes coupled to single cell sequencing providing both transcriptomic data and cell-surface proteome insights. We applied this technological approach to investigate transcriptional regulators of macrophage immune signaling and described novel functional insights. This data was analyzed and combined with high-quality time series RNA and chromatin data exploring a broader array of immune signals in primary macrophages. Overall, this study provides a robust approach to explore transcriptional regulation; contributes valuable, high-quality data sets; and describes novel biological connections between genes.

3.1.1 Descriptive investigation of transcriptional and epigenetic dynamics in macrophages

In the initial part of this thesis, we performed dense time series immune stimulation experiments with six different immune stimuli on *in vitro* differentiated bone-marrow derived murine macrophages with both transcriptome and chromatin accessibility readout from the same cell culture well. Gathering both readout modalities from the same cell population and adhering to best practices in next generation sequencing workflows we obtained high-quality data for each modality respectively.

We identified expected transcriptional patterns based on previous literature such as the rapid upregulation of immune pathways with a clear time-dependent dynamic. Pathogenic stimuli first engaged TLR and intracellular detection pathways leading to strong NFκB signaling with subsequent interferon response pathways. The latter being induced by the type I interferon, IFN-β, expressed by the macrophages themselves (Sheu & Hoffmann, 2022). Likewise, transcription of cell proliferation and maintenance pathways decreased drastically as reported previously (Cheng *et al*, 2019). Additionally, comparison with chromatin accessibility indicates that the cells epigenetic status retains openness for a potential subsequent reactivation. Indeed, in our arguable weakest treatment (based on number of differential genes and accessible loci), using UV-irradiated *C. albicans*, we observed an initial transcriptional drop in a regulon associated with cell cycle and subsequent return to homeostasis at our latest timepoint of 24 hours. In this treatment we also observed a return to homeostatic chromatin accessibility for all identified regulons, indicating that macrophages likely return to an inactive state and

continue to persist if the pathogenic threat is of minor severity. These cells may have altered parts of their epigenetic profile, such as histone modifications like H3K4me1 (Kaikkonen *et al*, 2013; Ostuni *et al*, 2013), that can remain irrespective of chromatin accessibility and convey a training or tolerance effect for subsequent encounters as has been described extensively for innate immune cells (Netea *et al*, 2019, 2011; Novakovic *et al*, 2016; Sheu & Hoffmann, 2022; Vuscan *et al*, 2024).

While the involved epigenetic mechanisms can vary, we decided to utilize ATAC-seq to robustly measure general chromatin accessibility. As exemplified by the IFN-β locus chromatin opens up by both *Listeria* and LPS challenge yet full transcriptional activation was only observed in the ongoing *Listeria* condition. Interestingly, LPS treatment alone is reported to induce IFN-β (Jacobs & Ignarro, 2001) yet in our data did not yield a significant increase on the transcriptional level. In order to assess shared regulatory patterns over the time course, we integrated transcriptional output with chromatin accessibility at the promoter region to allow a high-level view of epigenetic involvement (Krausgruber *et al*, 2020). Using this integrative approach we select genes divergent from the expected correlation between both data modalities. As in the original study, we used the term “epigenetic potential” where a gene is accessible yet not transcribed to the expected level. We additionally termed the opposite state of abundant mRNA without the expected level of chromatin openness as “relative transcriptional abundance”. This approach allowed us to observe dynamic shifts over the time points and comparison between conditions, such as LPS and *Listeria* in their establishment of epigenetic potential and its subsequent realization, that is, expression. Furthermore, we were able to augment transcription factor prediction analysis with our own perturbation data of various transcriptional regulators enhancing biological insights.

3.1.2 Functional screening results

Our screening setup aimed to identify transcriptional regulators with a strong focus on epigenetic modifiers. Overall, we use the term transcriptional regulator very loosely/inclusive including upstream receptor and signaling adaptor proteins. The reason being that the readout of the perturbation screen permits a rather unbiased representation of the transcriptome of the cell. In other words, measuring the resulting changes from a perturbation is inherently agnostic to the respective biological mechanism. This is best demonstrated by our results with the “high within time point similarity” found between the cell surface receptor IFNAR1, the adaptor kinases JAK1 and TYK2 and the transcription factors STAT2 and IRF9. All are part of the type I interferon response pathway (Gough *et al*, 2012). Our results support the idea, that inhibition of the interferon response in macrophages challenged with *Listeria* can be achieved independent of which component of this pathway is targeted. This ability to screen entire pathways

increases therapeutic options to select from a variety of target genes and thus circumvent traditionally “undruggable” pathway members.

However, even in unchallenged homeostatic macrophages the receptor IFNAR1 displayed strong within time point similarity with the other members. This supports a model in which tonic signaling maintains the expression of the ISGF3 complex members STAT1, STAT2 and IRF9 (Gough *et al*, 2012; Majoros *et al*, 2016) and in turn enables unphosphorylated STAT2-IRF9 complexes to drive basal ISG expression (Platanitis *et al*, 2019). Importantly, the latter study used a JAK inhibitor to demonstrate that short term perturbation of the receptor or signaling adaptors would fail to decrease homeostatic ISG expression.

For interpreting a screen it is therefore important to consider the technical details Especially, how and when a perturbation would affect the respective target gene expression and replace the unperturbed proteins still present in the cell. With these considerations in mind, our findings serve as an example of the screening paradigm that irrespective of the actual mechanisms screening hits can be grouped based on functional similarities.

Differences in STATs

The greater depth of the first screen enabled us to observe that the STAT1 knockout lead to an increase in certain ISGs, such as IFITs and OASLs at homeostatic conditions, a counter-intuitive finding at first. Likewise, the 6 h time point of the first screen indicates that STAT1 loss does not lead to a complete abrogation of interferon signaling as do other members of the JAK-STAT pathway such as JAK1, IRF9, and STAT2. A potential explanation for this observation could be found in studies that explored how both unphosphorylated STAT2-IRF9 complexes as well as phosphorylated STAT2 complexes can cover a majority of interferon signaling in the absence of STAT1 (Blaszczyk *et al*, 2015; Michalska *et al*, 2018; Platanitis *et al*, 2019). Additionally, compared to STAT1 knockouts, unphosphorylated STAT1 macrophages are paradoxically more susceptible to infection with *Legionella.* This intracellular pathogen replicates primarily in alveolar macrophages by suppressing STAT2-IRF9 signaling (Majoros *et al*, 2016). Additionally, in fibroblasts unphosphorylated STAT1 lead to an increase of several ISGs such as IFI27, BST2, OAS1-3, IFI44 and STAT1 (Cheon & Stark, 2009).

These findings support cell type specific fine-tuning of ISGs in homeostatic conditions where unphosphorylated STAT1 and STAT2-IRF9 complexes may compete to ensure proper ISG expression levels. Overall, our data indicate that loss of STAT1 in a context preserving paracrine tonic interferon signaling can lead to a stronger basal ISG expression.

Opposing interferon expression

The aforementioned agnostic nature regarding the mechanism of action is further exemplified by the grouping of EP300 and SFPQ into a functional relationship. This is best characterized by the shared upregulation of interferon response genes after knockout of either factor. The paraspeckle protein SFPQ has been previously observed to be involved in the gene regulation of endogenous genes. SFPQ acts as a transcriptional repressor at the promoter site of IL-8 and quickly relocates to paraspeckles upon stimulation, thus allowing IL-8 expression to occur (Imamura *et al*, 2014). The long-noncoding RNA *Neat1_2* involved in the recruitment of SFPQ was found by Imamura *et al.* to regulate around 85 genes, two of which, RIG-I and DDX60, were later confirmed to be also regulated by SFPQ in a similar manner (Ma *et al*, 2017). Our study discovered an even more widespread regulation of interferon response genes, implying that the inhibitory function of SFPQ is vital to keep unwanted expression of detrimental immune cascades in check. Further evidence for the importance of paraspeckle formation during immune activation comes from *Neat1_2* knockout mice which fail to mount an adequate immune response to LPS. However, their cytokine profile remains relatively stable without immune activation (Azam *et al*, 2024). This further supports a model in which transcriptional repression by SFPQ is a main immune regulator and requires active sequestration to paraspeckles via *Neat1* to allow initiation of a proper immune response.

Additionally, several viruses exploit SFPQ for its IRSE-trans activating function, which allows the translation of transcripts beginning at IRSE sites. Therefore, a therapeutic intervention at SFPQ may provide multiple benefits to the host. Namely the inhibition of viral protein translation, the activation of cGAS-STING pathway via paraspeckle destabilization and the de-repression of immune genes (Milcamps & Michiels, 2024). Taken together, our findings position SFPQ as a transcriptional regulator affecting a broad range of immune response genes like ISGs.

A counterintuitive HAT

Like SFPQ, EP300 loss led to an increase in interferon signaling in both homeostasis and after immune stimulation with *Listeria*. This piqued our interest as EP300 is predominantly thought of as a transcriptional activator. It is a histone acetyl transferase responsible for the placement of the H3K27ac mark, a prominent feature of active promoter and enhancer structures. Indeed, in macrophage biology H3K27ac is often found associated with active transcription of immune genes (Ghisletti *et al*, 2010; Kaikkonen *et al*, 2013; Kano *et al*, 2024). Nevertheless, in addition to our observation two lines of evidence speak for a nuanced role for EP300 in the context of overall immune activation. A functional screen utilizing shRNAs in a human macrophage cell line, THP-1s, explored macrophage polarization factors based on the classic M1 (LPS + IFN-

γ) and M2 (IL4 + IL13) polarization treatments (Surdziel *et al*, 2017). In this setup EP300 was observed to suppress the M1 phenotype while simultaneously supporting M2 polarization, an anti-inflammatory state. Furthermore, the function of HDACs has been proven vital for proper immune response gene transcription (Chang *et al*, 2004). Blocking the HDAC function with the inhibitor TSA resulted in suppression of the upregulation of several immune genes that we found upregulated upon EP300 knockout, such as the ISGs *Irf7* and *Usp18*, as well as genes associated with antigen processing and presentation like *Psmb1/8/9/10* and *Tap1/2/bp* (Roger *et al*, 2011). Interestingly, the latter study found that while HDAC inhibitors suppressed IFN response genes, the actual expression of IFN-β was increased upon stimulation.

Further exploration of EP300 involvement

Given the above findings we set out to validate EP300 function in our experimental model system using two complementary approaches.

To directly validate the findings from the CROP-seq screens we generated *Ep300* knockouts in an arrayed format. In other words, one gRNA introduced a single perturbation per well/dish and we utilized qPCR readout to validate the findings on several ISGs. Additionally, we tested the *Spp1* gene whose regulation was strongly anticorrelated in the screens. While this setup closely recapitulates the genetic perturbations in the screen, slight technical differences could impact the read out. In our pooled screen experiment, knockout cells were surrounded by a majority of unperturbed/wild type cells, which provided exogenous factors such as IFN-β. Based on the Mixscape results of perturbation efficiency in our screens we would expect at most 10-15% of cells to remain unperturbed after successful gRNA introduction in the validation experiment. In the validation experiment we selected for the gRNA construct via antibiotic resistance to puromycin to ensure no untransduced cells remained. Additionally, due to the strong antibiotic selection the experiment stretched to three weeks between genetic perturbation and stimulation/readout. Taken together, the successful recapitulation both validates the functional impact of *Ep300* perturbation and indicates that the effect is independent of surrounding wild type cells (though whether *EP300* knockout cells themselves preserve aforementioned exogenous secretion remains to be tested) and persists stably over a long timeframe.

As orthogonal strategy to genetic perturbation, we utilized small molecule inhibitors of the EP300 protein. Specifically, we tested both an inhibitor, A-485, of the catalytic function (writer) and an inhibitor, SGC-CBP30, of the bromodomain (reader) of EP300 and the closely related CREB-binding protein (CBP). Hence this experimental setup can reveal the involvement of the specific function of EP300 required for the phenotype though with the caveat of inhibiting acetylation at a larger scale by affecting two histone acetyltransferases simultaneously. While

a previous study by Piatnitski-Chekler *et al.* observed a more varied expression of IFN genes using CBP/EP300 inhibition with another bromodomain inhibitor PF-CBP1 (Chekler *et al*, 2015), our results clearly validate the findings of our CROP-seq screens. Compared to the gRNA perturbation results the readout was taken after 24 hours suggesting that EP300s effect on ISGs is established quite fast after loss of either reader or writer function. In both validation approaches, the effect was observed in homeostatic conditions and after 2 hours of stimulation with IFN-β. The latter lead to decreased variability between replicates, suggesting that the effect is linked to the amount of extracellular IFN-β.

Taken together, both genetic perturbation and protein inhibition validate a key finding of our CROP-seq screens, namely EP300s involvement in ISG expression.

Interestingly, the effect on *Spp1* expression was less clear. While genetic perturbation and bromodomain inhibition of EP300 led to the expected downregulation, inhibiting the catalytic site of EP300 surprisingly led to an upregulation. This suggests that regulation of ISGs and *Spp1* are not simply anticorrelated but follow different regulatory mechanisms requiring careful further study.

A potential mechanistic model suggests that histone acetylation balance is impacting transcription via BRD4 availability. Too much histone acetylation (e.g. due to a lack of deacetylase function) would sequester BRD4 and hence lead to a lack of BRD4 availability for inducible promoters (Marié *et al*, 2018). Consequently, the loss of EP300 could lead to global overabundance of available BRD4. However, the same screen that positioned EP300 as a M2 mediator and M1 suppressor found the same to be true for BRD4 (Surdziel *et al*, 2017). It would therefore be interesting to closely compare the function of both proteins in macrophage activation, with a particular focus on constitutive active promoters and stimulus responsive promoters. Unfortunately, BRD4 was not included in any of our screening experiments. Apart from histones both HATs and HDACs affect the post-translational status of other proteins, such as transcription factors. Indeed, another proposed mechanism involves the direct deacetylation of the transcription factor C/EBPβ by HDAC-1 allowing transcription to occur (Xu, 2003).

In summary, EP300 exerts an inhibitory role on IFN response gene expression and several other immune related genes in macrophage homeostasis and in response to immune signaling. These effects reflect the opposing side of the functional characteristics of HDACs and inhibition thereof, suggesting that the mechanism of EP300's immune regulation is largely dependent on the catalytic acetyltransferase function.

Several angles from a single experiment

Overall, our data supports findings of tonic IFN response gene expression, potentially by a subset of cells. Furthermore, we have identified several factors such as SPI1, EP300 and SFPQ, whose perturbation led to an increase in IFN response gene expression in macrophage homeostasis and immune response. Taken together, this supports a model of the interferon response that constantly balances activatory with inhibitory signals, or in a car analogy, whose gas and brake pedals are constantly pressed. The JAK-STAT signaling cascade is often used as an exemplary simple signaling cascade, yet the widespread involvement of co-transcription factors and epigenetic modifiers to the final outcome regarding transcriptional output holds promise to yield various novel therapeutic angles.

3.1.3 Screening improvements

With the power of hindsight, it is easy to expect the screen yielding more biological insights if the 24 hour timepoint would have been removed in favor of going into more depth/breadth for the other time points, or replaced with an earlier, intermediate time point. The effects of *Listeria* induced macrophage cell death, either via virulence factors such as LLO or self-induced pyroptosis reduced the number of cells below the expected outcome and thus impacted the ability to assess functional effects of the perturbations.

We found the CITE-seq readout, which labels proteins using oligo-tagged antibodies, to provide both complementary biological validation as well as a strong technical control. For two proteins (CSF1R/CD115 and FCGR1A/CD64) where we perturbed the respective gene we could not detect a broad impact on the transcriptome in our experimental model, yet observed the loss of the protein. In the case of CSF1R a reduction in *Csf1r* mRNA itself was also observed, potentially due to nonsense-mediated decay. As other perturbation effects are context dependent (such as *Rela* and *Irf8* in our experiments) it is useful to include protein directed readouts to monitor the successful perturbation across several genes, especially when other positive controls for the given experimental context are not yet established. Nowadays, widely available pre-titrated antibody cocktails aid in measuring over hundred proteins simultaneously and intracellular staining protein methods (Gerlach *et al*, 2019; Mimitou *et al*, 2021; Reimegård *et al*, 2021) will further enhance a holistic understanding of regulatory processes.

An additional advantage, specifically for infection-based screening setups, is the ease of specific enrichments of RNAs using 5'-based transcriptome capture. Next to capturing the transcriptome of the host cell and the exogenous gRNA, a specific capture probe can be designed against RNAs of the infectious agent itself. As a hypothetical example, we could have enriched for a *Listeria* gene in our screens. This way, an assessment of the pathogenic load of each analyzed cell can be performed and a better separation between bystander effects vs true

host cells attained. The power of assessing the infection state was already demonstrated early on using poly-T primers to capture influenza virus transcripts (Steuerman *et al*, 2018) and this approach can now be extended to a broader array of RNAs.

3.1.4 Screening cell lines to in vivo

Over the course of the thesis multiple screening approaches were performed in primary bone marrow derived macrophages (BMDMs, data not shown). Compared to the RAW 264.7 cell line we encountered several challenges that precluded us from gaining biological insights within the constraints of the project's expectations.

When it comes to macrophage models an early question to address is whether to focus on tissue resident macrophages or on bone-marrow derived macrophages. The former allows tissue specific insights but often comes with downsides regarding extraction of tissue resident macrophages or with lack of appropriate *ex vivo* culture models, though advancements are ongoing such as a novel differentiation culture toward alveolar macrophages (Gorki *et al*, 2022).

Overall, while tissue resident macrophages retain cell proliferation potential and CSF1 specifically stimulates cell cycle also in bone marrow derived macrophages (Hamilton, 1997; Raza *et al*, 2014) the capabilities are not comparable to transformed cell lines. This precludes most screening setups using proliferation rate as selective pressure such as negative selection screens relying on high coverage per target gene (Bock *et al*, 2022).

Genetic engineering of inherently antiviral cells such as primary macrophages, especially via viral vectors, provides another hurdle. A constitutive Cas9-expressing mouse model allowed us to generate genetically perturbed BMDMs with single knockouts (Boccuni *et al*, 2022) using transduction of bone-marrow after 2 days of differentiation with M-CSF. However, this timing may conflate a gene target's role in mature macrophages with its functional impact during various bone-marrow precursor differentiation states. Expectedly, we encountered reduced efficiency of viral transduction rates in primary bone marrow derived cells differentiated with M-CSF for 7 days compared to the RAW 264.7 cell line. Notably, in our attempts we did not provide VPX which can increase the efficiency of lentiviral transduction in myeloid cells by degrading the reverse transcription inhibitor SAMHD1 (Bobadilla *et al*, 2013). Other viral cell engineering efforts rely on adenoviral transduction (Klichinsky *et al*, 2020), however, similar to other non-viral approaches these do not lead to incorporation of exogenous genetic material into the host cell and thus may not be suitable for long-term screening setups reliant on continuous gRNA expression.

Timing of viral transduction is a critical factor when it comes to transducing primary cells. Successful screens of *ex vivo* differentiated macrophages and dendritic cells often choose a timepoint early in the differentiation process, likely transducing a heterogeneous mix of progenitor cells. This could lead to greater noise, increased risk for multiple gRNA insertions not based on Poisson's distribution, and results need to be interpreted with the knowledge that continuing differentiation processes provide an additional selective pressure. Nevertheless, this strategy avoids the inefficiencies observed by fully differentiated innate cells. Successful examples include a genome-wide CRISPR screen for macrophage efferocytosis by transducing bone marrow after one day of exposure to M-CSF (Shi *et al*, 2022) and perturbation screens of dendritic cells transduced after 2 days differentiation of bone marrow with GM-CSF (Jaitin *et al*, 2016; Parnas *et al*, 2015).

A further increase in complexity are *in vivo* screens, which most often include cells being transduced *ex vivo* and engrafted in a host. Most efforts are applied to screen cancer cells or T cells due to their proliferative advantages (Wang *et al*, 2023). A large-scale screening endeavor on hematopoietic stem cells (HSCs) and progenitor cells promises ubiquitous applications to immune related questions (Haney *et al*, 2022). Recent alternative approaches performed transduction of early mouse embryos, which result in many developing tissues being transduced (Renz *et al*, 2024; Zheng *et al*, 2024).

Taken together, the choice of macrophage model depends largely on logistic constrains, the biological question at hand and a careful consideration between model complexity and validation capabilities.

3.1.5 Macrophage engineering, transcriptional regulators as leverage points

The introduction states several of the hallmark functions a macrophage is capable of, as well as the fact that macrophages both exist and can repopulate every organ in the human body. Furthermore, precursor cells can be extracted and *ex vivo* differentiation protocols are established such as common differentiation of bone-marrow derived precursor cells with either M-CSF or GM-CSF (Fleetwood *et al*, 2009). These properties make it an ideal candidate for cell engineering strategies to combat a variety of diseases. An investigation of IL12 knock-in macrophages observed increased IFN-γ in solid tumor environments and prolonged survival in murine models (Brempelis *et al*, 2020). Similarly, activation of macrophages with IFN-γ within tumor environments via attached "backpacks" is enough to prevent depolarization towards tumor associated macrophages (TAMs) and in turn, slow tumor progression (Shields *et al*, 2020).

Another novel strategy are chimeric antigen receptor (CAR) macrophages (CAR-Ms) with early studies applying these modified macrophages in malignant diseases contexts (Hadiloo

et al, 2023; Sloas *et al*, 2021). We envision that a systemic understanding of macrophage regulation, with transcriptional regulators providing a prominent leverage point, can aid in better harnessing the beneficial, intrinsic properties of macrophages. An example for the synergistic effects of CAR engineering paired with modification of an epigenetic modifier was observed early on in CAR-T cells with a TET2 disruption (Fraietta *et al*, 2018) that lead to beneficial changes in CAR-T cell differentiation and proliferation. Similarly, CAR-Ms can exploit genetic modifications such as a mutation in the GTPase RAC leading to increased CAR-directed phagocytic engulfment (Mishra *et al*, 2023).

The above examples highlight that the context-dependent macrophage plasticity is amenable to therapeutic intervention and both their sentinel and effector functions can be harnessed. We envision that a better systemic understanding of macrophages can inform of beneficial functions and that transcriptional regulators provide important leverage points in fine-tuning specific therapeutic outcomes.

3.2 Conclusion and future prospects

This study optimized cutting-edge technologies and applied them to complex biological questions. Specifically, genome-wide transcriptomic and chromatin accessibility sequencing allowed us to create a dense time series data set of diverse immune stimulations of *ex vivo* differentiated macrophages. Our analysis revealed the expected fast transcriptional upregulation of immune pathways in favor of cell division and maintenance programs, yet the latter was not accompanied by the expected loss of chromatin accessibility. Integrating both data modalities allowed us to identify divergent genes whose regulation does not follow the expected correlation between chromatin accessibility and transcriptional regulation, providing a high-level view of their importance in the immune context.

Additionally, by developing high-content CRISPR screens we could simultaneously assess over a hundred transcriptional regulators in their homeostatic role or function during innate immune response. We observed context specific involvement by the regulators, like *Csf1r*/CD115 knockout which failed to affect the M-CSF independent cell line RAW 264.7 used in the screen, or *Irf8* and *Rela* which displayed a strong effect only as macrophages were challenged with *Listeria*. Using cross-prediction analysis we were able to identify functionally similar regulators independent of the underlying mechanism. Interestingly, next to affirming recent findings of basal JAK-STAT signaling, we additionally characterize known and novel regulators as interferon response inhibitors. Perturbations of *Spi1*, *Ep300* and *Sfpq* led to an increase of ISGs in both homeostatic macrophages as well as during immune challenge. This, suggests that macrophages continuously balance activatory and inhibitory signals in order to

respond in a timely manner. The findings on EP300 specifically may present the as of yet missing opposition to previously implicated HDACs in interferon regulation.

Finally, we highlighted a way forward how both descriptive and functional data sets can be combined to create a systems level understanding of gene regulation in dynamic contexts. Next to pairing novel epigenetic regulators to immune regulons we found homeostatic JAK-STAT pathway members associated with a regulon increasing epigenetic potential during immune response, suggesting a gene regulatory role of JAK-STAT signaling besides transcriptional upregulation.

Technological developments towards novel biological insights

Besides a deeper dive into the data generated throughout this thesis and mechanistic follow up of newly identified regulators, combining and applying emerging methods will expand our systems level knowledge of complex biological processes, such as the innate immune response. Among the developments relevant to the specific focus of this thesis are advancements in *ex-vivo* model systems, epigenetic engineering, novel sequencing modalities and direct translatable therapeutic approaches.

The plasticity of macrophages and tissue specific roles are hard to capture in *ex vivo* settings yet recent success' in tissue slice culture technologies offer a promising route to find ethical human model systems recapitulating *in situ* contexts. Meanwhile, epigenetic engineering such as CRISPR technology coupled with epigenetic writers, erasers, and transcriptional cofactors to specific loci can support mechanistic investigations, like the speculated histone acetylation/BRD4 mechanism involved in the opposing roles of EP300 and HDACs. Combining multiple readouts of single cells will increase the yield of high-content screens while technologies like Live-seq (Chen *et al*, 2022) open up new dimensions to investigate cellular behavior. Furthermore, exciting developments in cellular therapy offer direct avenues to translate findings from (epi-)genetic perturbation experiments such as optimizing CAR-Macrophages towards better clinical outcomes.

Technological developments as above enable new avenues of research and ensure ever growing efficiency increases in data generation enabling both a wider and deeper understanding of biology and consequently the various therapeutic angles to reestablish and maintain health.

References

Adamson B, Norman TM, Jost M, Cho MY, Nuñez JK, Chen Y, Villalta JE, Gilbert LA, Horlbeck MA, Hein MY, *et al* (2016) A Multiplexed Single-Cell CRISPR Screening Platform Enables Systematic Dissection of the Unfolded Protein Response. *Cell* 167: 1867-1882.e21

Adelaja A, Taylor B, Sheu KM, Liu Y, Luecke S & Hoffmann A (2021) Six distinct NFκB signaling codons convey discrete information to distinguish stimuli and enable appropriate macrophage responses. *Immunity* 54: 916-930.e7

Angermueller C, Clark SJ, Lee HJ, Macaulay IC, Teng MJ, Hu TX, Krueger F, Smallwood SA, Ponting CP, Voet T, *et al* (2016) Parallel single-cell sequencing links transcriptional and epigenetic heterogeneity. *Nat Methods* 13: 229–232

Anzalone AV, Randolph PB, Davis JR, Sousa AA, Koblan LW, Levy JM, Chen PJ, Wilson C, Newby GA, Raguram A, *et al* (2019) Search-and-replace genome editing without double-strand breaks or donor DNA. *Nature* 576: 149–157

Arango Duque G & Descoteaux A (2014) Macrophage Cytokines: Involvement in Immunity and Infectious Diseases. *Front Immunol* 5

Ashall F (1986) Cancer cells and parasites: two of a kind. *Trends in Biochemical Sciences* 11: 518–520

Asmamaw Mengstie M (2022) Viral Vectors for the in Vivo Delivery of CRISPR Components: Advances and Challenges. *Front Bioeng Biotechnol* 10: 895713

Azam S, Armijo KS, Weindel CG, Chapman MJ, Devigne A, Nakagawa S, Hirose T, Carpenter S, Watson RO & Patrick KL (2024) The early macrophage response to pathogens requires dynamic regulation of the nuclear paraspeckle. *Proc Natl Acad Sci USA* 121: e2312587121

Azizi E, Carr AJ, Plitas G, Cornish AE, Konopacki C, Prabhakaran S, Nainys J, Wu K, Kiseliovas V, Setty M, *et al* (2018) Single-Cell Map of Diverse Immune Phenotypes in the Breast Tumor Microenvironment. *Cell* 174: 1293-1308.e36

Barski A, Cuddapah S, Cui K, Roh T-Y, Schones DE, Wang Z, Wei G, Chepelev I & Zhao K (2007) High-Resolution Profiling of Histone Methylations in the Human Genome. *Cell* 129: 823–837

Bird JE, Marles-Wright J & Giachino A (2022) A User's Guide to Golden Gate Cloning Methods and Standards. *ACS Synth Biol* 11: 3551–3563

Blaszczyk K, Olejnik A, Nowicka H, Ozgyin L, Chen Y-L, Chmielewski S, Kostyrko K, Wesoly J, Balint BL, Lee C-K, *et al* (2015) STAT2/IRF9 directs a prolonged ISGF3-like transcriptional response and antiviral activity in the absence of STAT1. *Biochemical Journal* 466: 511–524

Boada-Romero E, Martinez J, Heckmann BL & Green DR (2020) The clearance of dead cells by efferocytosis. *Nat Rev Mol Cell Biol* 21: 398–414

Bobadilla S, Sunseri N & Landau NR (2013) Efficient transduction of myeloid cells by an HIV-1-derived lentiviral vector that packages the Vpx accessory protein. *Gene Ther* 20: 514–520

Boccuni L, Podgorschek E, Schmiedeberg M, Platanitis E, Traxler P, Fischer P, Schirripa A, Novoszel P, Nebreda AR, Arthur JSC, *et al* (2022) Stress signaling boosts interferon-induced gene transcription in macrophages. *Sci Signal* 15: eabq5389

Bock C, Datlinger P, Chardon F, Coelho MA, Dong MB, Lawson KA, Lu T, Maroc L, Norman TM, Song B, *et al* (2022) High-content CRISPR screening. *Nat Rev Methods Primers* 2: 8

Brempelis KJ, Cowan CM, Kreuser SA, Labadie KP, Prieskorn BM, Lieberman NAP, Ene CI, Moyes KW, Chinn H, Degolier KR, *et al* (2020) Genetically engineered macrophages persist in solid tumors and locally deliver therapeutic proteins to activate immune responses. *Journal for ImmunoTherapy of Cancer* 8

Brown DV, Anttila CJA, Ling L, Grave P, Baldwin TM, Munnings R, Farchione AJ, Bryant VL, Dunstone A, Biben C, *et al* (2024) A risk-reward examination of sample multiplexing reagents for single cell RNA-Seq. *Genomics* 116: 110793

Burioli EAV, Hammel M, Bierne N, Thomas F, Houssin M, Destoumieux-Garzón D & Charrière GM (2021) Traits of a mussel transmissible cancer are reminiscent of a parasitic life style. *Sci Rep* 11: 24110

Callaway E (2015) The tapeworm that turned into a tumour. *Nature*: nature.2015.18726

Carpenter S, Aiello D, Atianand MK, Ricci EP, Gandhi P, Hall LL, Byron M, Monks B, Henry-Bezy M, Lawrence JB, *et al* (2013) A Long Noncoding RNA Mediates Both Activation and Repression of Immune Response Genes. *Science* 341: 789–792

Carson MJ, Doose JM, Melchior B, Schmid CD & Ploix CC (2006) CNS immune privilege: hiding in plain sight. *Immunological Reviews* 213: 48–65

Casadevall A & Pirofski L-A (2002) What is a pathogen? *Annals of Medicine* 34: 2–4

Caughey B & Baron GS (2006) Prions and their partners in crime. *Nature* 443: 803–810

Chang HHY, Pannunzio NR, Adachi N & Lieber MR (2017) Non-homologous DNA end joining and alternative pathways to double-strand break repair. *Nat Rev Mol Cell Biol* 18: 495–506

Chang H-M, Paulson M, Holko M, Rice CM, Williams BRG, Marié I & Levy DE (2004) Induction of interferon-stimulated gene expression and antiviral responses require protein deacetylase activity. *Proc Natl Acad Sci USA* 101: 9578–9583

Chekler ELP, Pellegrino JA, Lanz TA, Denny RA, Flick AC, Coe J, Langille J, Basak A, Liu S, Stock IA, *et al* (2015) Transcriptional Profiling of a Selective CREB Binding Protein Bromodomain Inhibitor Highlights Therapeutic Opportunities. *Chemistry & Biology* 22: 1588–1596

Chen B, Gilbert LA, Cimini BA, Schnitzbauer J, Zhang W, Li G-W, Park J, Blackburn EH, Weissman JS, Qi LS, *et al* (2013) Dynamic Imaging of Genomic Loci in Living Human Cells by an Optimized CRISPR/Cas System. *Cell* 155: 1479–1491

Chen GY & Nuñez G (2010) Sterile inflammation: sensing and reacting to damage. *Nat Rev Immunol* 10: 826–837

Chen H, Ruiz PD, Novikov L, Casill AD, Park JW & Gamble MJ (2014) MacroH2A1.1 and PARP-1 cooperate to regulate transcription by promoting CBP-mediated H2B acetylation. *Nat Struct Mol Biol* 21: 981–989

Chen L-F, Lin YT, Gallegos DA, Hazlett MF, Gómez-Schiavon M, Yang MG, Kalmeta B, Zhou AS, Holtzman L, Gersbach CA, *et al* (2019) Enhancer Histone Acetylation Modulates Transcriptional Bursting Dynamics of Neuronal Activity-Inducible Genes. *Cell Reports* 26: 1174-1188.e5

Chen S, Ma J, Wu F, Xiong L, Ma H, Xu W, Lv R, Li X, Villen J, Gygi SP, *et al* (2012) The histone H3 Lys 27 demethylase JMJD3 regulates gene expression by impacting transcriptional elongation. *Genes Dev* 26: 1364–1375

Chen S, Yang J, Wei Y & Wei X (2020) Epigenetic regulation of macrophages: from homeostasis maintenance to host defense. *Cell Mol Immunol* 17: 36–49

Chen W, Guillaume-Gentil O, Rainer PY, Gäbelein CG, Saelens W, Gardeux V, Klaeger A, Dainese R, Zachara M, Zambelli T, *et al* (2022) Live-seq enables temporal transcriptomic recording of single cells. *Nature* 608: 733–740

Cheng CS, Behar MS, Suryawanshi GW, Feldman KE, Spreafico R & Hoffmann A (2017) Iterative Modeling Reveals Evidence of Sequential Transcriptional Control Mechanisms. *Cell Systems* 4: 330-343.e5

Cheng Q, Behzadi F, Sen S, Ohta S, Spreafico R, Teles R, Modlin RL & Hoffmann A (2019) Sequential conditioning-stimulation reveals distinct gene- and stimulus-specific effects of Type I and II IFN on human macrophage functions. *Sci Rep* 9: 5288

Cheng Z, Taylor B, Ourthiague DR & Hoffmann A (2015) Distinct single-cell signaling characteristics are conferred by the MyD88 and TRIF pathways during TLR4 activation. *Sci Signal* 8

Cheon H & Stark GR (2009) Unphosphorylated STAT1 prolongs the expression of interferon-induced immune regulatory genes. *Proc Natl Acad Sci USA* 106: 9373–9378

Chinnery HR, McMenamin PG & Dando SJ (2017) Macrophage physiology in the eye. *Pflugers Arch - Eur J Physiol* 469: 501–515

Chu VT, Graf R, Wirtz T, Weber T, Favret J, Li X, Petsch K, Tran NT, Sieweke MH, Berek C, *et al* (2016) Efficient CRISPR-mediated mutagenesis in primary immune cells using CrispRGold and a C57BL/6 Cas9 transgenic mouse line. *Proceedings of the National Academy of Sciences* 113: 12514–12519

Clark IC, Fontanez KM, Meltzer RH, Xue Y, Hayford C, May-Zhang A, D'Amato C, Osman A, Zhang JQ, Hettige P, *et al* (2023) Microfluidics-free single-cell genomics with templated emulsification. *Nat Biotechnol* 41: 1557–1566

Clow PA, Du M, Jillette N, Taghbalout A, Zhu JJ & Cheng AW (2022) CRISPR-mediated multiplexed live cell imaging of nonrepetitive genomic loci with one guide RNA per locus. *Nat Commun* 13: 1871

Cohen J (2021) CRISPR, the revolutionary genetic 'scissors,' honored by Chemistry Nobel.

Cohen-Tannoudji M, Robine S, Choulika A, Pinto D, El Marjou F, Babinet C, Louvard D & Jaisser F (1998) I-*Sce*I-Induced Gene Replacement at a Natural Locus in Embryonic Stem Cells. *Molecular and Cellular Biology* 18: 1444–1448

Cramer P (2019) Organization and regulation of gene transcription. *Nature* 573: 45–54

Crow YJ & Casanova J-L (2024) Human life within a narrow range: The lethal ups and downs of type I interferons. *Sci Immunol* 9: eadm8185

Datlinger P, Rendeiro AF, Boenke T, Senekowitsch M, Krausgruber T, Barreca D & Bock C (2021) Ultra-high-throughput single-cell RNA sequencing and perturbation screening with combinatorial fluidic indexing. *Nat Methods* 18: 635–642

Datlinger P, Rendeiro AF, Schmidl C, Krausgruber T, Traxler P, Klughammer J, Schuster LC, Kuchler A, Alpar D & Bock C (2017) Pooled CRISPR screening with single-cell transcriptome readout. *Nat Methods* 14: 297–301

De Groot R, Lüthi J, Lindsay H, Holtackers R & Pelkmans L (2018) Large-scale image-based profiling of single-cell phenotypes in arra yed CRISPR-Cas9 gene perturba–tion screens. *Molecular Systems Biology* 14: e8064

De Rop FV, Hulselmans G, Flerin C, Soler-Vila P, Rafels A, Christiaens V, González-Blas CB, Marchese D, Caratù G, Poovathingal S, *et al* (2024) Systematic benchmarking of single-cell ATAC-sequencing protocols. *Nat Biotechnol* 42: 916–926

De Santa F, Narang V, Yap ZH, Tusi BK, Burgold T, Austenaa L, Bucci G, Caganova M, Notarbartolo S, Casola S, *et al* (2009) Jmjd3 contributes to the control of gene expression in LPS-activated macrophages. *EMBO J* 28: 3341–3352

Deng H, Maitra U, Morris M & Li L (2013) Molecular Mechanism Responsible for the Priming of Macrophage Activation. *Journal of Biological Chemistry* 288: 3897–3906

Denisenko E, Guler R, Mhlanga MM, Suzuki H, Brombacher F & Schmeier S (2017) Genome-wide profiling of transcribed enhancers during macrophage activation. *Epigenetics & Chromatin* 10: 50

Dixit A, Parnas O, Li B, Chen J, Fulco CP, Jerby-Arnon L, Marjanovic ND, Dionne D, Burks T, Raychowdhury R, *et al* (2016) Perturb-Seq: Dissecting Molecular Circuits with Scalable Single-Cell RNA Profiling of Pooled Genetic Screens. *Cell* 167: 1853-1866.e17

Dvorkin S, Cambier S, Volkman HE & Stetson DB (2024) New frontiers in the cGAS-STING intracellular DNA-sensing pathway. *Immunity* 57: 718–730

Elewaut A, Estivill G, Bayerl F, Castillon L, Novatchkova M, Pottendorfer E, Hoffmann-Haas L, Schönlein M, Nguyen TV, Lauss M, *et al* (2025) Cancer cells impair monocyte-mediated T cell stimulation to evade immunity. *Nature* 637: 716–725

Emanuel G, Moffitt JR & Zhuang X (2017) High-throughput, image-based screening of pooled genetic-variant libraries. *Nat Methods* 14: 1159–1162

Fanucchi S, Fok ET, Dalla E, Shibayama Y, Börner K, Chang EY, Stoychev S, Imakaev M, Grimm D, Wang KC, *et al* (2019) Immune genes are primed for robust transcription by proximal long noncoding RNAs located in nuclear compartments. *Nat Genet* 51: 138–150

Fernández A, Josa S & Montoliu L (2017) A history of genome editing in mammals. *Mamm Genome* 28: 237–246

Fleetwood AJ, Dinh H, Cook AD, Hertzog PJ & Hamilton JA (2009) GM-CSF- and M-CSF-dependent macrophage phenotypes display differential dependence on Type I interferon signaling. *Journal of Leukocyte Biology* 86: 411–421

Foster SL, Hargreaves DC & Medzhitov R (2007) Gene-specific control of inflammation by TLR-induced chromatin modifications. *Nature* 447: 972–978

Fraietta JA, Nobles CL, Sammons MA, Lundh S, Carty SA, Reich TJ, Cogdill AP, Morrissette JJD, DeNizio JE, Reddy S, *et al* (2018) Disruption of TET2 promotes the therapeutic efficacy of CD19-targeted T cells. *Nature* 558: 307–312

Franchi L, Warner N, Viani K & Nuñez G (2009) Function of Nod-like receptors in microbial recognition and host defense. *Immunological Reviews* 227: 106–128

Ganesan A, Arimondo PB, Rots MG, Jeronimo C & Berdasco M (2019) The timeline of epigenetic drug discovery: from reality to dreams. *Clin Epigenet* 11: 174

Gao XD, Tu L-C, Mir A, Rodriguez T, Ding Y, Leszyk J, Dekker J, Shaffer SA, Zhu LJ, Wolfe SA, *et al* (2018) C-BERST: defining subnuclear proteomic landscapes at genomic elements with dCas9–APEX2. *Nat Methods* 15: 433–436

Gao Y, Han M, Shang S, Wang H & Qi LS (2021) Interrogation of the dynamic properties of higher-order heterochromatin using CRISPR-dCas9. *Molecular Cell* 81: 4287-4299.e5

Garber M, Yosef N, Goren A, Raychowdhury R, Thielke A, Guttman M, Robinson J, Minie B, Chevrier N, Itzhaki Z, *et al* (2012) A High-Throughput Chromatin Immunoprecipitation Approach Reveals Principles of Dynamic Gene Regulation in Mammals. *Molecular Cell* 47: 810–822

Gasperini M, Hill AJ, McFaline-Figueroa JL, Martin B, Kim S, Zhang MD, Jackson D, Leith A, Schreiber J, Noble WS, *et al* (2019) A Genome-wide Framework for Mapping Gene Regulation via Cellular Genetic Screens. *Cell* 176: 377-390.e19

Gaudelli NM, Komor AC, Rees HA, Packer MS, Badran AH, Bryson DI & Liu DR (2017) Programmable base editing of A•T to G•C in genomic DNA without DNA cleavage. *Nature* 551: 464–471

Gerlach JanP, Van Buggenum JAG, Tanis SEJ, Hogeweg M, Heuts BMH, Muraro MJ, Elze L, Rivello F, Rakszewska A, Van Oudenaarden A, *et al* (2019) Combined quantification of intracellular (phospho-)proteins and transcriptomics from fixed single cells. *Sci Rep* 9: 1469

Ghisletti S, Barozzi I, Mietton F, Polletti S, De Santa F, Venturini E, Gregory L, Lonie L, Chew A, Wei C-L, *et al* (2010) Identification and Characterization of Enhancers Controlling the Inflammatory Gene Expression Program in Macrophages. *Immunity* 32: 317–328

Gifford GE & Lohmann-Matthes M-L (1987) Gamma Interferon Priming of Mouse and Human Macrophages for Induction of Tumor Necrosis Factor Production by Bacterial Lipopolysaccharide. *JNCI: Journal of the National Cancer Institute* 78: 121–124

Gilbert LA, Horlbeck MA, Adamson B, Villalta JE, Chen Y, Whitehead EH, Guimaraes C, Panning B, Ploegh HL, Bassik MC, *et al* (2014) Genome-Scale CRISPR-Mediated Control of Gene Repression and Activation. *Cell* 159: 647–661

Gilbert LA, Larson MH, Morsut L, Liu Z, Brar GA, Torres SE, Stern-Ginossar N, Brandman O, Whitehead EH, Doudna JA, *et al* (2013) CRISPR-Mediated Modular RNA-Guided Regulation of Transcription in Eukaryotes. *Cell* 154: 442–451

Ginhoux F & Guilliams M (2016) Tissue-Resident Macrophage Ontogeny and Homeostasis. *Immunity* 44: 439–449

González-Rodríguez P, Füllgrabe J & Joseph B (2023) The hunger strikes back: an epigenetic memory for autophagy. *Cell Death Differ* 30: 1404–1415

Gorki A-D, Symmank D, Zahalka S, Lakovits K, Hladik A, Langer B, Maurer B, Sexl V, Kain R & Knapp S (2022) Murine *Ex Vivo* Cultured Alveolar Macrophages Provide a Novel Tool to Study Tissue-Resident Macrophage Behavior and Function. *Am J Respir Cell Mol Biol* 66: 64–75

Gough DJ, Messina NL, Clarke CJP, Johnstone RW & Levy DE (2012) Constitutive Type I Interferon Modulates Homeostatic Balance through Tonic Signaling. *Immunity* 36: 166–174

Gray EE & Cyster JG (2012) Lymph Node Macrophages. *J Innate Immun* 4: 424–436

Hadiloo K, Taremi S, Heidari M & Esmaeilzadeh A (2023) The CAR macrophage cells, a novel generation of chimeric antigen-based approach against solid tumors. *Biomark Res* 11: 103

Hamilton JA (1997) CSF-1 and cell cycle control in macrophages. *Mol Reprod Dev* 46: 19–23

Haney MS, Bohlen CJ, Morgens DW, Ousey JA, Barkal AA, Tsui CK, Ego BK, Levin R, Kamber RA, Collins H, *et al* (2018) Identification of phagocytosis regulators using magnetic genome-wide CRISPR screens. *Nat Genet* 50: 1716–1727

Haney MS, Shankar A, Hsu I, Miyauchi M, Pálovics R, Khoo HM, Igarashi KJ, Bhadury J, Munson C, Mack PK, *et al* (2022) Large-scale in vivo CRISPR screens identify SAGA complex members as a key regulators of HSC lineage commitment and aging. doi:10.1101/2022.07.22.501030 [PREPRINT]

Hao N, Shearwin KE & Dodd IB (2017) Programmable DNA looping using engineered bivalent dCas9 complexes. *Nat Commun* 8: 1628

Hargreaves DC, Horng T & Medzhitov R (2009) Control of Inducible Gene Expression by Signal-Dependent Transcriptional Elongation. *Cell* 138: 129–145

Hernández-García D, García-Meléndrez C, Hernández-Martínez R, Collazo-Navarrete O & Covarrubias L (2024) Macrophages allocate before apoptosis initiation and produce reactive oxygen species during interdigital phagocytosis. *Biology Open* 13: bio060492

Hill AJ, McFaline-Figueroa JL, Starita LM, Gasperini MJ, Matreyek KA, Packer J, Jackson D, Shendure J & Trapnell C (2018) On the design of CRISPR-based single-cell molecular screens. *Nat Methods* 15: 271–274

Hilton IB, D'Ippolito AM, Vockley CM, Thakore PI, Crawford GE, Reddy TE & Gersbach CA (2015) Epigenome editing by a CRISPR-Cas9-based acetyltransferase activates genes from promoters and enhancers. *Nat Biotechnol* 33: 510–517

Hoja S, Schulze M, Rehli M, Proescholdt M, Herold-Mende C, Hau P & Riemenschneider MJ (2016) Molecular dissection of the valproic acid effects on glioma cells. *Oncotarget* 7: 62989–63002

Hou Y, Guo H, Cao C, Li X, Hu B, Zhu P, Wu X, Wen L, Tang F, Huang Y, *et al* (2016) Single-cell triple omics sequencing reveals genetic, epigenetic, and transcriptomic heterogeneity in hepatocellular carcinomas. *Cell Res* 26: 304–319

Hu Y, Huang K, An Q, Du G, Hu G, Xue J, Zhu X, Wang C-Y, Xue Z & Fan G (2016) Simultaneous profiling of transcriptome and DNA methylome from a single cell. *Genome Biol* 17: 88

Imamura K, Imamachi N, Akizuki G, Kumakura M, Kawaguchi A, Nagata K, Kato A, Kawaguchi Y, Sato H, Yoneda M, *et al* (2014) Long Noncoding RNA NEAT1-Dependent SFPQ Relocation from Promoter Region to Paraspeckle Mediates IL8 Expression upon Immune Stimuli. *Molecular Cell* 53: 393–406

Immunological Genome Consortium, Gautier EL, Shay T, Miller J, Greter M, Jakubzick C, Ivanov S, Helft J, Chow A, Elpek KG, *et al* (2012) Gene-expression profiles and transcriptional regulatory pathways that underlie the identity and diversity of mouse tissue macrophages. *Nat Immunol* 13: 1118–1128

Ishii M, Wen H, Corsa CAS, Liu T, Coelho AL, Allen RM, Carson WF, Cavassani KA, Li X, Lukacs NW, *et al* (2009) Epigenetic regulation of the alternatively activated macrophage phenotype. *Blood* 114: 3244–3254

Jacobs AT & Ignarro LJ (2001) Lipopolysaccharide-induced Expression of Interferon-β Mediates the Timing of Inducible Nitric-oxide Synthase Induction in RAW 264.7 Macrophages. *Journal of Biological Chemistry* 276: 47950–47957

Jaeger MG, Schwalb B, Mackowiak SD, Velychko T, Hanzl A, Imrichova H, Brand M, Agerer B, Chorn S, Nabet B, *et al* (2020) Selective Mediator dependence of cell-type-specifying transcription. *Nat Genet* 52: 719–727

Jaitin DA, Weiner A, Yofe I, Lara-Astiaso D, Keren-Shaul H, David E, Salame TM, Tanay A, Van Oudenaarden A & Amit I (2016) Dissecting Immune Circuits by Linking CRISPR-Pooled Screens with Single-Cell RNA-Seq. *Cell* 167: 1883-1896.e15

Joung J, Konermann S, Gootenberg JS, Abudayyeh OO, Platt RJ, Brigham MD, Sanjana NE & Zhang F (2017) Genome-scale CRISPR-Cas9 knockout and transcriptional activation screening. *Nat Protoc* 12: 828–863

Joung JK & Sander JD (2013) TALENs: a widely applicable technology for targeted genome editing. *Nat Rev Mol Cell Biol* 14: 49–55

Kaikkonen MU, Spann NJ, Heinz S, Romanoski CE, Allison KA, Stender JD, Chun HB, Tough DF, Prinjha RK, Benner C, *et al* (2013) Remodeling of the Enhancer Landscape during Macrophage Activation Is Coupled to Enhancer Transcription. *Molecular Cell* 51: 310–325

Kaluscha S, Domcke S, Wirbelauer C, Stadler MB, Durdu S, Burger L & Schübeler D (2022) Evidence that direct inhibition of transcription factor binding is the prevailing mode of gene and repeat repression by DNA methylation. *Nat Genet* 54: 1895–1906

Kanfer G, Sarraf SA, Maman Y, Baldwin H, Dominguez-Martin E, Johnson KR, Ward ME, Kampmann M, Lippincott-Schwartz J & Youle RJ (2021) Image-based pooled whole-genome CRISPRi screening for subcellular phenotypes. *Journal of Cell Biology* 220: e202006180

Kano N, Miki T, Uehara Y, Ori D & Kawai T (2024) Identification and characterization of putative enhancer regions that direct *Il6* transcription in murine macrophages. *International Immunology*: dxae024

Kebschull JM & Zador AM (2018) Cellular barcoding: lineage tracing, screening and beyond. *Nature Methods* 15: 871–879

Khan SU, Khan MU, Azhar Ud Din M, Khan IM, Khan MI, Bungau S & Hassan SSU (2023) Reprogramming tumor-associated macrophages as a unique approach to target tumor immunotherapy. *Front Immunol* 14: 1166487

Klein AM, Mazutis L, Akartuna I, Tallapragada N, Veres A, Li V, Peshkin L, Weitz DA & Kirschner MW (2015) Droplet Barcoding for Single-Cell Transcriptomics Applied to Embryonic Stem Cells. *Cell* 161: 1187–1201

Klichinsky M, Ruella M, Shestova O, Lu XM, Best A, Zeeman M, Schmierer M, Gabrusiewicz K, Anderson NR, Petty NE, *et al* (2020) Human chimeric antigen receptor macrophages for cancer immunotherapy. *Nat Biotechnol* 38: 947–953

Komor AC, Kim YB, Packer MS, Zuris JA & Liu DR (2016) Programmable editing of a target base in genomic DNA without double-stranded DNA cleavage. *Nature* 533: 420–424

Korkmaz G, Lopes R, Ugalde AP, Nevedomskaya E, Han R, Myacheva K, Zwart W, Elkon R & Agami R (2016) Functional genetic screens for enhancer elements in the human genome using CRISPR-Cas9. *Nat Biotechnol* 34: 192–198

Krausgruber T, Fortelny N, Fife-Gernedl V, Senekowitsch M, Schuster LC, Lercher A, Nemc A, Schmidl C, Rendeiro AF, Bergthaler A, *et al* (2020) Structural cells are key regulators of organ-specific immune responses. *Nature* 583: 296–302

Kulle A, Thanabalasuriar A, Cohen TS & Szydlowska M (2022) Resident macrophages of the lung and liver: The guardians of our tissues. *Front Immunol* 13: 1029085

Lai Y & Gallo RL (2009) AMPed up immunity: how antimicrobial peptides have multiple roles in immune defense. *Trends in Immunology* 30: 131–141

Lavin Y, Winter D, Blecher-Gonen R, David E, Keren-Shaul H, Merad M, Jung S & Amit I (2014) Tissue-Resident Macrophage Enhancer Landscapes Are Shaped by the Local Microenvironment. *Cell* 159: 1312–1326

Lawson MJ, Camsund D, Larsson J, Baltekin Ö, Fange D & Elf J (2017) *In situ* genotyping of a pooled strain library after characterizing complex phenotypes. *Molecular Systems Biology* 13: 947

Liu X, Zhang Y, Chen Y, Li M, Zhou F, Li K, Cao H, Ni M, Liu Y, Gu Z, *et al* (2017) In Situ Capture of Chromatin Interactions by Biotinylated dCas9. *Cell* 170: 1028-1043.e19

Lucere KM, O'Malley MMR & Diermeier SD (2020) Functional Screening Techniques to Identify Long Non-Coding RNAs as Therapeutic Targets in Cancer. *Cancers* 12: 3695

Ma H, Han P, Ye W, Chen H, Zheng X, Cheng L, Zhang L, Yu L, Wu X, Xu Z, *et al* (2017) The Long Noncoding RNA NEAT1 Exerts Antihantaviral Effects by Acting as Positive Feedback for RIG-I Signaling. *J Virol* 91: e02250-16

Ma H, Tu L-C, Naseri A, Huisman M, Zhang S, Grunwald D & Pederson T (2016) Multiplexed labeling of genomic loci with dCas9 and engineered sgRNAs using CRISPRainbow. *Nat Biotechnol* 34: 528–530

Maass PG, Barutcu AR, Shechner DM, Weiner CL, Melé M & Rinn JL (2018) Spatiotemporal allele organization by allele-specific CRISPR live-cell imaging (SNP-CLING). *Nat Struct Mol Biol* 25: 176–184

Macosko EZ, Basu A, Satija R, Nemesh J, Shekhar K, Goldman M, Tirosh I, Bialas AR, Kamitaki N, Martersteck EM, *et al* (2015) Highly Parallel Genome-wide Expression Profiling of Individual Cells Using Nanoliter Droplets. *Cell* 161: 1202–1214

Mages J, Dietrich H & Lang R (2008) A genome-wide analysis of LPS tolerance in macrophages. *Immunobiology* 212: 723–737

Majoros A, Platanitis E, Szappanos D, Cheon H, Vogl C, Shukla P, Stark GR, Sexl V, Schreiber R, Schindler C, *et al* (2016) Response to interferons and antibacterial innate immunity in the absence of tyrosine-phosphorylated STAT 1. *EMBO Reports* 17: 367–382

Mak TW (2007) Gene Targeting in Embryonic Stem Cells Scores a Knockout in Stockholm. *Cell* 131: 1027–1031

Makuch M, Stepanechko M & Bzowska M (2024) The dance of macrophage death: the interplay between the inevitable and the microenvironment. *Front Immunol* 15: 1330461

Mali P, Yang L, Esvelt KM, Aach J, Guell M, DiCarlo JE, Norville JE & Church GM (2013) RNA-Guided Human Genome Engineering via Cas9. *Science* 339: 823–826

Mao YS, Zhang B & Spector DL (2011) Biogenesis and function of nuclear bodies. *Trends in Genetics* 27: 295–306

Marié IJ, Chang H-M & Levy DE (2018) HDAC stimulates gene expression through BRD4 availability in response to IFN and in interferonopathies. *Journal of Experimental Medicine* 215: 3194–3212

Mazumder A, Bose M, Chakraborty A, Chakrabarti S & Bhattacharyya SN (2013) A transient reversal of miRNA-mediated repression controls macrophage activation. *EMBO Reports* 14: 1008–1016

Mereu E, Lafzi A, Moutinho C, Ziegenhain C, McCarthy DJ, Álvarez-Varela A, Batlle E, Sagar, Grün D, Lau JK, *et al* (2020) Benchmarking single-cell RNA-sequencing protocols for cell atlas projects. *Nat Biotechnol* 38: 747–755

Michalska A, Blaszczyk K, Wesoly J & Bluyssen HAR (2018) A Positive Feedback Amplifier Circuit That Regulates Interferon (IFN)-Stimulated Gene Expression and Controls Type I and Type II IFN Responses. *Front Immunol* 9: 1135

Michlits G, Jude J, Hinterndorfer M, De Almeida M, Vainorius G, Hubmann M, Neumann T, Schleiffer A, Burkard TR, Fellner M, *et al* (2020) Multilayered VBC score predicts sgRNAs that efficiently generate loss-of-function alleles. *Nat Methods* 17: 708–716

Milcamps R & Michiels T (2024) Involvement of paraspeckle components in viral infections. *Nucleus* 15: 2350178

Mimitou EP, Cheng A, Montalbano A, Hao S, Stoeckius M, Legut M, Roush T, Herrera A, Papalexi E, Ouyang Z, *et al* (2019) Multiplexed detection of proteins, transcriptomes, clonotypes and CRISPR perturbations in single cells. *Nat Methods* 16: 409–412

Mimitou EP, Lareau CA, Chen KY, Zorzetto-Fernandes AL, Hao Y, Takeshima Y, Luo W, Huang T-S, Yeung BZ, Papalexi E, *et al* (2021) Scalable, multimodal profiling of chromatin accessibility, gene expression and protein levels in single cells. *Nat Biotechnol* 39: 1246–1258

Mishra AK, Rodriguez M, Torres AY, Smith M, Rodriguez A, Bond A, Morrissey MA & Montell DJ (2023) Hyperactive Rac stimulates cannibalism of living target cells and enhances CAR-M-mediated cancer cell killing. *Proc Natl Acad Sci USA* 120: e2310221120

Mohr SE, Smith JA, Shamu CE, Neumüller RA & Perrimon N (2014) RNAi screening comes of age: improved techniques and complementary approaches. *Nat Rev Mol Cell Biol* 15: 591–600

Moore LD, Le T & Fan G (2013) DNA Methylation and Its Basic Function. *Neuropsychopharmacol* 38: 23–38

Morgens DW, Wainberg M, Boyle EA, Ursu O, Araya CL, Tsui CK, Haney MS, Hess GT, Han K, Jeng EE, *et al* (2017) Genome-scale measurement of off-target activity using Cas9 toxicity in high-throughput screens. *Nat Commun* 8: 15178

Mowat AM & Bain CC (2011) Mucosal Macrophages in Intestinal Homeostasis and Inflammation. *J Innate Immun* 3: 550–564

Muntjewerff EM & Meesters LD (2020) Antigen Cross-Presentation by Macrophages. *Frontiers in Immunology* 11

Neal JT, Li X, Zhu J, Giangarra V, Grzeskowiak CL, Ju J, Liu IH, Chiou S-H, Salahudeen AA, Smith AR, *et al* (2018) Organoid Modeling of the Tumor Immune Microenvironment. *Cell* 175: 1972-1988.e16

Netea MG, Quintin J & van der Meer JWM (2011) Trained Immunity: A Memory for Innate Host Defense. *Cell Host & Microbe* 9: 355–361

Netea MG, Schlitzer A, Placek K, Joosten LAB & Schultze JL (2019) Innate and Adaptive Immune Memory: an Evolutionary Continuum in the Host's Response to Pathogens. *Cell Host & Microbe* 25: 13–26

Niu Y, Chen J & Qiao Y (2022) Epigenetic Modifications in Tumor-Associated Macrophages: A New Perspective for an Old Foe. *Front Immunol* 13: 836223

Novakovic B, Habibi E, Wang S-Y, Arts RJW, Davar R, Megchelenbrink W, Kim B, Kuznetsova T, Kox M, Zwaag J, *et al* (2016) β-Glucan Reverses the Epigenetic State of LPS-Induced Immunological Tolerance. *Cell* 167: 1354-1368.e14

Olins AL & Olins DE (1974) Spheroid Chromatin Units (v Bodies). *Science* 183: 330–332

Ostuni R, Piccolo V, Barozzi I, Polletti S, Termanini A, Bonifacio S, Curina A, Prosperini E, Ghisletti S & Natoli G (2013) Latent Enhancers Activated by Stimulation in Differentiated Cells. *Cell* 152: 157–171

Palazzo AF & Lee ES (2015) Non-coding RNA: what is functional and what is junk? *Front Genet* 6

Paludan SR, Pradeu T, Masters SL & Mogensen TH (2021) Constitutive immune mechanisms: mediators of host defence and immune regulation. *Nat Rev Immunol* 21: 137–150

Papalexi E, Mimitou EP, Butler AW, Foster S, Bracken B, Mauck WM, Wessels H-H, Hao Y, Yeung BZ, Smibert P, *et al* (2021) Characterizing the molecular regulation of inhibitory immune checkpoints with multimodal single-cell screens. *Nat Genet* 53: 322–331

Park MD, Silvin A, Ginhoux F & Merad M (2022) Macrophages in health and disease. *Cell* 185: 4259–4279

Parnas O, Jovanovic M, Eisenhaure TM, Herbst RH, Dixit A, Ye CJ, Przybylski D, Platt RJ, Tirosh I, Sanjana NE, *et al* (2015) A Genome-wide CRISPR Screen in Primary Immune Cells to Dissect Regulatory Networks. *Cell* 162: 675–686

Pavletich NP & Pabo CO (1991) Zinc Finger-DNA Recognition: Crystal Structure of a Zif268-DNA Complex at 2.1 Å. *Science* 252: 809–817

Peterson VM, Zhang KX, Kumar N, Wong J, Li L, Wilson DC, Moore R, McClanahan TK, Sadekova S & Klappenbach JA (2017) Multiplexed quantification of proteins and transcripts in single cells. *Nat Biotechnol* 35: 936–939

Platanitis E, Demiroz D, Schneller A, Fischer K, Capelle C, Hartl M, Gossenreiter T, Müller M, Novatchkova M & Decker T (2019) A molecular switch from STAT2-IRF9 to ISGF3 underlies interferon-induced gene transcription. *Nat Commun* 10: 2921

Platt RJ, Chen S, Zhou Y, Yim MJ, Swiech L, Kempton HR, Dahlman JE, Parnas O, Eisenhaure TM, Jovanovic M, *et al* (2014) CRISPR-Cas9 Knockin Mice for Genome Editing and Cancer Modeling. *Cell* 159: 440–455

Policarpi C, Munafò M, Tsagkris S, Carlini V & Hackett JA (2024) Systematic epigenome editing captures the context-dependent instructive function of chromatin modifications. *Nat Genet* 56: 1168–1180

Pope SD & Medzhitov R (2018) Emerging Principles of Gene Expression Programs and Their Regulation. *Molecular Cell* 71: 389–397

Prasad R, Yen TJ & Bellacosa A (2021) Active DNA demethylation—The epigenetic gatekeeper of development, immunity, and cancer. *Advanced Genetics* 2: e10033

Price JV & Vance RE (2014) The Macrophage Paradox. *Immunity* 41: 685–693

Quénet D (2018) Histone Variants and Disease. In *International Review of Cell and Molecular Biology* pp 1–39. Elsevier

Ramirez-Carrozzi VR, Braas D, Bhatt DM, Cheng CS, Hong C, Doty KR, Black JC, Hoffmann A, Carey M & Smale ST (2009) A Unifying Model for the Selective Regulation of Inducible Transcription by CpG Islands and Nucleosome Remodeling. *Cell* 138: 114–128

Raza S, Barnett MW, Barnett-Itzhaki Z, Amit I, Hume DA & Freeman TC (2014) Analysis of the transcriptional networks underpinning the activation of murine macrophages by inflammatory mediators. *Journal of Leukocyte Biology* 96: 167–183

Recoules L, Heurteau A, Raynal F, Karasu N, Moutahir F, Bejjani F, Jariel-Encontre I, Cuvier O, Sexton T, Lavigne A-C, *et al* (2022) The histone variant macroH2A1.1 regulates RNA polymerase II-paused genes within defined chromatin interaction landscapes. *Journal of Cell Science* 135: jcs259456

Reece MD, Taylor RR, Song C & Gavegnano C (2021) Targeting Macrophage Dysregulation for Viral Infections: Novel Targets for Immunomodulators. *Front Immunol* 12: 768695

Reimegård J, Tarbier M, Danielsson M, Schuster J, Baskaran S, Panagiotou S, Dahl N, Friedländer MR & Gallant CJ (2021) A combined approach for single-cell mRNA and intracellular protein expression analysis. *Commun Biol* 4: 624

Reisbeck M, Helou MJ, Richter L, Kappes B, Friedrich O & Hayden O (2016) Magnetic fingerprints of rolling cells for quantitative flow cytometry in whole blood. *Sci Rep* 6: 32838

Renz PF, Ghoshdastider U, Baghai Sain S, Valdivia-Francia F, Khandekar A, Ormiston M, Bernasconi M, Duré C, Kretz JA, Lee M, *et al* (2024) In vivo single-cell CRISPR uncovers distinct TNF programmes in tumour evolution. *Nature* 632: 419–428

Replogle JM, Norman TM, Xu A, Hussmann JA, Chen J, Cogan JZ, Meer EJ, Terry JM, Riordan DP, Srinivas N, *et al* (2020) Combinatorial single-cell CRISPR screens by direct guide RNA capture and targeted sequencing. *Nat Biotechnol* 38: 954–961

Replogle JM, Saunders RA, Pogson AN, Hussmann JA, Lenail A, Guna A, Mascibroda L, Wagner EJ, Adelman K, Lithwick-Yanai G, *et al* (2022) Mapping information-rich genotype-phenotype landscapes with genome-scale Perturb-seq. *Cell* 185: 2559-2575.e28

Rival C, Theas M, Suescun M, Jacobo P, Guazzone V, Van Rooijen N & Lustig L (2008) Functional and phenotypic characteristics of testicular macrophages in experimental autoimmune orchitis. *The Journal of Pathology* 215: 108–117

Rivello F, Van Buijtenen E, Matuła K, Van Buggenum JAGL, Vink P, Van Eenennaam H, Mulder KW & Huck WTS (2021) Single-cell intracellular epitope and transcript detection reveals signal transduction dynamics. *Cell Reports Methods* 1: 100070

Roche PA & Furuta K (2015) The ins and outs of MHC class II-mediated antigen processing and presentation. *Nat Rev Immunol* 15: 203–216

Roger T, Lugrin J, Le Roy D, Goy G, Mombelli M, Koessler T, Ding XC, Chanson A-L, Reymond MK, Miconnet I, *et al* (2011) Histone deacetylase inhibitors impair innate immune responses to Toll-like receptor agonists and to infection. *Blood* 117: 1205–1217

Roth DB (2014) V(D)J Recombination: Mechanism, Errors, and Fidelity. *Microbiol Spectr* 2: 2.6.18

Saeed S, Quintin J, Kerstens HHD, Rao NA, Aghajanirefah A, Matarese F, Cheng S-C, Ratter J, Berentsen K, Van Der Ent MA, *et al* (2014) Epigenetic programming of monocyte-to-macrophage differentiation and trained innate immunity. *Science* 345: 1251086

Sanson KR, Hanna RE, Hegde M, Donovan KF, Strand C, Sullender ME, Vaimberg EW, Goodale A, Root DE, Piccioni F, *et al* (2018) Optimized libraries for CRISPR-Cas9 genetic screens with multiple modalities. *Nat Commun* 9: 5416

Sapozhnikov DM & Szyf M (2021) Unraveling the functional role of DNA demethylation at specific promoters by targeted steric blockage of DNA methyltransferase with CRISPR/dCas9. *Nat Commun* 12: 5711

Schmidt SV, Krebs W, Ulas T, Xue J, Baßler K, Günther P, Hardt A-L, Schultze H, Sander J, Klee K, *et al* (2016) The transcriptional regulator network of human inflammatory macrophages is defined by open chromatin. *Cell Res* 26: 151–170

Schmidtmann E, Anton T, Rombaut P, Herzog F & Leonhardt H (2016) Determination of local chromatin composition by CasID. *Nucleus* 7: 476–484

Shang R, Lee S, Senavirathne G & Lai EC (2023) microRNAs in action: biogenesis, function and regulation. *Nat Rev Genet* 24: 816–833

Sheu KM & Hoffmann A (2022) Functional Hallmarks of Healthy Macrophage Responses: Their Regulatory Basis and Disease Relevance. *Annu Rev Immunol* 40: 295–321

Shi J, Wu X, Wang Z, Li F, Meng Y, Moore RM, Cui J, Xue C, Croce KR, Yurdagul A, *et al* (2022) A genome-wide CRISPR screen identifies WDFY3 as a regulator of macrophage efferocytosis. *Nat Commun* 13: 7929

Shields CW, Evans MA, Wang LL-W, Baugh N, Iyer S, Wu D, Zhao Z, Pusuluri A, Ukidve A, Pan DC, *et al* (2020) Cellular backpacks for macrophage immunotherapy. *Sci Adv* 6: eaaz6579

Sloas C, Gill S & Klichinsky M (2021) Engineered CAR-Macrophages as Adoptive Immunotherapies for Solid Tumors. *Front Immunol* 12: 783305

Smithies O, Gregg RG, Boggs SS, Koralewski MA & Kucherlapati RS (1985) Insertion of DNA sequences into the human chromosomal β-globin locus by homologous recombination. *Nature* 317: 230–234

Smyth LCD & Kipnis J (2025) Redefining CNS immune privilege. *Nat Rev Immunol*

Statello L, Guo C-J, Chen L-L & Huarte M (2021) Gene regulation by long non-coding RNAs and its biological functions. *Nat Rev Mol Cell Biol* 22: 96–118

Steuerman Y, Cohen M, Peshes-Yaloz N, Valadarsky L, Cohn O, David E, Frishberg A, Mayo L, Bacharach E, Amit I, *et al* (2018) Dissection of Influenza Infection In Vivo by Single-Cell RNA Sequencing. *Cell Systems* 6: 679-691.e4

Stik G, Vidal E, Barrero M, Cuartero S, Vila-Casadesús M, Mendieta-Esteban J, Tian TV, Choi J, Berenguer C, Abad A, *et al* (2020) CTCF is dispensable for immune cell

transdifferentiation but facilitates an acute inflammatory response. *Nat Genet* 52: 655–661

Stoeckius M, Hafemeister C, Stephenson W, Houck-Loomis B, Chattopadhyay PK, Swerdlow H, Satija R & Smibert P (2017) Simultaneous epitope and transcriptome measurement in single cells. *Nat Methods* 14: 865–868

Surdziel E, Clay I, Nigsch F, Thiemeyer A, Allard C, Hoffman G, Reece-Hoyes JS, Phadke T, Gambert R, Keller CG, *et al* (2017) Multidimensional pooled shRNA screens in human THP-1 cells identify candidate modulators of macrophage polarization. *PLoS ONE* 12: e0183679

Tanenbaum ME, Gilbert LA, Qi LS, Weissman JS & Vale RD (2014) A Protein-Tagging System for Signal Amplification in Gene Expression and Fluorescence Imaging. *Cell* 159: 635–646

Tang S, Wu X, Liu J, Zhang Q, Wang X, Shao S, Gokbag B, Fan K, Liu X, Li F, *et al* (2022) Generation of dual-gRNA library for combinatorial CRISPR screening of synthetic lethal gene pairs. *STAR Protocols* 3: 101556

Taxman DJ, Moore CB, Guthrie EH & Huang MT-H (2010) Short Hairpin RNA (shRNA): Design, Delivery, and Assessment of Gene Knockdown. In *RNA Therapeutics*, Sioud M (ed) pp 139–156. Totowa, NJ: Humana Press

Tong A-J, Liu X, Thomas BJ, Lissner MM, Baker MR, Senagolage MD, Allred AL, Barish GD & Smale ST (2016) A Stringent Systems Approach Uncovers Gene-Specific Mechanisms Regulating Inflammation. *Cell* 165: 165–179

Traxler P, Reichl S, Folkman L, Shaw L, Fife V, Nemc A, Pasajlic D, Kusienicka A, Barreca D, Fortelny N, *et al* (2025) Integrated time-series analysis and high-content CRISPR screening delineate the dynamics of macrophage immune regulation. *Cell Systems* 16: 101346

Trescher S & Leser U (2019) Estimation of Transcription Factor Activity in Knockdown Studies. *Sci Rep* 9: 9593

Tyagi M, Imam N, Verma K & Patel AK (2016) Chromatin remodelers: We are the drivers!! *Nucleus* 7: 388–404

Uribe-Querol E & Rosales C (2020) Phagocytosis: Our Current Understanding of a Universal Biological Process. *Front Immunol* 11: 1066

Valinluck V (2004) Oxidative damage to methyl-CpG sequences inhibits the binding of the methyl-CpG binding domain (MBD) of methyl-CpG binding protein 2 (MeCP2). *Nucleic Acids Research* 32: 4100–4108

Van Der Oost J, Jore MM, Westra ER, Lundgren M & Brouns SJJ (2009) CRISPR-based adaptive and heritable immunity in prokaryotes. *Trends in Biochemical Sciences* 34: 401–407

Van Epps HL (2006) Ignoring endotoxin. *The Journal of Experimental Medicine* 203: 1137–1137

Van Goethem E, Poincloux R, Gauffre F, Maridonneau-Parini I & Le Cabec V (2010) Matrix Architecture Dictates Three-Dimensional Migration Modes of Human Macrophages:

Differential Involvement of Proteases and Podosome-Like Structures. *The Journal of Immunology* 184: 1049–1061

Van Steensel B & Belmont AS (2017) Lamina-Associated Domains: Links with Chromosome Architecture, Heterochromatin, and Gene Repression. *Cell* 169: 780–791

Vojta A, Dobrinić P, Tadić V, Bočkor L, Korać P, Julg B, Klasić M & Zoldoš V (2016) Repurposing the CRISPR-Cas9 system for targeted DNA methylation. *Nucleic Acids Res* 44: 5615–5628

Vuscan P, Kischkel B, Joosten LAB & Netea MG (2024) Trained immunity: General and emerging concepts. *Immunological Reviews* 323: 164–185

Wang H, Xu X, Nguyen CM, Liu Y, Gao Y, Lin X, Daley T, Kipniss NH, La Russa M & Qi LS (2018) CRISPR-Mediated Programmable 3D Genome Positioning and Nuclear Organization. *Cell* 175: 1405-1417.e14

Wang T, Birsoy K, Hughes NW, Krupczak KM, Post Y, Wei JJ, Lander ES & Sabatini DM (2015) Identification and characterization of essential genes in the human genome. *Science* 350: 1096–1101

Wang Y, Khalil A, Kamar A, Du M, Dinh T, McFarland C & Wang Z (2023) Unveiling immune checkpoint regulation: exploring the power of in vivo CRISPR screenings in cancer immunotherapy. *Front Genet* 14: 1304425

Wu Y & Hirschi KK (2021) Tissue-Resident Macrophage Development and Function. *Front Cell Dev Biol* 8: 617879

Wynn TA, Chawla A & Pollard JW (2013) Macrophage biology in development, homeostasis and disease. *Nature* 496: 445–455

Wynn TA & Vannella KM (2016) Macrophages in Tissue Repair, Regeneration, and Fibrosis. *Immunity* 44: 450–462

Xie K, Minkenberg B & Yang Y (2015) Boosting CRISPR/Cas9 multiplex editing capability with the endogenous tRNA-processing system. *Proc Natl Acad Sci USA* 112: 3570–3575

Xie S, Duan J, Li B, Zhou P & Hon GC (2017) Multiplexed Engineering and Analysis of Combinatorial Enhancer Activity in Single Cells. *Molecular Cell* 66: 285-299.e5

Xu M (2003) STAT5-induced Id-1 transcription involves recruitment of HDAC1 and deacetylation of C/EBPbeta. *The EMBO Journal* 22: 893–904

Yan X, Stuurman N, Ribeiro SA, Tanenbaum ME, Horlbeck MA, Liem CR, Jost M, Weissman JS & Vale RD (2021) High-content imaging-based pooled CRISPR screens in mammalian cells. *Journal of Cell Biology* 220: e202008158

Zaccone P, Burton OT & Cooke A (2008) Interplay of parasite-driven immune responses and autoimmunity. *Trends in Parasitology* 24: 35–42

Zheng GXY, Terry JM, Belgrader P, Ryvkin P, Bent ZW, Wilson R, Ziraldo SB, Wheeler TD, McDermott GP, Zhu J, *et al* (2017) Massively parallel digital transcriptional profiling of single cells. *Nat Commun* 8: 14049

Zheng X, Wu B, Liu Y, Simmons SK, Kim K, Clarke GS, Ashiq A, Park J, Li J, Wang Z, *et al* (2024) Massively parallel in vivo Perturb-seq reveals cell-type-specific transcriptional networks in cortical development. *Cell* 187: 3236-3248.e21

Zhou P, Wan YK, Chan BKC, Choi GCG & Wong ASL (2021) Extensible combinatorial CRISPR screening in mammalian cells. *STAR Protocols* 2: 100255

Zhu S, Cao Z, Liu Z, He Y, Wang Y, Yuan P, Li W, Tian F, Bao Y & Wei W (2019) Guide RNAs with embedded barcodes boost CRISPR-pooled screens. *Genome Biol* 20: 20